MECHANISM OF TRANSCRIPTIONAL CONTROL OF ONCOGENIC TRANSCRIPTION FACTOR FUSIONS IN TUMOR DEVELOPMENT

By

Susu Zhang

Dissertation

Submitted to the Faculty of the

Graduate School of Vanderbilt University

in partial fulfillment of the requirements

for the degree of

DOCTOR OF PHILOSOPHY

In

Biochemistry

June 30, 2022

Nashville, Tennessee

Approved:

Scott Hiebert, Ph.D.

Kevin Schey, Ph.D.

Emily Hodges, Ph.D.

Yi Ren, Ph.D.

William Tansey, Ph.D.

Copyright © 2022 Susu Zhang
All Rights Reserved

To my wonderful parents and grandparents

ACKNOWLEDGEMENTS

This project would not have been possible without the support of many amazing people during my time at Vanderbilt. First and most important, I would like to express my deepest gratitude to my advisor Scott for providing me the opportunity to study at Vanderbilt and work in his lab. Through my training, Scott is always supportive of my research and encourages me when I have failed experiments. I would like to extend my sincere thanks to the rest of my committee: Emily, Yi, Kevin, and Bill, for their insightful advice and guidance to improve my critical thinking throughout my project.

I'm extremely grateful to work with a group of smart lab mates. Special thanks to Kristy for her always being supportive in troubleshooting all my questions, and for a lot of discussions during paper writing. A special thanks also goes to former postdoc Yue for teaching me all the new experimental skills when I first came to the lab. Thanks should also go to Clare, Gretchen, Monica, Hillary, and Jake for their help with protocol troubleshooting, and encouragement, especially Jake for doing all the PRO-seq for the lab. I feel very lucky to work with them, and they are the best lab mates. I also want to thank Steven and Brenda for their help with all the reagents and instruments to make the experiment much easier. Many thanks to the lab's bioinformatics collaborators Qi and Jing for their assistance with my data analysis questions. I thank also want to thank Patty for her help with all the program training documents.

I would like to thank all my friends in Nashville: Diane Jordan, Kathy Zhao, Adam Wang, Jiayi Yu, Sixie Yu, Simeng Zhao, Zhaobo Zheng, Shuang Xie, Pengfei Wang,

Peitong Wei, Liang Tong, Xiao Li, Xiaojia Li, Tengyu Ma, Lei su, Ling Chen, Yan Sun, Yongtai Liu, Betty Xie, Yue Gao, etc.

Finally, I want to thank my parents and grandparents for their support and love during these years of my life. I am especially thankful to my husband Chao for the support and for being my chauffeur every day for the past years even though he can work at home, and for having a “lab meeting” on the way home to discuss my research accomplishment of the day.

TABLE OF CONTENTS

LIST OF FIGURES

LIST OF ABBREVIATIONS

ABL1: ABL Proto-Oncogene 1

ALK: ALK Receptor Tyrosine Kinase

ALK: anaplastic lymphoma kinase

AML: acute myeloid leukemia

APEX2: Apurinic/Apyrimidinic Endo deoxyribonuclease 2

APL: acute promyelocytic leukemia

AR: Androgen Receptor

ARID1A: AT-Rich Interaction Domain 1A

aRMS: alveolar rhabdomyosarcoma

ASXL2: ASXL Transcriptional Regulator 2

ATAC-seq: Assay for Transposase-Accessible Chromatin with high-throughput sequencing

BCL2: BCL2 Apoptosis Regulator

BCR: BCR Activator Of RhoGEF And GTPase

BET: bromodomain and extra-terminal

BrdU: Bromodeoxyuridine

CBP: CREB binding protein

CCND1: cyclin D1

CCND2: cyclin D2

CCNT1: Cyclin T1

CDK: cyclin-dependent kinase

CDK8: Cyclin Dependent Kinase 8

CDK9: Cyclin Dependent Kinase 9

CDKN1A: Cyclin Dependent Kinase Inhibitor 1A

CDKN1C: Cyclin Dependent Kinase Inhibitor 1C

CEBPA: CCAAT Enhancer Binding Protein Alpha

ChIP-seq: chromatin immunoprecipitation and DNA sequencing

CIC: Capicua Transcriptional Repressor

CML: chronic myeloid leukemia

CMML: chronic myelomonocytic leukemia

CRISPR: clustered regularly interspaced short palindromic repeats

CTD: C-terminal domain

CUT&RUN: Cleavage Under Targets and Release using Nuclease

DBD: DNA-binding domain

DDIT3: DNA Damage Inducible Transcript 3

DHX15: DEAH-Box Helicase 15

DNMT3A: DNA Methyltransferase 3 Alpha

DRB: 5,6-dichloro-1-b-d-ribofuranosylbenzimidazole

DSIF: DRB sensitivity-inducing factor

dTAG: degradation tag

DUX4: Double Homeobox 4

E2F2: E2F Transcription Factor 2

E2F8: E2F Transcription Factor 8

ECAR: extracellular acidification rates

ENL: MLLT1, MLLT1 Super Elongation Complex Subunit

ERG: ETS Transcription Factor

eRMS: embryonal rhabdomyosarcoma

ESR1: Estrogen Receptor 1

ETS1: ETS Proto-Oncogene 1

ETV6 : ETS Variant Transcription Factor 6

EWS: EWS RNA Binding Protein 1

EZH2: enhancer of zeste 2

FACT: facilitates chromatin transactions

FCCP: p-trifluoromethoxy carbonyl cyanide phenyl hydrazine

FGF8: Fibroblast Growth Factor 8

FGFR2: Fibroblast Growth Factor Receptor 2

FGFR4: Fibroblast Growth Factor Receptor 4

FGGY: FGGY Carbohydrate Kinase Domain Containing

FLI1: Fli-1 Proto-Oncogene

FLT3: Fms Related Receptor Tyrosine Kinase 3

FOXO1: forkhead box O1

FUS: FUS RNA Binding Protein

GPS2: G Protein Pathway Suppressor 2

GSEA: gene set enrichment analysis

H2AX: H2A histone family member X

HDACs: histone deacetylases

HEB: TCF12, Transcription Factor 12

IgH: immunoglobulin heavy-chain H

JUN: Jun Proto-Oncogene

KIT: KIT Proto-Oncogene

KLF4: Kruppel Like Factor 4

LBD: ligand binding domain

LC-MS: liquid chromatography coupled with mass spectrometry

MCL1: MCL1 Apoptosis Regulator

MET: MET Proto-Oncogene

MIB1: MIB E3 Ubiquitin Protein Ligase 1

MLL4: KMT2B, Lysine Methyltransferase 2B

MPAL: mixed-phenotype acute leukemia

MTG16: CBFA2T3, CBFA2/RUNX1 Partner Transcriptional Co-Repressor 3

MYC: Myelocytomatosis

MYCN: MYCN Proto-Oncogene

MYOD1: Myogenic Differentiation 1

MYOG: Myogenin

NELF: negative elongation factor

NELFB: Negative Elongation Factor Complex Member B

NELL1: Neural EGFL Like 1

NES: nuclear export sequence

NFE2: Nuclear Factor, Erythroid 2

NFR: nucleosome free regions

NLS: nuclear localization signal

NRAS: NRAS Proto-Oncogene

NRSA: nascent RNA-sequencing analysis

NTRK: Neurotrophic Receptor Tyrosine Kinase

NTRK3: Neurotrophic Receptor Tyrosine Kinase 3

OCR: oxygen consumption rate

P-TEFb: positive transcription elongation factor b

PAX3: paired box gene 3

PCR: polymerase chain reaction

PI: propidium iodide

PIC: preinitiation complex

PLZF: Zinc Finger And BTB Domain Containing 16

PML: promyelocytic leukemia

Pol II: RNA polymerase II

PRDM12: PR/SET Domain 12

PRO-seq: precision nuclear run-on sequencing

PROTAC: proteolysis targeting chimera

RAD21: RAD21 Cohesin Complex Component

RARA: retinoic acid receptor alpha

RMS: rhabdomyosarcoma

RUNX1: RUNX Family Transcription Factor 1

RUNX1T1: RUNX1 Partner Transcriptional Co-Repressor 1

RUNX2: RUNX Family Transcription Factor 2

SEs: super-enhancers

SPT16: SPT16 Homolog

SS18: SS18 Subunit of BAF Chromatin Remodeling Complex

SSB: signal-sensing domain

SSRP1: structure-specific recognition protein-1

SSX1: SSX Family Member 1

SWI/SNF: SWItch/Sucrose Non-Fermentable

T-ALL: T cell acute lymphoblastic leukemia

TAD: transactivation domain

TBP: TATA box-binding protein

TET2: Tet Methylcytosine Dioxygenase 2

TF: transcription factor

TFAP2B: Transcription Factor AP-2 Beta

WT1: WT1 Transcription Factor

YY1: Yin Yang 1

CHAPTER 1

Introduction

1.1 Overview of transcriptional regulation

1.1.1 Transcriptional programs

1.1.1.1 Gene regulatory structures and DNA-binding transcription factor

Transcription represents the first level of gene expression. Generally, the main components of a protein-coding gene include the cis-regulatory element promoter and the coding region. Enhancers are also cis-regulatory elements in the genome that regulate gene expression in cooperation with promoters. For most eukaryotic genes, introns segment the coding region into exons. After the entire gene is transcribed to an RNA molecule, the exons are spliced to the mature mRNA as the template of protein translation. The promoter is a DNA sequence to which the transcriptional machinery binds, and can be separated into a core element and regulatory elements (Verrijzer et al., 1995).

The core promoter refers to the minimal elements required to mediate Pol II recruitment for transcription initiation (Roeder, 1996; Valen and Sandelin, 2011; Danino et al., 2015; Haberle and Stark, 2018). TATA box (consensus sequence: TATAWAWR) is the most characterized sequence of the core promoter that is recognized and bound by TATA box-binding protein (TBP), a subunit of the general transcription factors TFIID (Tanese et al., 1991; Chen et al., 1994). The TBP-DNA complex then recruits other general transcription factors (TFIIA, -B, -E, -F, and -H) and Pol II to the promoter to form the preinitiation complex. While ~76% of human core promoters lack TATA-like elements,

other consensus DNA motifs, such as SCGGAAGY, GGGCGGR, and TGCGCANK are identified as enriched in TATA-less promoters, suggesting novel DNA motifs might play a selective role in TATA-independent transcription (Yang et al., 2006; Yang et al., 2007).

Apart from the core promoter, the regulatory element of the promoter contains gene-specific sequences and controls the transcription initiation rate (Levine and Tjian, 2003). Transcription factors bind to the promoter regulatory element to facilitate transcription by recruiting other transcription complexes. For example, a gene with E-box (consensus sequence: CACGTG) in the promoter can be bound by a basic-helix-loop-helix (bHLH) motif-containing protein, like c-Myc (Blackwell et al., 1990). More often, the promoter regulatory regions are postulated to enable the communication of enhancers to core promoters, and this communication also relies on transcription factors (Su et al., 1991; Calhoun et al., 2002)

Enhancer is another type of cis-regulatory element, which are non-coding sequences in the genome. The enhancers can be upstream or downstream of their target promoters, in introns (typically the first intron of the gene), and even in the gene body of another gene (Levine, 2010). The distance of enhancers to the target promoters also varies. While some of the enhancers can be found near the promoter, some of the enhancers can be very distantly localized, such as 1Mb away (Bejerano et al., 2006; Borsari et al., 2021). The chromosome conformation capture (3C) methodology reveals that the long-range looping interaction between genomic elements is common (van Berkum et al., 2009). The regulation of distal enhancers is enabled by DNA looping or genome folding to place the enhancers and promoters in physical proximity (Robson et al., 2019; Schoenfelder and Fraser, 2019).

The mechanism of communication between promoters and enhancers over large distances action is still poorly understood. The specific regions in the enhancer might function differently according to the enhancer-promoter space. When a particular region in a distal enhancer is critical for the enhancer to activate transcription, the region can become unnecessary when this transcriptionally mutant distal enhancer is placed at a more proximal position to the promoter (Swanson et al., 2010). In addition, the enhancer-promoter interaction may exist before transcription is activated, or the contact might occur after association with a transcription factor (Li et al., 2012; Jin et al., 2013; Krivega et al., 2012).

The development of computational and functional genomic methods has enabled the identification of putative enhancers and their locations across the genome. It is generally accepted that transcriptionally active regions are less compacted chromatin to allow transcription machinery binding. Therefore, assays of the chromatin accessibility have been exploited to identify potential active regulatory regions, such as DNase I hypersensitive sites sequencing (DNase-seq) and the Assay of Transposase-Accessible Chromatin sequencing (ATAC-seq) (Wu et al., 1979; Song and Crawford, 2010; Tsompana and Buch, 2014; Shlyueva et al., 2014). Histone modification patterns are also widely used as signatures to identify active enhancers (Heintzman et al., 2007). Genome-wide studies show that enhancers are generally marked by histone H3 lysine 27 acetylation (H3K27ac) and histone H3 lysine 4 monomethylation (H3K4me1), while H3K4me1 and histone H3 lysine 4 tri-methylation (H3K4me3) are often present at the promoter sites (Rada-Iglesias et al., 2011; Creyghton et al., 2011; Zentner et al., 2011; Calo et al., 2013).

The discovery of a large number of putative enhancers raises the question of how many enhancers are actually functional and whether a small number of enhancers are essential in a particular cell type or condition. In the study of enhancer function, the term super-enhancer is used to describe a cluster of enhancers that are densely bound by transcription factors and have high levels of chromatin modification (Whyte et al., 2013). The super-enhancers are defined as enhancers within 12.5 kb of each other and meet the cutoff levels of enhancer signatures, like H3K27ac enrichment, or other transcription coactivators (Di Micco et al., 2014). One postulated model of super-enhancer function is that super-enhancers trigger condensates to facilitate the compartmentalization and concentration of transcriptional components at their associated genes to ensure robust transcription (Sabari et al., 2018).

In cancer, super-enhancers have been identified to be associated with critical oncogenes (Loven et al., 2013; Hnisz et al., 2013; Chapuy et al., 2013; Mansour et al., 2014). Super-enhancers associated with *MYC* are found in various cancer cell lines (Loven et al., 2013; Hnisz et al., 2013). For specific genes, tumor cells are more likely to associate with super-enhancers compared with the related healthy cells (Hnisz et al., 2013; Loven et al., 2013). In some cases, genetic alterations in cancers, such as rearrangement, encompass the super-enhancers or bring super-enhancer regions to oncogenes (Affer et al., 2014; Walker et al., 2014; Hayday et al., 2014). Somatic mutations in a super-enhancer can introduce new binding motifs to oncogenic transcription factors to reinforce the expression of associated genes (Mansour et al., 2014).

Transcription factors are the essential proteins that recognize promoters and enhancers to regulate transcription. A prototypical DNA-binding transcription factor contains a DNA-binding domain (DBD), a functional domain including a transactivation domain (TAD) or repression domain, and an optional signal-sensing domain (SSD) (Latchman, 1997). The DNA-binding domain forms a module that recognizes a specific sequence within enhancer or promoter DNA sequences. Transcription factors in a family with the same types of DNA-binding domains tend to have similar DNA-binding specificities. The transactivation domain is also a module domain containing binding sites for other transcription coregulators. These tend to be unstructured domains for facilitating the flexibility binding of diverse proteins (Dyson and Wright, 2005; Minezki et al., 2006).

Transcription factors regulate gene expression by a variety of mechanisms. Some transcription factors bind to DNA promoter sequences to help the formation of the transcription initiation complex, while others bind to enhancer sequences to either stimulate or repress transcription of the related gene (Yankulov et al., 1994; Yankulov et al., 1995; Rahl et al., 2010; Zhou et al., 2012). DNA-binding transcription factors integrate the communication between the promoter and distal enhancer to regulate transcription by recruiting coactivating complexes (Wilson et al., 2010; Taatjes, 2010; Stadler et al., 2011; Spaeth et al., 2011;).

1.1.1.2 Complexes recruited by DNA-binding transcription factors

The majority of the DNA is wrapped onto histones to form the units of chromatin: nucleosomes. The structure of local chromatin affects the access of transcription factors to regulatory elements: enhancers and promoters. When a gene is being transcribed,

chromatin regulators need to be recruited to move, eject, or restructure nucleosomes, thus exposing promoter and enhancer regions to allow access to proteins involved in transcription. Also, during the transcription elongation, the transcription machinery needs to overcome the nucleosome barriers and unwrap the DNA from nucleosomes to allow the polymerase machinery to melt the DNA duplex and transcribe the coding strand. Once accomplished, nucleosome integrity needs to be re-established (Lai et al., 2017). Therefore, transcription factors recruit various proteins, including Mediator, SWI/SNF, FACT, and histone modifying enzymes, to help the assembly and activity of the transcription machinery.

Mediator of Pol II transcription (Mediator) is a multiprotein complex identified as a coactivator (Malik and Roeder et al., 2000). In human cells, up to 30 subunits in the Mediator complex are required for transcription, and its structure is divided into four modules: the head, middle, tail, and CDK8 kinase module (Bourbon et al., 2008; Tsai et al., 2014). The head module subunit of Mediator (Med11) directly interacts with the general transcription factor TFIIH, while Med17, and Med22 are required to recruit TFIIE (Esnault et al., 2008). Other than initiation, subunit Med26 in the middle module of Mediator can function to switch the interaction from TFIID to proteins involved in elongation (Takahashi et al., 2011). The CDK8 kinase module regulates transcription through phosphorylation and control of Pol II binding with the middle module (Tsai et al., 2013).

SWItch/Sucrose Non-Fermentable (SWI/SNF) is one of the essential classes of chromatin-remodeling factors. SWI/SNF complex act to reposition nucleosomes through the displacement of the histone octamer, thus providing access to the promoter and

enhancer (Cote et al., 1994; Kwon et al., 1994; Whitehouse et al., 1999). The model of. SWI/SNF complex nucleosome remodeling is to slide or eject the nucleosomes that were initially equally spaced (Saha et al., 2006; Kassabov et al., 2003). *ARID1A* is one of the SWI/SNF subunits frequently mutated in cancers (Jones et al., 2010; Gui et al., 2010). *ARID1A* mutations cause loss of SWI/SNF complex occupancy on chromatin and result in loss of chromatin accessibility at enhancers followed by rapid downregulation of transcription (Mathur et al., 2017; Blumli et al., 2021).

Facilitates chromatin transcription (FACT) complex, comprised of suppressor of Ty 16 (SPT16) and structure-specific recognition protein-1 (SSRP1), is also involved in nucleosome remodeling, and is required for transcription (Orphanides et al., 1999). During transcription, FACT destabilizes nucleosomes by the interaction of SPT16 to H2A-H2B dimers and that of SSRP1 to H3-H4 tetramers (Belotserkovskaya et al., 2003). On the other hand, FACT facilitates the nucleosome reassembly by maintaining the tetrameric confirmation of H3-H4 and then DNA displaces FACT to bind the tetramer (Liu et al., 2019). In addition to transcription, the FACT complex is also involved in DNA replication and DNA repair (Charles Richard et al., 2016; Yang et al., 2016).

The modifications of the N-terminal tails of histones H2A, H3B, H3, and H4 are also involved in the regulation of local chromatin structure to affect transcription. Transcription factors recruit the proteins that can write, read, or erase these histone modification marks to regulate local chromatin structure. Transcription factors and histone modifications tend to co-localize at promoter and enhancer and different patterns of histone modifications indicate the activation or repression of gene transcription (Costa et al., 2011; Benveniste et al., 2014). For example, the histone acetyltransferase (HAT) p300

and CREB binding protein (CBP) are recruited and activated by transcription factors to introduce H3K27ac (Ortega et al., 2018). H3K27ac neutralizes the positive charge of the histone tail to attenuate the interaction of DNA and histone to presumably facilitate the access of enhancers (Eberharter et al., 2002). H3K27ac is established as an essential enhancer mark that distinguishes active enhancers from poised enhancers (Creyghton et al., 2010). In comparison, the recruitment of histone methyltransferase enhancer of zeste 2 (EZH2) in the Polycomb repressive complex 2 (PCR2) catalyzes the H3K27me3 leading to a more condensed chromatin state and transcription repression (Yoo et al., 2012; Cai et al., 2021).

1.1.1.3 Transcription apparatus

RNA polymerase II is the main enzyme for the transcription of protein-coding genes and several no-coding nuclear RNAs. It is a 12-subunit enzyme and is conserved throughout eukaryotes. The subunit Rpb1 contains a C-terminal domain (CTD) that plays a vital role during the transcription cycle. The CTD consists of 52 consensus repeats of Tyr1-Ser2-Pro3-Thr4-Ser5-Pro6-Ser7 in human cells. CTD is highly phosphorylated by different kinases at specific positions throughout the transcription cycle.

There are three stages of transcription: initiation, elongation, and termination. The transcription initiation begins when Pol II and general transcription factors are recruited to the promoter to form the preinitiation complex (PIC). The PIC is defined to consist of eight factors including general transcription factors (TFIIA, TFIIB, TFIID, TFIIE, TFIIF, TFIIH), Pol II, and Mediator (Hahn et al., 2004; Murakami el., 2013). Then the helicase activity of TFIIH unwinds the double-strand DNA to allow the formation of the transcription

bubble. The CTD ser5 is phosphorylated by the TFIIH kinase cyclin-dependent kinase 7 (CDK7) at the onset of initiation, and plays a critical role in the mRNA processing including the nascent pre-mRNA 5' terminus capping and co-transcriptional splicing (Lu et al., 1992; Rodriguez et al., 2000; Nojima et al., 2018).

Shortly after initiation, TFIIB, TFIIF, and TFIIE dissociate from pol II to allow the binding of two factors: the 5,6-dichloro-1-β-d-ribofuranosylbenzimidazole (DRB) sensitivity-inducing factor (DSIF) and the negative elongation factor (NELF) to the Pol II. A post-initiation block of Pol II occurs after the synthesis of ~30 nucleotide-long nascent RNA, and Pol II accumulates just proximal to the promoter (Figure 1.1). DSIF and NELF were defined during the *in vivo* study of Pol II elongation inhibition caused by DRB, which is a kinase inhibitor (Wada et al., 1998; Yamaguchi et al., 1999). The cryo-electron microscopy (cryo-EM) structure analysis of paused elongation complex suggests that NELF restrains Pol II mobility, and the paused Pol II helps prevent new initiation (Shao et al., 2017; Vos et al., 2018).

After pausing, the paused Pol II begins active elongation through the recruitment and activation of positive transcription elongation factor b (p-TEFb) by phosphorylation of the CTD Ser2 of paused Pol II through its CDK9 catalytic subunit, as well as phosphorylation of DSIF and NELF to dissociate NELF from Pol II (Wu et al., 2003; Adelman and Lis, 2012; Lu et al., 2016) (Figure 1.1). P-TEFb can be recruited by transcription factors, Mediator proteins, and bromodomain protein BRD4 (Yang et al., 2005; Donner et al., 2010). BRD4 interacts with the P-TEFb CDK9 subunit to release it from the binding of the inhibitory subunit, thus stimulating the kinase activity of P-TEFb for phosphorylation of Pol II CTD (Itzen et al., 2014). The CTD Ser2 can also be

phosphorylated by CDK12 and CDK13 during the transcription of long genes with high numbers of exons (Bartkowiak et al., 2010; Blazek et al., 2011). After the full length of the gene is transcribed, the CTD coupled pre-mRNA 3' end cleavage and polyadenylation provide a signal for the transcription termination (Connelly and Manley, 1988; Batt et al., 1994; de Almeida et al., 2008; Mayer et al., 2012).

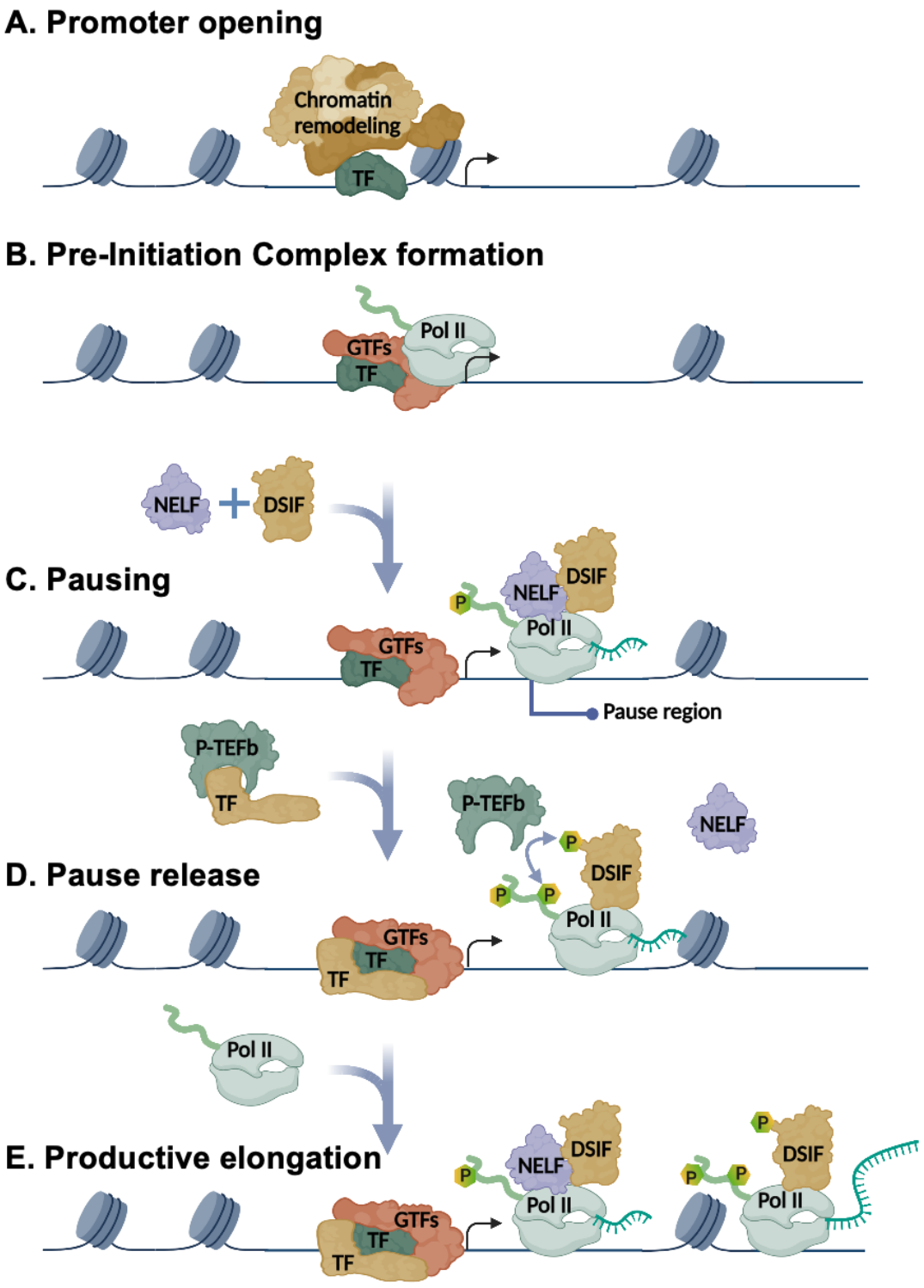

Figure 1.1. Mechanisms of Pol II pausing and releasing. (A) A sequence-specific transcription factor binds to chromatin and brings in chromatin remodelers to open chromatin around TSS and render the promoter accessible for recruitment of the transcription machinery. (B) Specific transcription factors facilitate the recruitment of a set

of general transcription factors and Pol II to form a Pre-Initiation Complex (PIC) to proceed with the initiation of RNA synthesis. (C) Pol II pausing occurs shortly after transcription initiation and involves the association of pausing factors DSIF and NELF. The paused Pol II is phosphorylated on its CTD. (D) The recruitment of the P-TEFb kinase triggers pause release by the transcription factor. P-TEFb kinase phosphorylate the DSIF/NELF complex to release paused Pol II. Phosphorylation of DSIF/NELF dissociates NELF from the elongation complex and transforms DSIF into a positive elongation factor associated with Pol II throughout the gene. (E) The paused Pol II proceeds to productive elongation and another Pol II enters the paused site, allowing for efficient RNA production.

1.1.2 Dysregulation of transcription in cancer

Transcription factors are frequently dysregulated in human cancer via various mechanisms including gene amplification or deletion, point mutations, and chromosomal translocation to alter gene expression. *E2F1* is a cell cycle regulatory factor that is amplified, whereas another cell cycle factor, *FOXM1* is over-expressed in different types of cancers (Xiao et al., 2007; Suh et al., 2008; Liao et al., 2018; Barger et al., 2019). The tumor suppressor *p53* mutation is the most frequently mutated gene in cancer (Muller and Vousden, 2013; Mantovani et al., 2018). The mutations give rise to loss of function of p53 or dominant-negative activity by inserting into the p53 tetramer to inactivate the wild-type counterpart. The dysregulation of *TAL1* can be caused by either rearrangement to create a STIL-TAL1 fusion, or by non-coding mutations to create an enhancer that is responsive to oncogenetic transcription factor MYB (Mansour et al., 2014; Girardi et al., 2017).

Transcription factors are also often disrupted by chromosomal translocations in cancer (Mitelman et al., 2007, Mertens et al., 2015). These translocations connect enhancers to oncogenic transcription factors to cause aberrant expression of the oncogene, like MYC, or create new transcription factors, like the t(8;21)-AML-ETO and the t(2;13)-PAX3-FOXO1 (Rowley JD. 1973, Turc-Carel et al. 1986) (Figure 1.2). Many

of these translocations create fusion proteins containing functional domains of two different transcription factors, making a new transcription factor with oncogenic activities (Rabbitts, 1994). Mainly, the genes produce in-frame fusion proteins with new and altered activities. Recently, a large genome study indented that there are 17% of tumors contain oncogenic gene fusions, demonstrating that translocations are a common cause of malignancy (Gao et al., 2018).

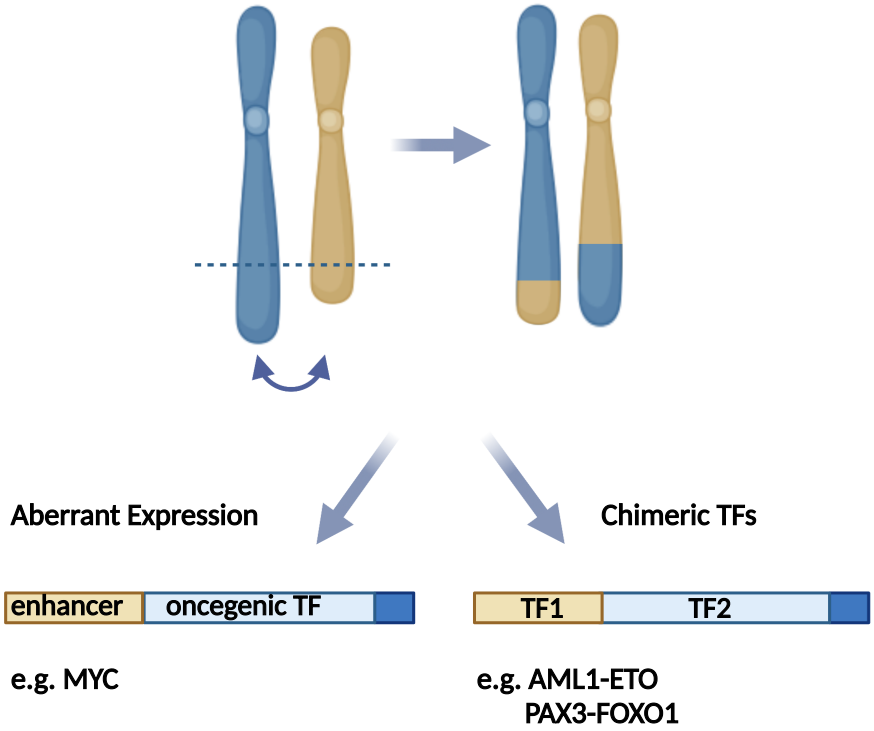

Figure 1.2. Model of chromosomal translocation target master transcription factors.

Other than transcription factors, nearly all components involved in transcription control can be affected by different genetic alterations in cancer. The cis-regulatory elements in enhancers and promoters can be mutated to cause abnormal binding sites for oncogenic transcription factors, such as in the TAL1 enhancer (Mansour et al., 2014). MED12 from the Mediator is found mutated in uterine leiomyomas and prostate

cancer, and the different mutations of MED12 show different effects on the interaction with other Mediator components (Mittal et al., 2015; Kampjarvi et al., 2016). Chromatin writer proteins such as MLL have been reported to fuse with over 90 partners in acute myeloid leukemia (AML) or acute lymphocytic leukemia (ALL) (Slany et al., 2005). Chromatin reader protein, for example, BRD4 is reported to disrupt by translocation in midline carcinoma to drive the stem cell-like proliferation (Wang et al., 2014). Pol II mutation is also found to drive tumorigenesis in meningioma (Clark et al., 2016).

1.1.3 Targeting transcription in cancer therapy

Transcription programs are critical therapeutic targets for cancer treatment. Chromatin regulators are enzymes that can influence gene transcription control and be the target of cancer therapy. Examples of chromatin regulators that have been targeted in the clinic include the inhibitors of “eraser” proteins such as histone deacetylases (HDACs) and histone demethylase (Montalban-Bravo and Garcia-Manero, 2015; De Souza et al., 2015; Johnston et al., 2020).

Kinase inhibitors that target CTD phosphorylation have been used to inhibit the transcriptional process. Inhibitors of CDK7, such as THZ1, show sensitivity in T-cell acute lymphoblastic leukemia (T-ALL) due to the inhibition of core transcriptional control of transcription factor RUNX1 expression (Kwiatkowski et al., 2015). Also, CDK9 has been shown to cause Pol II pausing to slow the rate of elongation and trigger cell apoptosis in t(8;21) AML (Sampathi et al., 2019; Mandal et al., 2021).

The bromodomain and extraterminal (BET) proteins that recruit P-TEFb are promising therapeutic targets in cancer. BET consists of 4 family members including

BRD2, BRD3, BRD4, and BRDT. These BET proteins bind to acetylated lysine in the tail of histones as well as other non-histone proteins through two conserved N-terminal bromodomains (Dey et al., 2003; Filippakopoulos and Knapp, 2012). Small molecule inhibitors of BET proteins, such as JQ1, I-BET, and MS417 mimic the acetylated lysine moiety and competitively bind to the two bromodomains (BD1, BD2) to displace BET proteins from chromatin. Gene expression studies showed that BETi induced down-regulation of mRNAs including key oncogenes important for cell cycle progression, such as *MYC* and *E2F1*, genes that control cell death such as *BCL2*, and lineage-specific oncogenes such as *BCL6* (Zhao et al., 2016).

Although DNA-binding transcription factors are thought of as 'undruggable' targets, many of the fusion proteins in cancer are composed of domains from two transcription factors, transcriptional co-regulators or non-enzymatic proteins. The main strategies to modulate the activity of transcription factors with small compounds focus on inhibition of protein/protein interactions to block the interaction between TFs and co-factors or dimerization of TFs, or the approach is based on blockage of protein/DNA binding by manipulating the transcription factor DNA binding domain or competing with TFs (Hagenbuchner et al., 2016, Bushweller, 2019).

The development of proteolysis targeting chimera (PROTAC) makes it possible to target transcription factors directly. PROTAC is a bifunctional small molecule composed of two active domains and a linker (Sakamoto et al.,2001) (Figure 1.3). It requires high selectivity of binding of its targets rather than inhibition of the protein function. The development of PROTACs that link transcription factors to ubiquitin E3 ligases to rapidly induce the destruction of the protein has been applied to next-generation drug discovery

in cancer. For CML with fusion oncoprotein BCR-ABL, the BCR-ABL-targeting PROTACs are shown high potency to inhibit CML K562 cell growth. (Lai et al., 2016; Demizu et al., 2016; Bruslem et al., 2019). The PROTAs target STAT3 efficiently inhibit STAT3, and exhibit potent antitumor in cell line and mouse model studies (Zhou et al., 2019; Bai et al., 2019).

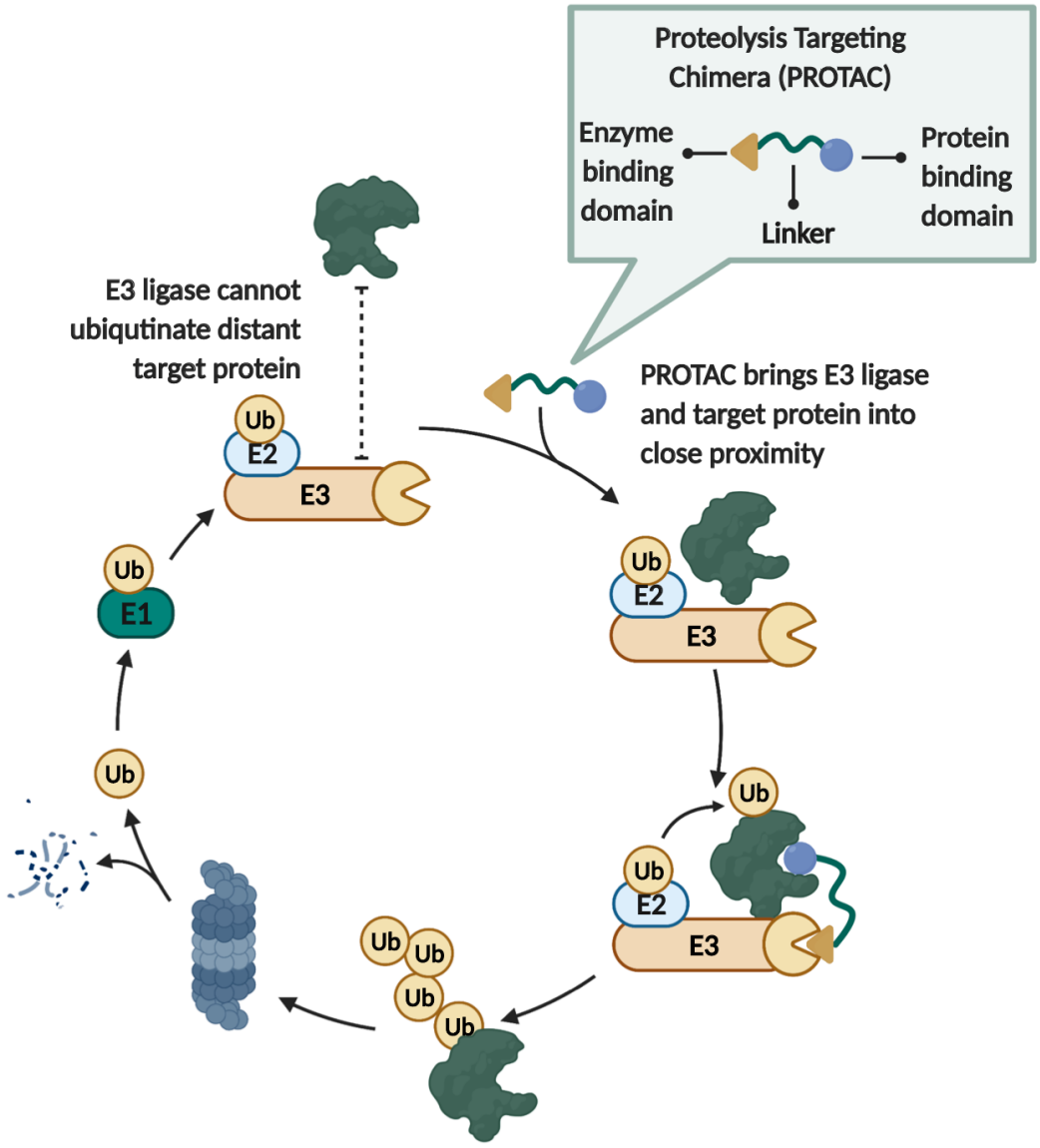

Figure 1.3. Schematic model of selective PROTAC-induced targeted protein degradation. PROTACs are heterobifunctional small molecules composed of two active

domains and a linker. The two functional domains are covalently linked protein-binding molecules: one capable of engaging E3 ubiquitination, and another binds to a target protein. E3 ligase cannot ubiquitinate distant target protein. When PROTAC brings E3 ligase and target protein into proximity, the E3 ligase targets protein and covalently attaches the ubiquitin to the protein. After a ubiquitin chain is formed, the protein is recognized and degraded by the 26S proteasome. The E1 ligase recycles the ubiquitin, and the E1 ligase activates and conjugates the ubiquitin to the E2 ligase which forms a complex with the E3 ligase.

For the molecular mechanism of transcriptional regulation, transcription factors are often the last link in a signal transduction cascade and transcription can change within 15 to 30 minutes of such a signaling event (Swift et al., 2017). Rapid inhibition of the fusion transcriptional factors is critical to understanding the mechanism(s) by which oncogenic transcription factors facilitate tumor development by defining their direct transcriptional targets. One of the challenges to studying fusion transcription factors is that it is difficult to rapidly inhibit their function to assess the immediate targets, in the same way, that kinase inhibitors have been used to define signal transduction cascades. While utilizing PROTACs has been shown to degrade cancer-causing proteins successfully, it is still challenging to synthesize PROTACs to target every cancer driver protein.

Previous studies to define the gene network of transcription factors rely on genetic inactivation through gene deletion or RNAi approaches, and the subsequent steady-state mRNA level changes. The obvious limitation of these approaches is timeliness. After days of genetic inactivation, it is hard to distinguish direct transcriptional events from indirect ones. Rather than genetic inactivation or inhibiting protein function, the degradation TAG (dTAG) system is a tag-based strategy that enables the degradation of targeted proteins (Nabet et al., 2018). The targeted protein expressing an $FKBP12^{F36V}$ chimera is linked to the E3 ligases such as cereblon (CRBN) or von Hippel-Lindau (VHL) by small molecule

degrader (Winter et al., 2015; Weintraub et al., 2017; Nabet et al., 2018). Compared to traditional genetic approaches, dTAG system provides a rapid depletion of the protein-of-interest with high selectivity.

The dTAG system has been employed to evaluate the function of factors in transcriptional regulation. Degradation of ENL in MLL-AF4 rearranged AML reveals that ENL suppressed the initiation and elongation of RNA Pol II (Erb et al., 2017). Degradation of Yin Yang 1 (YY1) shows that YY1 contributes to enhancer-promoter structural interactions by forming dimers that facilitate the interaction of DNA elements (Weintraub et al., 2017). The rapid degradation of endogenous AML1-ETO fusion protein suggests that rather than maintaining or activating gene expression defined after several days of *AML1-ETO* knockdown, AML1-ETO functions primarily as a transcriptional repressor and represses only ~60 direct targets instead of hundreds to thousands of genes (Berget al., 2008; Stengel et al., 2021).

1.2 Oncogenic transcription factor fusions in hematological malignancies

1.2.1 Chromosomal translocation in hematological malignancies

Leukemia is the most common type of pediatric cancer, around 30% of total cases. Most fusion genes are identified in leukemias. Many of the translocations affect transcription factors. t(15;17) translocation is found in acute promyelocytic leukemia (APL), which accounts for 5-10% of AML. The fusion gene *PML-RARA* results from the translocation of t(15;17) that fuses the gene for retinoic acid receptor alpha (*RARA*) with promyelocytic leukemia (*PML*) (Grignani et al., 1993). In the absence of ligands, PML-

RARA functions to repress the transcription of genes that are critical to myeloid differentiation (Segalla et al., 2003; Noguera et al., 2016). All-trans retinoic acid (ATRA) and arsenic relieve the block of myeloid differentiation by binding to RARA and PML, respectively, and are associated with high clinical complete remission (CR) (Yoshida et al., 1996; Zhu et al., 1999; Shen et al., 2004; Lalllemand-Breitenbach et al., 2008; Jeanne et al., 2010).

Chromosomal translocations that connect enhancers to oncogenic transcription factors can cause aberrant expression of the oncogene. For example, the translocation between chromosome 14 and chromosome 8 was reported in Burkitt lymphomas (Manolov and Manolova, 1972; Zech et al., 1976). One of the molecular targets of the translocations is the transcription factor MYC, which binds to the enhancer box sequence (E-box) to regulate transcription elongation (Grandori et al., 1997). The t(8;14) translocation juxtaposes the *c-MYC* gene to the immunoglobulin heavy-chain (*IgH*) enhancer loci and results in constitutive deregulation of MYC expression, and MYC upregulation leads to activation of genes related to proliferation and apoptosis. (Dalla-Favera et al., 1982; Taub et al., 1982; Hamlyn and Rabbitts, 1983).

While there is frequent involvement of transcription factors by chromosomal translocations, kinases are also frequently affected by these translocations, such as the proto-oncogene tyrosine-protein kinase (*ABL1*) gene on chromosome 9 and the breakpoint cluster region (*BCR*) gene on chromosome 22 fuse to encode (BCR-ABL1) oncogenic protein, which enhances the tyrosine kinase activity of BCR, and results in maintenance of proliferation, inhibition of differentiation, and resistance of cell death (Rowley, 1973; Collins, 1983; Kurzrock, 1988; Li, 1999).

There are also translocations that fuse transcription factors with receptor tyrosine kinases. The ETS family transcription factor ETS variant transcription factor 6 (ETV6) is reported to be involved in different translocations with tyrosine kinases, such as ETV6-PDGFβR (platelet-derived growth factor β) resulting from the t(5;12) balanced translocation in chronic myelomonocytic leukemia (CMML), and ETV6-NTRK3 (neurotrophic tropomyosin receptor kinase gene 3) resulting from t(5;12) in acute lymphoblastic leukemia (ALL) (Golub et al., 1994; Knezevich et al., 1998; Roberts et al., 2018). The function of these fusion proteins seems more dependent on the kinase activity. The fusion proteins contain the dimerization domain of ETV6 and the tyrosine kinase domain of PDGFβR and NTRK3 protein. The dimerization of fusion proteins mimics the ligand-induced dimerization to cause continuous activation of phosphorylating tyrosine residues to promote the growth, proliferation, and survival of cells (Golub et al., 1994; Carroll et al., 1996; Knezevich et al., 1998).

1.2.2 AML1-ETO in AML

t(8;21) is the first chromosomal translocation discovered in AML (Rowley, 1973). The translocation fuses the DNA binding domain of AML1 (or RUNX1) to nearly all the ETO (or MTG8/RUNX1T1) (Miyoshi et al., 1991). While RUNX1 associates with multiple DNA binding proteins and/or histone-modifying complexes to activate or repress transcription, the presence of the ETO moiety skews the activity of the fusion protein towards repression of RUNX1-regulated genes (Lutterbach et al., 1998; Linggi et al., 2002). ETO associates with histone acetyltransferases, but recruits class I histone deacetylases, and global studies of t(8;21) cells suggest that this latter effect is the

predominant mechanism of action (Amann et al., 2001; Wang et al., 2011; Ptasinska et al., 2014). However, ETO family members are associated with the “E proteins” HEB and LYL1 (LYL1 basic helix-loop-helix family member) in a complex containing LDB1 (LIM domain-binding protein 1), LMO2 (LIM domain only 2), and CDK9 (cyclin-dependent kinase 9), making it possible that ETO family members regulate transcriptional elongation (Zhang et al., 2004; Meier et al., 2006).

Previous studies sought to underlie the role of *AML1-ETO* in AML from the transcriptional aspect by defining the core AML1-ETO transcriptional program. After days of *AML1-ETO* knockdown or knockout, AML1-ETO down-regulation led to hundreds to thousands of gene changes. While many existing studies indicate the transcriptional repression function of AML1-ETO, numerous studies also reported that AML1-ETO activates gene expression. However, with a more rapid endogenous AML1-ETO degradation, Stengel et al were able to define a surprisingly small core network of ~60 genes that are directly regulated by AML1-ETO (Stengel et al., 2021). The network includes critical mediators of myeloid differentiation and cell fate decision genes such as *CEBPA* (CCAAT enhancer binding protein alpha), *PLZF* (promyelocytic leukemia zinc finger), *NFE2* (nuclear factor, erythroid 2), and *MTG16* (myeloid translocation gene 16).

Today, t(8;21) is used to define a distinct subgroup of patients which is usually considered a “good” prognostic marker. Around 6-8% of adult and 10% of pediatric cases harbors this fusion gene (Nucifora et al., 1994). In mice, the expression of AML1-ETO alone is not sufficient to cause leukemia (Rhoades et al., 2000; Yuan et al., 2001). When investigating the secondary mutations that contribute to AML1-ETO-mediated leukemogenesis, an alternatively spliced AML1-ETO isoform AE9a (alternative splicing

at exon 9) is identified to strongly indeces leukemia development (Yan et al., 2004; Yan et al., 2006; Link et al., 2016). The AE9a lacks the C-terminal of the NHR3/4 domain of ETO, which is critical for NCoR/SMRT (nuclear receptor corepressor/silencing mediator of retinoic acid and thyroid hormone receptor) interaction, therefore leading to the differential regulation of AML1-ETO target genes, such as the p21 cell cycle inhibitor CDKN1A (cyclin-dependent kinase inhibitor 1) to facilitate growth (Yan et al., 2004; Link et al., 2016). Additionally, mutational landscape analysis shows that in cooperating with t(8;21), somatic variants that might overcome the growth arrest induced by AML1-ETO are detected in both diagnosis and relapse, including *FLT3* (fms-like tyrosine kinase 3), *KIT* (KIT proto-oncogene), *NRAS* (NRAS proto-oncogene), *WT1* (Wilms's tumor gene), *DHX15* (DEAH-box helicase 15), *ASXL2* (ASXL transcriptional regulator 2), *DNMT3A* (DNA methyltransferase 3 alpha), *TET2* (tet methylcytosine dioxygenase 2), and *RAD21* (double-strand-break repair protein rad21 homology) (Madan et al., 2018).

BETi show efficacy in preclinical models of AML, multiple myeloma, and certain types of lymphoma as well as other cancer types (Bartholomeeusen et al., 2013; Filippakopoulos et al., 2010; Delmore et al., 2011; Ott et al., 2012). AML containing chromosomal translocations involving MLL appear to be especially sensitive to BET inhibitor, perhaps due to the translocations that fuse the N-terminal domain of MLL with components of the super elongation complex to stimulate the expression of key regulators of hematopoietic stem cell self-renewal such as Hox family members. In the early studies, t(8;21) showed the most pronounced sensitivity (Zuber et al., 2011). A recent study in t(8;21) AML cells shows that BETi impairs RNA polymerases II pausing the release of over 1400 genes including the stem cell factor receptor tyrosine kinase KIT ((Zhao et al.,

2016). BETi also shows the ability to repression of microRNAs that target the antiapoptotic factor (MCL1), which suggests the BETi resistance mechanism and the combination treatment with antiapoptotic protein inhibitor Venetoclax in AML (Ramsey et al., 2021).

1.3 Oncogenic transcription factor fusions in solid tumors

For pediatric solid tumors, there are several fusion genes that are considered oncogenic drivers of tumorigenesis in children, as well as diagnostic markers or new therapeutic targets. One of the most described bones and soft-tissue tumors in children is Ewing's sarcoma. Over 90% of Ewing's sarcomas contain a t(11;22) translocation which fuses the *EWS* gene with the *FLI1* genes generating a novel transcription factor (Delattre et al., 1992). Apart from the common *EWS-FLI1*, the *FUS-ERG* (fused in sarcoma/ETS transcription factor ERG) fusion gene resulting from t(16;21) is also been observed in Ewing's tumors. *FUS* rearrangement has also been reported in myxoid liposarcoma (Rabbitts et al., 1993). FUS-DDIT3 (DNA damage-inducible transcript 3) fusion is the signature onco-transcription factor which fuses the FUS N-terminal SYGQ-rich low complexity domain to the full-length DDIT3.

There are also translocations been found in rare cancers associated with poor survival like MLL4-GPS2 (t(5;8)) in spindle cell sarcoma, SS18-SSX1 (t(X;18)) in synovial sarcoma, and CIC-DUX4 (t(4;19)) in undifferentiated round cell sarcoma (O'Meara et al., 2014; Storlazzi et al., 2004; Kawamura-Saito et al., 2006). PAX3/7-FOXO1, which is due to the translocation t(2;13), is a novel transcription factor with high transcriptional activity

due to the translation of the transactivation domain of FOXO1 to the DNA binding domain of PAX3 in certain subtypes of rhabdomyosarcoma (RMS) (Barr et al., 1993).

1.3.1 PAX3-FOXO1 in aRMS

1.3.1.1 Overview of RMS

Rhabdomyosarcoma (RMS) is one of the most common solid tumors in children, accounting for approximately 50% of all soft tissue sarcomas or around 3-8% of all pediatric cancers (Dagher et al., 1998, Ward et al., 2014). In the United States, about 400-500 people are diagnosed with RMS each year, and more than half of the patients are under age 10. The overall 5-year survival rate is 70% for children under 15, and 50% for teens over 15. Epidemiology and End Results database shows that 40% of all RMS are diagnosed in adults over 20 years of age, with an overall survival rate of 30% (Sultan et al., 2009).

RMS tumors are thought to originate from myogenic precursor cells of muscle, and they show histologically aberrant muscle differentiation state (Dagher and Helman, 1999). There is evidence showing that both myogenic and non-myogenic lineage can contribute to the development of RMS-like tumors (Rubin et al., 2011; Hatley et al., 2012). Also, the tumors arise from a variety of anatomic sites, and are not limited to skeletal muscle. Based on the histology, the classification of RMS is listed as four subtypes: embryonal, alveolar, pleomorphic, and spindle cell/sclerosing. Embryonal rhabdomyosarcoma (eRMS) and alveolar rhabdomyosarcoma (aRMS) are the most common subtypes, they comprise ~60% and ~30% of RMS cases respectively (Ognjanovic et al., 2009). ERMS has a more

favorable prognosis, and the five-year survival rate of eRMS patients is greater than 85%. ERMS cases are reported with mutations of *p53* loss, *RAS* pathway activation, *MYOD1* (myogenic differentiation 1) mutation, and *VGLL2* (vestigial like family member 2) rearrangement (Stratton et al., 1989; Taylor et al.,2000; Kohsaka et al., 2014).

ARMS is the other major subtype of RMS, which have a relatively low 5-year overall survival, with a high chance of metastasis and relapse (Sorensen et al., 2002, Missiaglia et al., 2012). In contrast to eRSM, the t(2;13) (*PAX3-FOXO1*) or t(1;13) (*PAX7-FOXO1*) fusion gene is a signature genetic change of pediatric aRMS. Around 60% aRMS cases harbor *PAX3-FOXO1* fusion, and 20% with *PAX7-FOXO1* fusion, while 20% of tumors are fusion-negative aRMS. The patient outcome of aRMS is different between patients with *PAX3-FOXO1* fusion or *PAX7-FOXO1* fusion. In non-metastatic patients, the 5-year survival rate is 39% in *PAX3-FOXO1* patients, 74% in *PAX7-FOXO1* patients, and 84% in fusion-negative patients. The survival rates vary even more strikingly in patients with metastasis, 8% for *PAX3-FOXO1* fusion contain patients and 75% for *PAX7-FOXO1* fusion contain patients (Sorensen et al., 2002; Kubo et al., 2015).

For the past decades, the treatment of aRMS had remained unchanged with both local therapy, such as surgery and radiation therapy, and chemotherapy, which is toxic to normal cells. However, approximately one-third of the tumors will relapse, and the relapse rate rises to 70% for the metastatic cases (Pappo et al., 1999; Hibbitts et al., 2019). In addition, there is a limited number of secondary genomic mutations in aRMS tumors, which is 6.4 mutations per tumor and only 2.5 mutations are in a transcribed gene (Shern et al., 2014). This makes it even harder to develop potential targeted therapy.

1.3.1.2 PAX3-FOXO1

1.3.1.2.1 PAX3

The paired box gene 3 (PAX3) is a transcription factor. Characterized by a highly conserved paired DNA binding domain, PAX family transcription factors are essential regulators during the development of the nervous system and the formation of various organs (Tremblay and Gruss, 1994). The PST-rich region of the C-terminus is the transcriptional activation domain of PAX3 (Tanaka and Herr, 1990; Chalepakis et al., 1994). For PAX3 and PAX7, the C-terminal transactivation domains appear to be potently inhibited by a domain located in the first 90 N-terminal amino acid of PAX3 (Chalepakis et al., 1994; Fredericks et al., 1995; Bennicelli et al., 1995; Bennicelli et al., 1999). As a transcription factor, PAX3 has the capability to form homodimers (PAX3/PAX3) and heterodimers (PAX3/PAX7) (Schafer et al., 1994). PAX can also recruit other transcription factors to regulate the downstream gene.

PAX3 dysregulation is found in different human diseases. *PAX3* germline mutations are reported in Waardenburg syndrome, and most of these mutations are localized to exons 2 through 6, which affect the DNA binding domain of PAX3 (Hoth et al., 1993; Pingault et al., 2010). High expression of wild-type PAX3 has also been reported in cancer. Tumors related to neural tube-derived lineages are detected with high PAX3 expressions, such as melanoma, neurofibroma, and Ewing's sarcoma (Schulte et al., 1997; Gershon et al., 2005; He et al., 2010). Tumors associated with deregulation of myogenic differentiation like Embryonal rhabdomyosarcoma also detected a high level of PAX3 expression (Frascella et al., 1998).

1.3.1.2.2 FOXO1

The forkhead box O (FOXO1) family includes four members: FOXO1, FOXO3, FOXO4, and FOXO6, and they are characterized by a conserved DNA-binding domain (forkhead domain). FOXO1 is the first identified member of the FOXO subfamily. It consists of four domains: the highly conserved forkhead DNA-binding domain, a nuclear localization signal (NLS), a nuclear export sequence (NES), and a C-terminal transactivation domain. As a downstream target of AKT, FOXO1 is involved in the control of cell cycle, apoptosis, metabolism, and adipocyte differentiation (Dowell et al., 2003; Battiprolu et al., 2012; Song et al. 2015). FOXO1 can upregulate the negative regulators of the cell cycle, such as p21, and p27, to arrest cells in G0/G1 phase, and this is also responsible for the regulation of adipocyte differentiation (Huang and Tindall, 2007; Adachi et al., 2007; Nakea et al., 2003).

The regulation of FOXOs is primarily through phosphorylation, and its transcriptional activity is dependent on its phosphorylation state (Rena et al., 1999; Guo et al., 1999). In its un-phosphorylated state, FOXO is localized to the nucleus. The nuclear localization of FOXO proteins indicates transcriptional activity (Lin et al., 2001). Posttranslational modifications are triggered under different types of environmental stresses to lead to the nuclear translocation of FOXO proteins (Eijkelenboom and Burgering, 2013). FOXO transcription factors are normally inactivated by sequestration into the cytoplasm under homeostatic conditions. FOXO transcriptional targets are mainly involved in the regulation of the cell cycle, apoptosis, oxidative stress resistance, and metabolism in response to environmental changes to maintain homeostasis (van der Horst and Burgering, 2007; Eijkelenboom and Burgering, 2013).

FOXO1 plays an important role in tumorigenesis through the regulation of apoptosis. Without a growth factor, the FOXO1 phosphorylation pathway phosphatidylinositol 3-kinase (PI3K)-AKT is inactivated. The dephosphorylated FOXO1 in the nucleus triggers apoptosis (Brunet et al., 2004). Tumor suppressor PTEN (phosphatase and tensin homolog) functions as an antagonist of the PI3K-AKT pathway. When *PTEN* is mutated in tumor cells, FOXO1 is constitutively phosphorylated and apoptosis is inhibited (Nakamura et al., 2000). In contrast, a constitutively active of FOXO1 relocates in the nucleus and restores its transcriptional activation to induce apoptosis (Nakamura et al., 2000; Brunet et al., 2004). Furthermore, *FOXO1* is found in human cancers at chromosomal translocations, indicating an important role in the tumor development of FOXO1 protein.

1.3.1.2.3 Protein structure of PAX3-FOXO1

PAX3-FOXO1 results from the stable reciprocal translocation of chromosomes 2 and 13, which fuses the DNA binding domain of PAX3 with the transactivation domain of FOXO1 (Shapiro et al., 1993, Galili et al., 1993) (Figure 1.4). The breakpoint separates most of the PAX3 transactivation domain and disrupt the forkhead DNA binding domain. Therefore, the potent transactivation domain of FOXO1 in the fusion protein results in increased activity at both functional and expression levels comparing to the wild type PAX3 and FOXO1. It is possible that the the N-terminus of PAX3 is insensitive to inhibit the FOXO1 activation domain (Chalepakis et al., 1994; Fredericks et al., 1995; Bennicelli et al., 1995; Bennicelli et al., 1999). This is also supported by previous studies showing that the PAX3-FOXO1 fusion protein is a stronger activator of genes with PAX3 binding

sites (Bennicelli et al., 1995; Fredericks et al., 1995; Bennichelli et al., 1996). Therefore, in aRMS, the resulting fusion protein of PAX3 and FOXO1 acts as novel transcription factor with altered transcriptional functions, inducing aberrant expression of genes containing the PAX3 DNA binding site (Linardic et al., 2009).

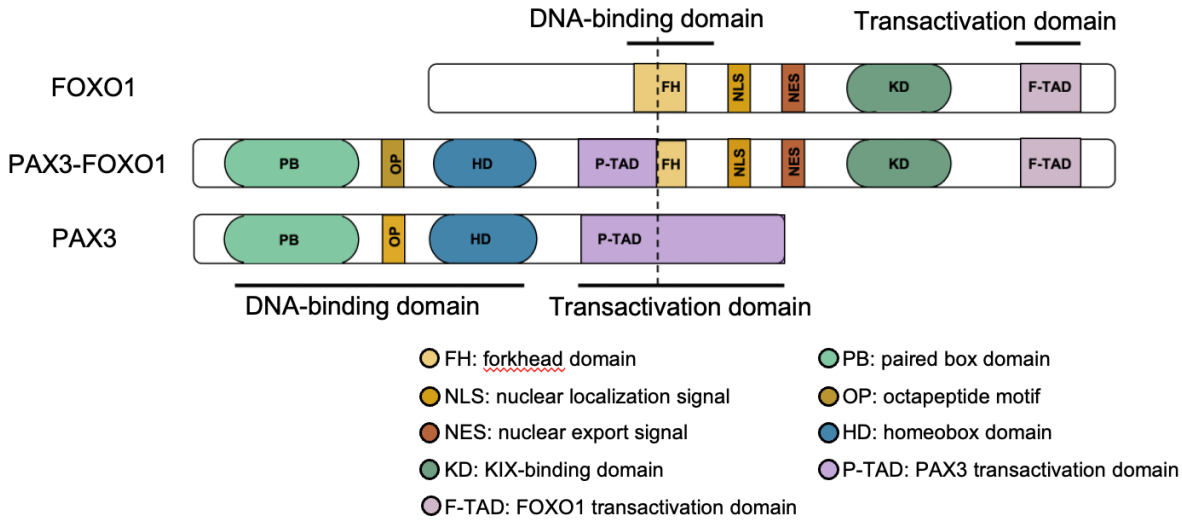

Figure 1.4. Schematic model of protein domain structures of the wild-type PAX3, FOXO1, and PAX3-FOXO1 fusion protein.

1.3.1.2.4 Contribution to tumorigenesis of PAX3-FOXO1

PAX3-FOXO1 contributes to tumorigenesis through multiple paths. The ectopic expression of PAX3-FOXO1 in fusion-negative embryonal rhabdomyosarcoma (eRMS) tumor cells resulted in an increased proliferation (Anderson et al., 2001). *PAX3-FOXO1* containing aRMS having increased cell proliferation is also supported by the increased expression of an immunohistochemical marker of proliferation (MIB1) in *PAX3-FOXO1*-containing tumors (Collins et al., 2001). siRNA knockdown of PAX3-FOXO1 in human aRMS cells shows the accumulation of cells in the G1 phase, inhibition of proliferation, and reduction of cell motility (Kikuchi et al., 2008). In mouse C2C12 myoblasts, PAX3-

FOXO1 can induce cell cycling and promote proliferation while blocking myogenesis (Wang et al., 1998). Also, PAX3-FOXO1 induced the angiogenic cytokine VEGF and stabilized its high expression level (Wang et al., 1998).

PAX3-FOXO1 may contribute to the phenotype of aRMS by preventing terminal differentiation. The study in mouse C2C12 myoblasts showed that PAX3-FOXO1 inhibited differentiation (Wang et al., 1998). This may be due to the property of wild-type PAX3, since PAX3 can inhibit myogenic differentiation of C2C12 myoblasts which is induced by the condition of low serum, and the inhibition can be abolished by PAX3 DNA binding domain mutation (Epstein et al., 1995). The inhibition of differentiation is confirmed in transgenic mice expressing PAX3-FOXO1 in a later study. The myoblasts were unable to complete myogenic differentiation might be due to the repression of the key cell cycle and differentiation regulator CDKN1C (cyclin dependent kinase inhibitor 1C) by PAX3-FOXO1 (Roeb et al., 2007).

1.3.1.2.5 Pioneer factor activity of PAX3-FOXO1

Chromatin is compacted by linker histone H1 to block the access of transcription factors to their target DNA sequence. Pioneer factors are a subset of transcription factors that bind directly to condensed chromatin to affect transcription. They are important in recruiting other transcription factors and histone modifying enzymes to the open chromatin. The forkhead family proteins contain a conserved winged-helix DNA-binding domain that mimics the structural features of histone H1 to disrupt H1-compacted chromatin (Cirillo et al., 2002). As a member of the forkhead family proteins, FOXO1 also

contains the conserved winged-helix DNA-binding domain to bind to and de-condense linker histone H1-compacted chromatin (Hatta and Cirillo, 2007).

Among the identified pioneer factors, PAX7 functions to remodel chromatin to allow the binding of other factors for gene activation (Budry et al., 2012). Introduction of mutation impairing either the paired or homeodomain impaired this activity, indicating both domains are required for PAX7 pioneer factor function (Pelletier et al., 2021). As a paralog of PAX7, PAX3 might also have the pioneer factor function since PAX3 shows chromatin binding behavior which is the ability to bind mitotic chromosomes (Wu et al., 2015). The evidence that suggests PAX3-FOXO1 might have pioneer factor activity includes that fusion protein PAX3-FOXO1 contains the PAX3 paired domain and homeobox domain and part of the FOXO1 DNA-binding domain, and PAX3-FOXO1 is shown to bind to compact chromatin (Sunkel et al., 2021). However, whether the binding to compact chromatin could affect transcription or not still need to be further investigated.

1.3.1.2.6 PAX3-FOXO1 transcriptional targets

Because PAX3-FOXO1 is specific for aRMS and inhibition of fusion transcription factors is challenging, the development of new drugs has focused on the transcriptional targets of PAX3-FOXO1. Antibody-based PAX3-FOXO1 chromatin immunoprecipitation and DNA sequencing (ChIP-seq), and ChIP-seq of active and repressive histone marks identified more than one thousand potential PAX3-FOXO1 regulatory sites (Cao et al., 2010; Gryder et al., 2017). These assays show that PAX3-FOXO1 predominantly binds sites within either promoters or distal enhancers of the putative target genes (Cao et al., 2010; Gryder et al., 2017; Sunkel et al., 2021). For example, apoptotic gene *TFAP2B*

(transcription factor AP-2 bata) (Ebauer et al., 2007), and histone demethylase gene *JARID2* (Jumonji and AT-rich interaction domain containing 2) (Walters et al., 2014), are reported as direct targets of PAX3-FOXO1 through binding to the promoter of these genes. Since more than 99% of PAX3-FOXO1 sites are more than 2.5 kb distal from the nearest transcriptional start site, RMS hallmark genes *IGF2* (insulin like growth factor 2)*, MYC, ALK* (anaplastic lymphoma kinase)*, MET* (MET proto-oncogene)*,* FGFR4 (fibroblast growth factor receptor 4)*, MYOD1* (myoblast determination protein 1)*, MYOG* (myogenin) are reported as targets of PAX3-FOXO1 through binding to the super-enhancer of these genes (Cao et al., 2010, Gryder et al., 2017; Marshall et al., 2012, Souza et al., 2012).

However, the majority of current studies have been done through gene expression profiling after knock-in, exogenous expression of PAX3-FOXO1, or shRNA knockdown of the endogenous *PAX3-FOXO1*. While knockdown or re-expression studies coupled with RNA-seq analysis can identify genes with an altered expression such as *PPP2R1A* (Akaike et al., 2018) and *HES3* (Kendall et al., 2018), some of these changes could be indirect or compensatory transcriptional changes resulting from chronic transcription factor loss or re-expression.

Despite the lack of understanding of PAX3-FOXO1 contribution to tumorigenesis, PAX3-FOXO1 in aRMS is associated with a worse outcome for the patient. The interfering techniques to inhibit PAX3-FOXO1 not only influenced PAX3-FOXO1, but also the endogenous PAX3, which makes the results hard to interpret. Moreover, the cell origin of RMS is still unknown, as well as the difference between eRMS and aRSM. Therefore, to address the detailed transcriptional mechanism of PAX3-FOXO1 to provide insight into the cellular aspect of tumorigenesis and for the clinical significance aspect of therapy

development, a comprehensive investigation of PAX3-FOXO1 in aRMS still needs to be continued.

1.4 Scope of the dissertation

Given the critical role of oncogenic transcription factor fusion in cancer development, these transcription factors and their regulatory targets are being developed to define new therapeutic agents. In my dissertation work, I focused on two main questions. First, in Chapter 3, I focused on investigating the action of BETi in t(8;21) AML cells. The data of this part has been published in *J Cell Biochem* (Zhang et al., 2018). Chapter 4 focused on the mechanism of PAX3-FOXO1 transcriptional control in aRMS. The data of this part is currently under revision by *Molecular Cell*. Chapter 5 provide an overview of the conclusions and future directions.

CHAPTER 2

Methods and materials

Materials Availability

All the materials generated in this study are accessible upon request.

Data Availability

All genomic datasets are available at GEO accession GSE153281. The reviewer token is yhkfqqgghvstxil**.**

Cell lines

The cell lines were obtained from ATCC. Rh30 cells were cultured in RPMI-1640 (Corning by Mediatech, Inc.) containing 10% FetalPlex (Corning by Mediatech, Inc.) and supplemented with 1% L-Glutamine (Corning by Mediatech, Inc.) and 1% penicillin/streptomycin (Corning by Mediatech, Inc.). Rh4 cells were cultured in RPMI-1640 (Corning by Mediatech, Inc.) containing 10% FBS (Corning by Mediatech, Inc.) and supplemented with 1% L-Glutamine (Corning by Mediatech, Inc.) and 1% penicillin/streptomycin (Corning by Mediatech, Inc.). Kasumi-1 cells were cultured in RPMI-1640 (Corning by Mediatech, Inc.) containing 15% FBS (Corning by Mediatech, Inc.) and supplemented with 1% L-Glutamine (Corning by Mediatech, Inc.) and 1% penicillin/streptomycin (Corning by Mediatech, Inc.). *Drosophila* S2 cells (Schneider media supplemented with 10% FBS, 1% penicillin and streptomycin) were a gift from Dr. Emily Hodges.

dTAG-47

dTAG-47 was synthesized by the Vanderbilt University Medical Center (VUMC) Molecular Design and Synthesis Center (VICB, kk-25-065) as described (Nabet et al., 2018), and reconstituted in DMSO (Sigma).

Generation of endogenous PAX3-FOXO1-tagged Rh30 and Rh4 cell lines

The endogenous allele of PAX3-FOXO1 in Rh30 and Rh4 cells was engineered to express C-terminal FKBP12^{F36V}-2xHA, APEX2-2xHA, or 3X-FLAG tags using homology-directed DNA repair (Layden et al., 2021). 180 bp upstream of the stop codon and 500 bp after the *FOXO1* top codon were cloned into pUC19 containing FKBP12^{F36V}-2xHA-P2A-mCherry derived from Addgene #104370 (pAW62(Weintraub et al., 2017)) using the Gibson Assembly Cloning Kit (NEB #E5510S). The APEX2 sequence (Addgene #97421) or a 3xFLAG tag was cloned into the HDR donor plasmids to create the *FOXO1-APEX2* and *FOXO1-3xFLAG* plasmids respectively. Cas9, gRNA and the HDR template plasmid were delivered into Rh30 cells by electroporation. mCherry positive cells were sorted and single cell cloning was performed to generate PAX3-FOXO1-tagged and FOXO1-tagged clones.

Primers used to construct template plasmid are listed below:

Primers to generate 5’ homology gene block:

F:GCCAAGTGGGTTGATGTCTGGTTTTTCCTTGAGAGAAGCTCCCAAGTGACTTGG
ATGGCATGTTC

R:GGGGAGATGGTTTCCACCTGCACTCCTCCGGATCCGCCTGACACCCAGCTATGT
GTCGTTGTCTTG

Primers to generate 3’homology gene block:

Cherry-F:

ACTCCACCGGCGGCATGGACGAGCTGTACAAGTAAGGGTTAGTGAGCAGGTAAGT

TCACCCCAAT

BFP-F:

ACCTCCCTAGCAAACTGGGGCACAAGCTTAATTAAGGGTTAGTGAGCAGGTAAGTT

CACCCCAAT

R:CGGCCAGTGAATTCGAGCTCGGTACCCGGGGATCCCCAAGAAAACTAAAAGGG

AGTTGGTGAAAG

5’Gibson Cloning Primers:

F:CAAGACAACGACACATAGCTGGGTGTCAGGCGGATCCGGAGGAGTGCAGGTGG

AAACCATCTCCCC

R:GAACATGCCATCCAAGTCACTTGGGAGCTTCTCTCAAGGAAAAACCAGACATCA

ACCCACTTGGC

3’Gibson Cloning Primers:

Forward:

CTTTCACCAACTCCCTTTTAGTTTTCTTGGGGATCCCCGGGTACCGAGCTCGAATT

CACTGGCCG

Cherry-R:

ATTGGGGTGAACTTACCTGCTCACTAACCCTTACTTGTACAGCTCGTCCATGCCGC

CGGTGGAGT

BFP-R:

ATTGGGGTGAACTTACCTGCTCACTAACCCTTAATTAAGCTTGTGCCCCAGTTTGCT

AGGGAGGT

FOXO1 crRNA: 5’-CAGGCTGAGGGTTAGTGAGC

Guide RNAs and primers used for enhancer knockdown is listed below:

KLF4 PAX3-FOXO1-regulated enhancer:

singe guide RNA_1: gcatttgggaaaaggtgagg

singe guide RNA_2: cttaagtaaaggaaagaact

genome PCR primer_F: agctgggttcagctttcact

genome PCR primer_R: tggaaactcagccaagaattg

KLF4 non-PAX3-FOXO1-regulated enhancer:

singe guide RNA_1: CTCTGCAGTTGGGCACACCC

singe guide RNA_2: cacacagctactaaaactcg

genome PCR primer_F: TGAGATGCAGAGTCCCCATT

genome PCR primer_R: gatcttgcggatcagagagg

qPCR primer_F: CAAGCCAAAGAGGGGAAGAC

qPCR primer_R: CGTCCCAGTCACAGTGGTAA

RUNX2 PAX3-FOXO1-regulated enhancer:

singe guide RNA_1: cacc**G**CGGGCGGTGAGCTAACACAT

singe guide RNA_2: aaacATGTGTTAGCTCACCGCCCG**C**

singe guide RNA_3: cacc**G**CAGTTGGATGAGATCAAGCA

singe guide RNA_4: aaacTGCTTGATCTCATCCAACTG**C**

genome PCR primer_F: CGGGCGGTGAGCTAACACAT

genome PCR primer_R: CAGTTGGATGAGATCAAGCA

RUNX2 non-PAX3-FOXO1-regulated enhancer:

singe guide RNA_1: caccGGCAGCTGTAGCCCGCGGTT

singe guide RNA_2: aaacAACCGCGGGCTACAGCTGCC

singe guide RNA_3: caccGCTGATTCTGACGCCATCTG

singe guide RNA_4: aaacCAGATGGCGTCAGAATCAGC

genome PCR primer_F: GGCAGCTGTAGCCCGCGGTT

genome PCR primer_R: GCTGATTCTGACGCCATCT

qPCR primer_F: TGGTTACTGTCATGGCGGGTA

qPCR primer_R: TCTCAGATCGTTGAACCTTGCTA

ACTB qPCR primer_F: ACCTTCTACAATGAGCTGCG

ACTB qPCR primer_R: CCTGGATAGCAACGTACATGG

Western Blot

Cells were collected and lysed with RIPA buffer (50 mM Tris pH8.0, 150 mM NaCl, 1% NP-40, 0.5% sodium deoxycholate, 0.1% SDS) containing protease inhibitor. After sonication, lysates were cleared by centrifugation and subjected to SDS-PAGE and electrophoretic transfer to membranes before incubation with antibodies directed against HA (Abcam, ab18181), FLAG (Sigma, F1804), GAPDH (Santa Cruz, sc-365062), Lamin B (Santa Cruz, sc-6217). Signal was visualized with secondary IR-Dye conjugated antibodies (Licor) and detected using the Licor Odyssey imaging system.

Cell growth

Cells were seeded at a density of 2 x 10^5 cells/ml on day 0 in 6-well culture plates and treated with DMSO or 500 nM dTAG-47. The cells were reseeded every 3 days at 2 x 10^5 cells/ml and maintained in DMSO/dTAG-47 treatment for the duration of the assay. Viable cell were counted with Trypan Blue dye exclusion every day for 9 days consecutive.

Quantification was performed in triplicate and the values averaged and shown with standard deviations.

Cell cycle analysis

Cells were treated with DMSO or dTAG-47 for 3, 6, and 9 days. Before staining, cells in a 10-mm-dish at 80% confluence were pulsed with 20μM 5-bromo-2'-deoxyuridine (BrdU) for 2 hours and fixed overnight with 70% ethanol at 4°C. Cells were stained with fluorescein isothiocyanate (FITC)-conjugated anti-BrdU and counterstained with propidium iodide (PI) before analysis by flow cytometry. All flow cytometry figures were generated using FlowJo software.

Apoptosis assay

Cells were treated with DMSO or dTAG-47 for 1, 2, and 3 days. Cells were stained with FITC-AnnexinV/7-AAD Apoptosis detection kit (cat # 556547, BD Pharmingen). All flow cytometry figures were generated by FlowJo software.

Soft Agar colony formation assay

Cells were treated with DMSO or dTAG-47 for 3, 6, and 9 days, and then were plated in 0.3% agarose medium. Cells were fed with culture media with DMSO/dTAG-47 once per week. After 4 weeks, plates were stained with 0.005% Crystal Violet (Sigma), and colonies were counted using a dissecting microscope.

Oxygen consumption rate and extracellular acidification rate measurements.

Cells were seeded on Cell-Tak adhesive coated Seahorse XF96 Cell Culture Microplates to prepare adherent monolayer cultures. Seahorse XFe96 Extracellular flux analyzer (Agilent, Inc.) was utilized to determine the oxygen consumption rate (OCR) and extracellular acidification rate (ECAR) by measuring the concentration of oxygen

and free protons in the medium surrounding the monolayer of cells in real-time. The XF Cell Mito Stress Test Kit (Agilent, Inc.) was used to access the mitochondrial function after serially injecting oligomycin, FCCP and a mix of rotenone and antimycin A to measure ATP production, maximal respiration, and non-mitochondrial respiration, respectively. The XF Glycolysis Stress Test Kit (Agilent, Inc.) was used to access the glycolysis capacity after three sequential injections of glucose, oligomycin and 2-deoxy-glucose (2-DG).

Optical Metabolic Imaging.

Multi-photon fluorescence lifetime imaging was performed on a Nikon Ti:E inverted microscope equipped with time-correlated single photon counting electronics. NAD(P)H and FAD fluorescence were excited with a titanium:sapphire laser (Chameleon Ultra II, Coherent, Inc.) tuned to 750 nm and 890 nm, respectively. A 400–480 nm bandpass filter was used to isolate NAD(P)H fluorescence emission, and a 500 nm high pass dichroic mirror and 500–600 nm bandpass filter were used to isolate FAD fluorescence emission. Fluorescence signal was collected through a 40× oil-immersion objective across a 170 × 170 μm field of view, capturing approximately 40–60 cells. Four fields of view per sample were acquired, yielding 125–250 cells for each of three biological replicates. Images were processed with custom software previously described[34]. Briefly, the NAD(P)H and FAD intensities were calculated by integrating the fluorescence lifetime decay within each pixel. Then, the ratio of NAD(P)H intensity divided by FAD intensity (the optical redox ratio) was calculated at each pixel. Pixels within the cell cytoplasm were averaged and statistical differences were calculated on a per-cell level.

Immunofluorescence

Cells were seeded on coverslips and treated with DMSO or dTAG-47 for 3, 6, and 9 days. Cell were then fixed with 3.7% paraformaldehyde in PBS at room temperature for 15 minutes. The coverslips were then washed three times with phosphate buffered saline (PBS) and the cells were permeabilized using 0.3% Triton X-100 in PBS at room temperature for 30 minutes. In a humidified chamber, cells were blocked by adding 1% serum in PBS for 30 minutes, and then incubated with primary antibodies (Myogenin, Abcam, ab1835; Myosin Heavy Chain, R&D, MAB4470; HA, Cell Signaling, (C29F4) #3724) with appropriate dilution in 0.5% NP-40 and 1% serum in PBS at 37 °C for 1 hour. After washing 3 times with PBS, cells were incubated in Alexa Fluor secondary antibody (Abcam ab150117, Invitrogen A-11034) with Phalloidin (Thermo Fisher Scientific, A12380) and DAPI diluted in 0.5% NP-40, and 1% serum in PBS at 37 °C for 45 minutes. Coverslips were mounted on slides with Prolong Gold Antifade reagent (Thermo Fisher Scientific, P36930) and dried overnight in the dark. Images were collected using a Nikon fluorescent microscope.

Nuclei isolation

30 million Rh30 cells were treated with DMSO or dTAG-47 and collected at indicated time points. Cells were washed with ice cold PBS and lysed with cell lysis buffer (10mM Tris-Cl pH7.4, 300mM sucrose, 3mM $CaCl_2$, 2mM $MgCl_2$, 0.5% NP-40, 5mM DTT, 1mM PMSF, EDTA free protease cocktail inhibitor tablet) using dounce homogenization, nuclei were pelleted by centrifugation and washed with nuclei storage buffer (50mM Tris-Cl pH8.3, 40% glycerol, 5mM MgCl2, 5mM DTT, 0.1 mM EDTA, 1mM PMSF, EDTA free protease

cocktail inhibitor tablet). After counting, pelleted nuclei were resuspended in storage buffer, and stored at -80 °C.

Precision nuclear run-on and sequencing (PRO-seq)

PRO-seq was performed in biological replicates as previously described using approximately 20 million nuclei per run on with GTP, ATP, UTP, and biotin-11-CTP (PerkinElmer) using 0.5% Sarkosyl (Fisher Scientific) to prevent transcription initiation (Mahat et al., 2016; Zhao et al., 2016). RNA was reversed transcribed and amplified to make the cDNA library for sequencing by the Vanderbilt University Medical Center (VUMC) VANTAGE Genome Sciences Shared Resource on an Illumina Nextseq 500 (SR-75, 50 million reads). The sequences were aligned using bowtie2 (v2.2.2) before using the Nascent RNA Sequencing Analysis (NRSA) pipeline (Wang et al., 2018) to determine the gene body and eRNA changes.

RNA sequencing and data processing

All RNA-seq experiments were performed in biological duplicate. Total RNA was extracted using TRIzol. RNA was submitted to the VUMC VANTAGE core for library preparation and sequencing (Illumima NovaSeq, PE-150, 30 million reads). Adaptors were trimmed using Trimmomatic-0.32 and aligned to the human genome (hg19) using TopHat (v. 2.0.11) (Trapnell et al., 2012). Differential analysis was performed using CuffDiff (v. 2.1.1) (Trapnell et al., 2013).

Cleavage under targets and release using nuclease (CUT&RUN)

CUT&RUN experiments were performed in biological duplicate as described (Skene and Henikoff, 2017). Briefly, cells were treated with DMSO or dTAG-47 for the indicated times and 250,000 cells were collected and incubated with Concanavalin A-coated beads

(Bangs Laboratories, BP531) for 10 minutes at room temperature, and i with 0.01% freshly dissolved digitonin. Anti-HA (Cell Signaling, (C29F4) #3724), anti-BRD4 (BETHYL, #A301-985A50), anti-H3K4me3 (Abcam, ab12209), anti-MYOD (Santa Cruz, sc-377460), anti-RUNX1 (Santa Cruz, sc-365644), anti-HEB (Santa Cruz, sc-357), anti-ARID1A (Cell Signaling, (D2A8U) #12354), anti-SPT16 (Cell Signaling, D7I2K #12191), anti-CDK8 (Santa Cruz, sc-13155), and anti-PAX3 (Abcam, ab69856) primary antibodies were added and incubated at 4 °C overnight, before washing and binding of secondary antibody (anti-Rabbit, #ab31238, anti-Mouse, #ab46540) for 1hr. After washing, CUTANA pAG-MNase (EpiCypher, #15-1116) fusion protein was added and incubated at 0 °C for 60-90 mins to digest targeted regions of the genome. DNA was then extracted using phenol-chloroform(Skene and Henikoff, 2017) and sequencing libraries were generated using the NEBNext Ultra II DNA Library Prep Kit for Illumina (NEB #E7645S/L). Sequencing was performed by the VUMC VANTAGE core Illumina NovaSeq (PE-150, 10 million reads).

Chromatin Immunoprecipitation Sequencing (ChIP-seq)

Cells were treated with dTAG-47 for 0, 2, 4, and 24 hours. Five million cells were used to perform anti-H3K27ac ChIP-seq with *Drosophila* S2 cell spike-in. Cells were cross-linked with 1% formaldehyde for 8 minutes and quenched with 125mM Glycine. Following nuclei isolation, chromatin fragments within 300~600 bp range were generated by sonication for 25 cycles (30s-on, 30s-off) for 25 cycles with a Biorupter (Diagenode). Chromatin fragments were immunoprecipitated with anti-H3K27ac (Abcam, #ab4729) plus Protein A beads. NEBNext Ultra II DNA Library Prep Kit for Illumina was used to make the DNA

libraries (NEB, #E7645S/L), which were sequenced on the Illumina NovaSeq (PE-150, 30 million reads) at the VUMC VANTAGE Shared Resource.

CUT&RUN and ChIP-seq data analysis

Raw FASTQ data were trimmed using Trimmomatic (v0.32) and paired end reads were aligned to a concatenated human and *E.coli* genome (hg19 and ecK12MG1655) for CUT&RUN, or *Drosophila* genome (hg19 and dm3) genome for ChIP-seq using Bowtie2 in very sensitive local mode (--local --very-sensitive-local --no-unal --no-mixed --no-discordant --phred33 -I 10 -X 700) (Langmead and Salzberg, 2012). Peaks were called using MACS2 with a threshold of $q<0.01$. Peaks were annotated to the nearest TSS using HOMER. Differential analysis was performed using DiffBind and DESeq2. Significantly changed peaks were defined by a 1.5-fold change threshold and FDR<0.05. BigWig files were generated and normalized with the DESeq2 size factors using Deeptools. Heatmaps were created by Deeptools using the DESeq2 size factor normalized bigwig files.

Assay for Transposase Accessible Chromatin using sequencing (ATAC-seq)

ATAC-seq was performed in biological duplicate using the ATAC-Seq Kit (Active Motif, catalog No.53150) (Buenrostro et al., 2015). Briefly, 100,000 Rh30 cells and 2,000 *Drosophila* S2 cells were used to isolate nuclei. Nuclei were incubated with tagmentation Master Mix at 37 °C for 30 minutes after lysing the cells in ice-cold ATAC Lysis Buffer and the DNA was purified with the DNA purification column. PCR amplification of tagmented DNA was performed to make libraries with the appropriate indexed primers. After SPRI bead clean-up, the DNA libraries were sequenced on the Illumina NovaSeq (PE-150, 50 million reads) at the VUMC VANTAGE core.

ATAC-seq data analysis

Raw FASTQ data were trimmed by Trimmomatic (v0.32), and paired end reads were aligned to a concatenated human and *Drosophila* genome (hg19 and dm3) using Bowtie2 (-X 2000 -q --no-mixed --no-discordant). Peaks were called using Genrich (v. 0.6.1) (https://github.com/jsh58/Genrich) with the following options -j -y -r -e chrM -q 0.01 -a 20. Peaks were annotated to the nearest TSS using HOMER. Differential analysis was performed using DiffBind and DESeq2. Significantly changed peaks were defined by a 1.5-fold change threshold and FDR<0.05. BigWig files were generated and normalized using the DESeq2 size factors using Deeptools. Heatmaps were created by Deeptools using the DESeq2 size factor normalized bigwig files.

APEX2 in-cell biotinylation

APEX2 in-cell biotinylation was performed as described (Hung et al., 2017). Briefly, 100 million cells were incubated with 500 μm biotin phenol (Iris, LS-3500, dissolved in DMSO) at 37 °C for 1 hour. Hydrogen peroxide (H_2O_2) was added for 1 minute. After quenching, nuclei were isolated, lysed, and nuclear protein was harvested in RIPA buffer. Protein concentration was determined using DC Protein Assay (BioRad). Biotinylated proteins were purified with streptavidin beads (Thermo Fisher Scientific, #88817) and eluted by boiling in Laemmli sample buffer. Parental Rh30 cells were used as negative control to determine proteins specifically identified in Rh30-PAX3-FOXO1-APEX2 samples. Proteins from parental Rh30 cells and Rh30-PAX3-FOXO1-APEX2 cells were analyzed as biological triplicates that were processed independently.

FLAG affinity purification

Nuclei were isolated from 100 million cells per sample. The nuclei were then “extracted” by incubating with Pierce Universal Nuclease (Thermo Fisher Scientific, #88701) in co-IP

buffer (20 mM Tris pH 8, 150 mM NaCl, 2 mM $MgCl_2$, 0.1% NP-40, with protease inhibitors) on ice for 1 hour. Cleared lysates were passed over a 0.45 um cellulose acetate column (Corning) to remove any remaining particulates. Samples were incubated with 60 µl of equilibrated EZ Red Flag M2 bead slurry (EZview by Millipore Sigma, F2426) at 4°C for 2hr in co-IP buffer, after washing, purified proteins were eluted twice with 50 ul of 1 mg/ml 3X flag peptide (Sigma) in co-IP buffer on the nutator for 10 minutes at room temperature.

Mass Spectrometry

Eluents from Apex or FLAG purifications were prepared for analysis via S-trap trypsin digests using manufacturer's protocol (S-Trap™ – ProtiFi). The peptides were separated on a self-packed 100 µm x 20 cm reversed phase (Phenomonex - Jupiter 3 micron, 300A) column from which peptides were ionized directly via nano-electrospray into an Exploris 480 (Thermo-Fisher) mass spectrometer. Both full-scan and peptide fragmentation (MS/MS) were collected over the course of a 70-minute aqueous to organic gradient elution in a data-dependent manner using dynamic exclusion to reduce redundancy of peptide acquisition. Resulting MS/MS spectra were searched using SEQUEST (Eng et al., 1994) against a human database containing common contaminants and reversed copies of each entry. Resulting identifications were filtered to a 5% false-discovery threshold, collated back to the protein level, and compared across samples using Scaffold (Proteome Software). Filtered total spectral count values were used for fold-change comparisons and p-value estimations.

CHAPTER 3

Mechanism of action of BETi in t(8;21) AML

3.1 Background

Inhibitors of the bromodomain and extra-terminal domain family (BETi) offer a new approach of treating hematological malignancies. Intriguingly, in these early studies, the t(8;21) cell line Kasumi-1 showed the most pronounced sensitivity (Zuber et al., 2011). By using precision nuclear run-on sequencing (PRO-seq), we previously identified many of the earliest targets of BET inhibitor action and demonstrated that these compounds cause transcriptional pausing of drivers of the cell cycle and metabolic activity, and affect eRNA synthesis in the *MYC* super-enhancer (Zhao et al., 2016). Here, we extended our study by showing that t(8;21) AML are not only very sensitive to BETi, but rather than induce cell death, treatment with JQ1 or MS417 dramatically reduced cell size and induced cell cycle arrest. Cell cycle analyses and assessment of mitochondrial function and glycolysis indicated that the BETi-induced cell cycle arrest was reversible. However, the metabolic stress and impaired transcription of *BCL2* after JQ1 treatment provides further molecular rationale for combination therapy using BETi and venetoclax.

3.2 Results

3.2.1 BET inhibitors affect Kasumi-1 cell proliferation without inducing apoptosis.

High throughput screens of cancer cell lines identified the t(8;21) cell line Kasumi-1 as the most sensitive cell type to the BET inhibitor (BETi) JQ1 using alamarBlue assays

as a surrogate for cell proliferation (Zhao et al., 2016). Consistent with these previous studies, we found that Kasumi-1 cells, as well as the t(8;21)-containing SKNO-1 cell line that requires GM-CSF for growth (Matozaki et al., 1995), were more sensitive than MOLM13, and MV4-11 that contain MLL disruptions (Fig. 3.1A) when using alamarBlue assays. However, alamarBlue measures metabolic output, rather than cell death. When we tested for cell death using JQ1 and another potent BET inhibitor, MS417 (Zhang et al., 2012), which shares molecular and transcription targets with JQ1 (Zhao et al., 2016), both JQ1 and MS417 only had minor effects on triggering apoptosis in Kasumi-1 cells, whereas SKNO-1 showed more cell death at 48 hr (Fig. 3.1B). In addition, while MOLM13 and MV4-11 cells required more BETi to show an effect in Alamar blue assays, MOLM13 cells showed very little apoptosis, while BETi more robustly induced apoptosis in MV4-11 (Fig. 3.1B). Consistent with these observations and in contrast to the Alamar blue data, when we manually counted viable cells using Trypan Blue dye exclusion, JQ1 and MS417 had a cytostatic rather than cytotoxic effect on cell growth in Kasumi-1 cells but reduced the number of viable cells in cultures of MV4-11 cells (Fig. 3.1C).

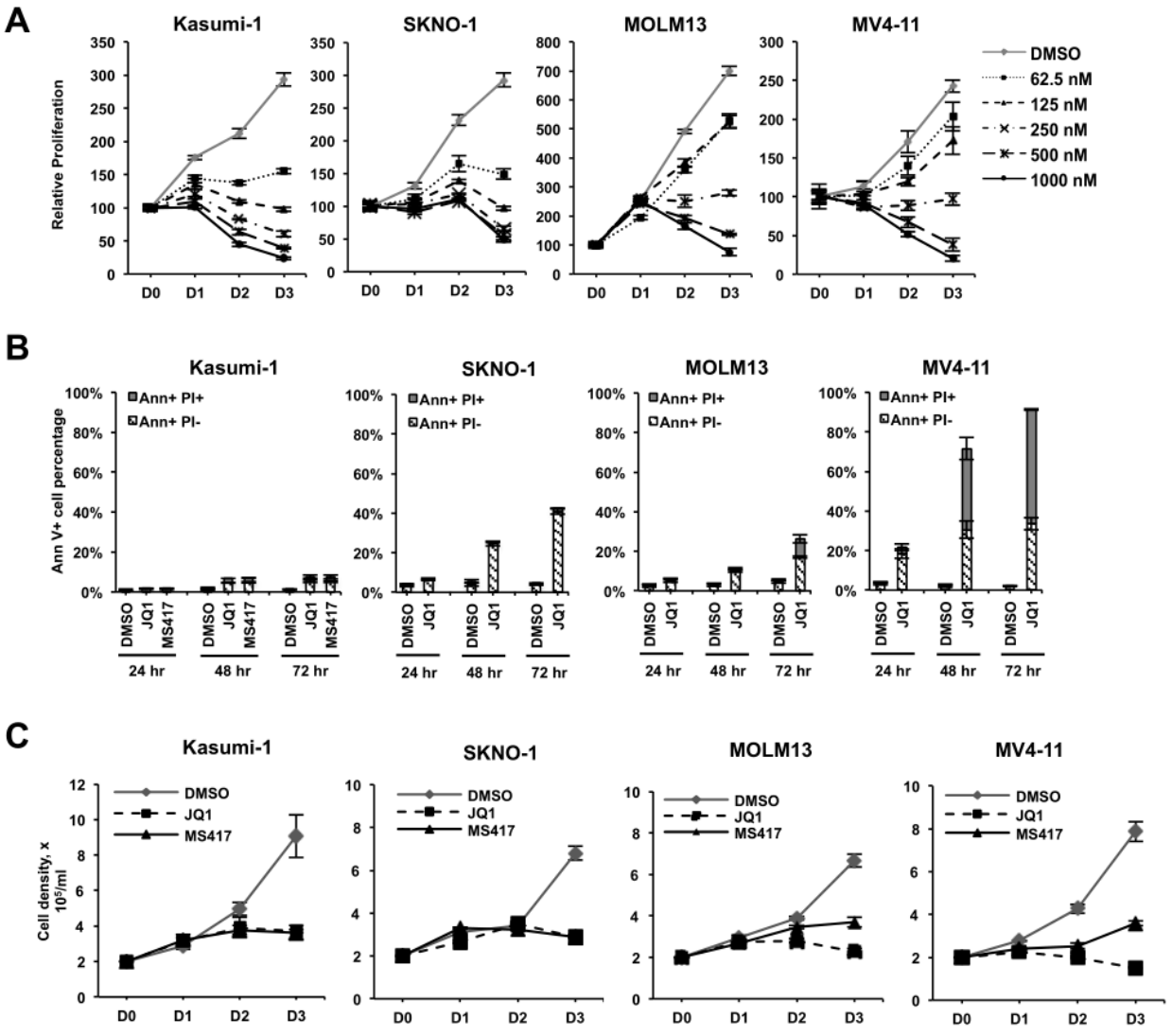

Figure 3.1. BETi inhibit proliferation, but induce variable levels of cell death in AML cell lines. (A) AlamarBlue assays show a dose-dependent loss of cellular metabolism after JQ1 treatment of Kasumi-1, SKNO-1, MOLM13, and MV4–11 cells for 3 days (D0-D3). Data are mean ± SEM (n=3). (B) BETi induce variable levels of apoptosis. Kasumi-1 cells were treated with 250 nM JQ1 or 125 nM MS417. SKNO-1 were treated with 250 nM JQ1. MOLM13 and MV4–11 were treated with 500 nM JQ1. The levels of dying cells were quantified using Annexin V positivity (Ann+) and uptake of propidium iodide (PI). Data are mean ± SEM (n=4). (C) SKNO and Kasumi-1 cells were treated with 250 nM JQ1 or 125 nM MS417, whereas MOLM13 and MV4–11 were treated with twice these levels. Cell counts were determined by Trypan Blue dye exclusion. Data are mean ± SEM (n=4).

BETi disrupts the communication between enhancers and RNA polymerases that are paused just after transcriptional initiation. Inhibitors of pTEFb (that is, CDK9 inhibitors), such as flavopiridol, also block RNA polymerase elongation and cause DNA damage. However, we did not detect any phosphorylated H2AX in the nuclei of JQ1 or MS417 treated cells (Fig. 3.2). This indicated that BETi inhibited cell proliferation without DNA double-strand breaks and without causing apoptosis in Kasumi-1 cells. Moreover, these compounds did not trigger a DNA damage-dependent cell cycle arrest or apoptosis of Kasumi-1 cells. These results raised the possibility that BETi directly or indirectly affected the metabolic rate as measured by alamarBlue.

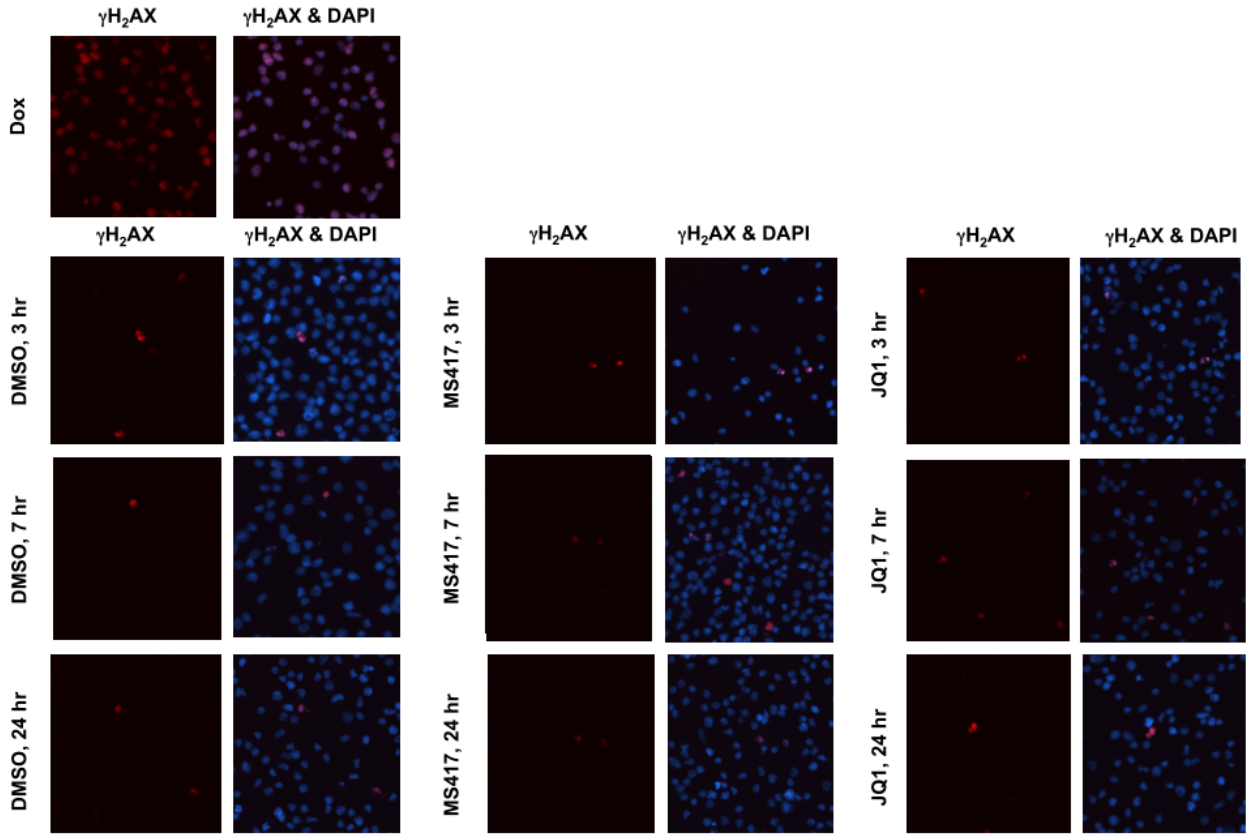

Figure 3.2. DNA damage analysis of BETi-treated Kasumi-1 cells. Immunofluorescence to detect phosphorylated H2AX. Upper panels, cells treated with 2 mg/ml doxorubicin (Dox) for 18 hr as a positive control. Nuclei were counterstained with DAPI for visualization.

3.2.2 BET inhibitors reduce cell size

We extended this analysis by using propidium iodide (PI) staining of DNA, which showed that Kasumi-1 cells treated with JQ1 and MS417 rapidly accumulated in the G_0/G_1 phase of the cell cycle (Fig. 3.3A). Interestingly, we noted that treatment with BETi led to dramatic reductions in cell size in Kasumi-1 and SKNO-1cells within 24 hr of treatment with JQ1, as assessed by diminished forward scatter in flow cytometry analysis (Fig. 3.3B). JQ1 also reduced cell size in MOLM13 cells but the response was delayed (Fig. 3.3B) relative to Kasumi-1 cells. While there were no apparent morphological changes toward myeloid differentiation, Wright-Giemsa staining confirmed the smaller cell size and condensed nuclei of Kasumi-1 cells (Fig. 3.4).

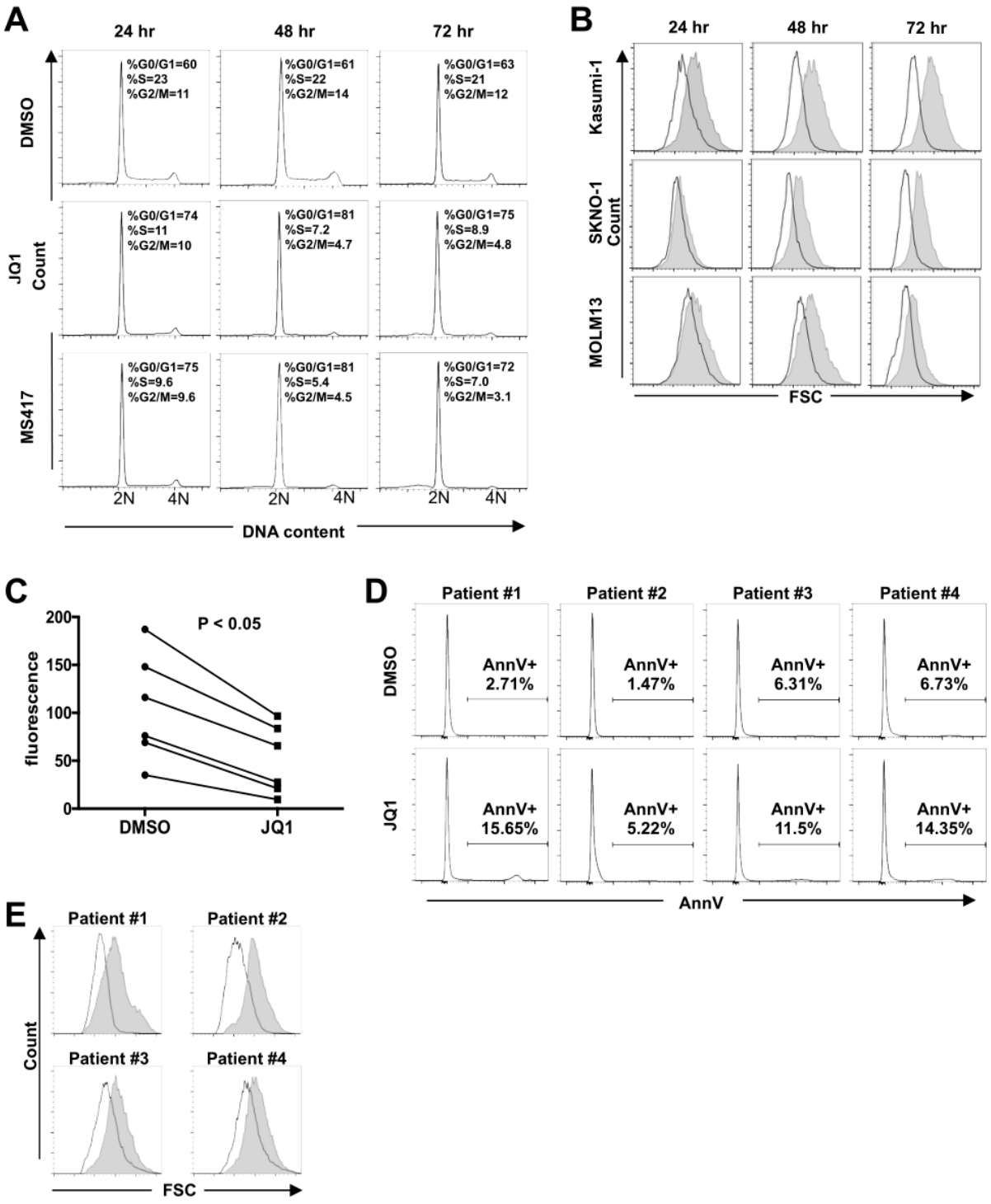

Figure 3.3. BETi induce cell cycle arrest and reduce cell size in t(8;21) AML cells. (A) Cell cycle analyses of Kasumi-1 cells treated with BETi show cell cycle arrest with modest cell death 24–72 hr after treatment. Representative graphs of DNA content (2N to 4N) are shown (n=4). (B) Flow cytometry analyses showing forward scatter plots indicate that t(8;21) cells are distinctly smaller after treatment with 250 nM JQ1.

Representative graphs are shown (n=4). Shaded area represents DMSO and white plots represent JQ1. (C and D) High blast count t(8;21) AML patient samples (n=6) were treated with 250 nM JQ1 for 3 days. AlamarBlue assays show the inhibition of cell growth $p < 0.05$ by two-sided Wilcoxon signed-rank test (C). (D) Shows the lack of Annexin V positive cells for four of the samples in C. (E) Forward scatter plots of flow cytometry analyses show that t(8;21) AML patient cells are distinctly smaller after JQ1 treatment for 3 days. Representative flow cytometry plots are shown. Shaded area represents DMSO and empty area represents JQ1.

Given the apparent sensitivity of t(8;21) cell lines, we extended this analysis to primary AML samples containing this translocation. Again, JQ1 inhibited cell growth as measured by alamarBlue staining without inducing high amounts of Annexin V, and these primary AML cells also showed a reduction in cell size (Fig. 3.3C-E).

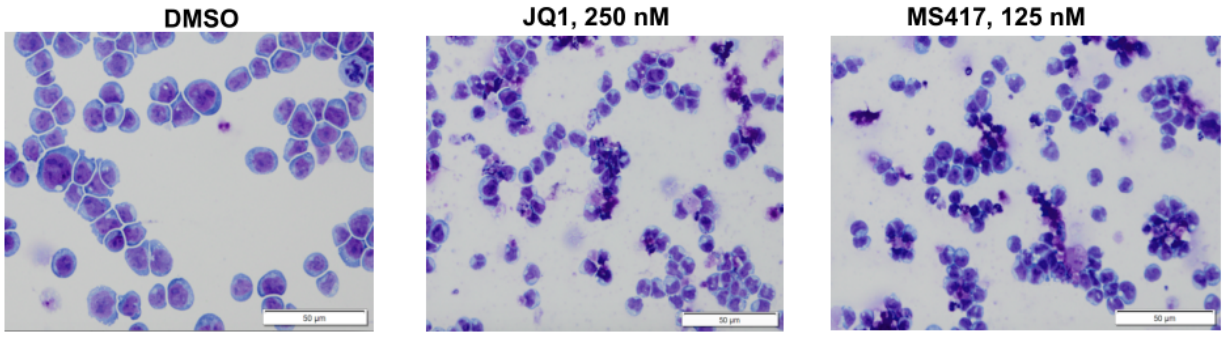

Figure 3.4. BETi cause Kasumi-1 cells to shrink. Kasumi-1 cells were treated with DMSO, JQ1 or MS417 for 3 days. Wright staining shows the smaller cell size upon BETi. (X200)

We further extended these observations to other leukemia/lymphoma cell lines, including Raji, K562, and MOLT4. JQ1 treatment reduced cell size in all cell lines tested (Fig. 3.5A and D). This reduction in cell size was associated with a robust cell cycle arrest in all cell lines while the annexin V positive population was not greatly increased (Fig. 3.5B-C) in the first 48 hr. Taken together, our data suggested that BET proteins are required for maintaining cell metabolism and cell size if the cells do not undergo rapid cell death.

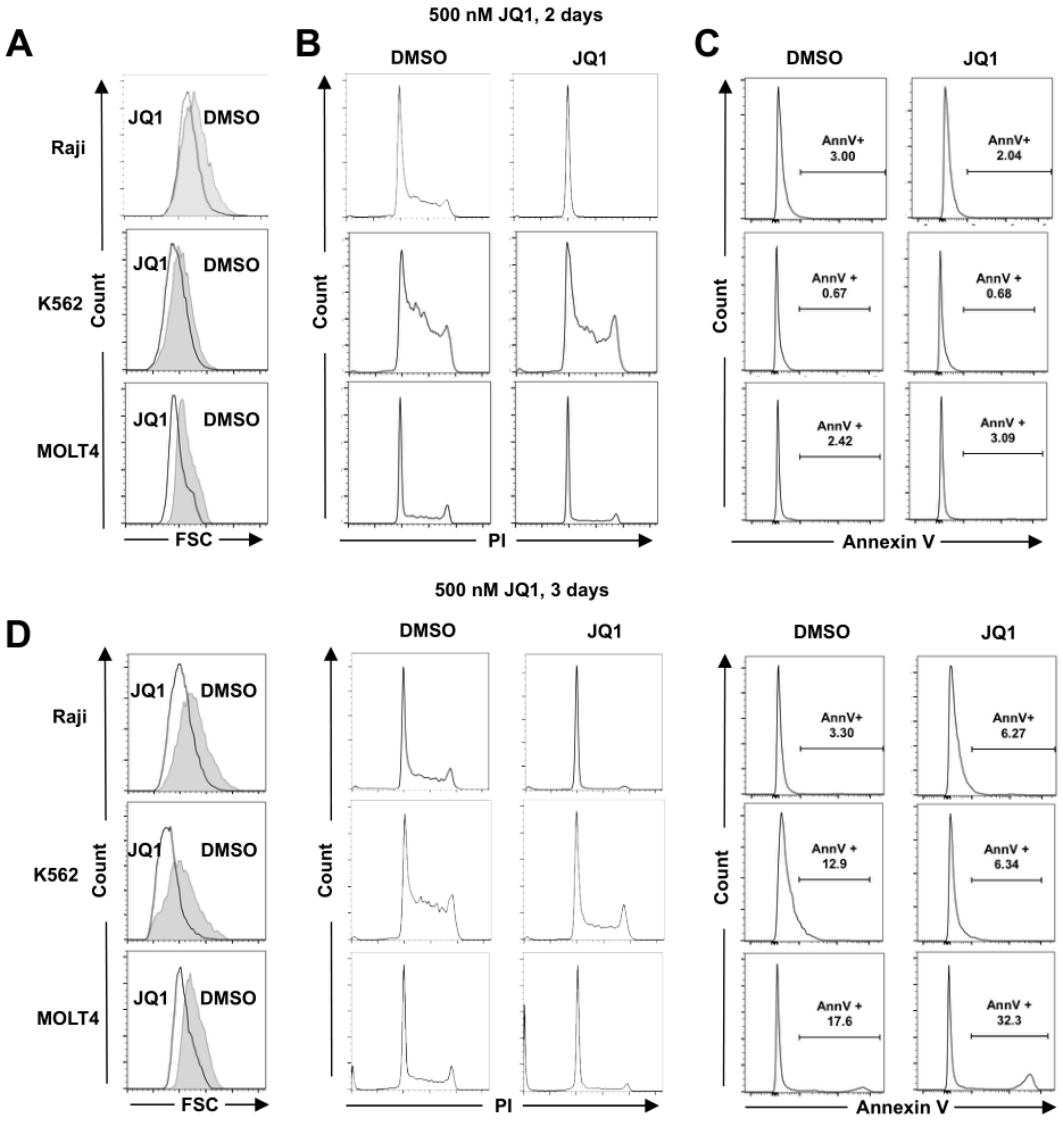

Figure 3.5. BETi reduces cell size in leukemia and lymphoma cell lines. (A) Cell size was assessed using forward light scatter in flow cytometry. (B) Cell cycle progression was assessed using propidium iodide staining. Representative graphs are shown. (C) Apoptosis was assessed using Annexin V (AnnV+) on viable cells. (D) Similar analyses as in (A-C), but performed at day 3 with the indicated cell lines. Statistical analysis was performed as described in Figure 2.

3.2.3 BET inhibitors reduce metabolic rate

The reduction in cell size is a classical phenotype associated with the loss of *MYC* expression and we observed a rapid loss of *MYC* transcription in Kasumi-1 cells treated

with JQ1 (Zhao et la., 2016). Western blot analysis confirmed that MYC levels dropped within two hours in both Kasumi-1 cells and MV4-11 cells (Fig. 3.6A). Therefore, we used pathway analysis tools to determine whether BET inhibitors affect the expression of MYC targets and metabolic genes using our previously published precision nuclear run-on sequencing (PRO-seq) data that were generated in Kasumi-1 cells with JQ1 or MS417 treatment for 1 and 3 hrs (Zhao et al., 2016). PRO-seq provides a high-resolution map of the actively elongating RNA polymerases, which pinpoint the genes that are directly affected by small molecule inhibitors of transcription. Genes that were inhibited by both JQ1 and MS417 (GFOLD < -0.585) at 1 hr were enriched with signaling pathways mediated by cytokines and/or growth factors regulating cell proliferation that drive the accumulation of cell mass as the cells cycle (Fig. 3.6B). Genes inhibited at 3 hr were enriched with metabolic pathways and ribosome biogenesis (Fig. 3.6B), which is consistent with reduced metabolism and cell size. MYC controls many of these genes regulating metabolism and ribosomal genes to control cell size (Mateyak et al., 1997; Mateyak et al., 1999; Grewal et al., 2005; Graves et al., 2012). Gene set enrichment analysis (GSEA) supported this idea and showed that genes inhibited by BET inhibitors at both 1 and 3 hr were enriched with previously identified MYC target genes including genes regulating ribosomal biogenesis (Fig. 3.6C) (Ji et al., 2011; Sabo et al., 2014; Walz et al., 2014; Heaster et al., 2018). This suggests that BET inhibitors decrease the expression of genes regulating cell metabolism and cell size by impairing the transcription of MYC.

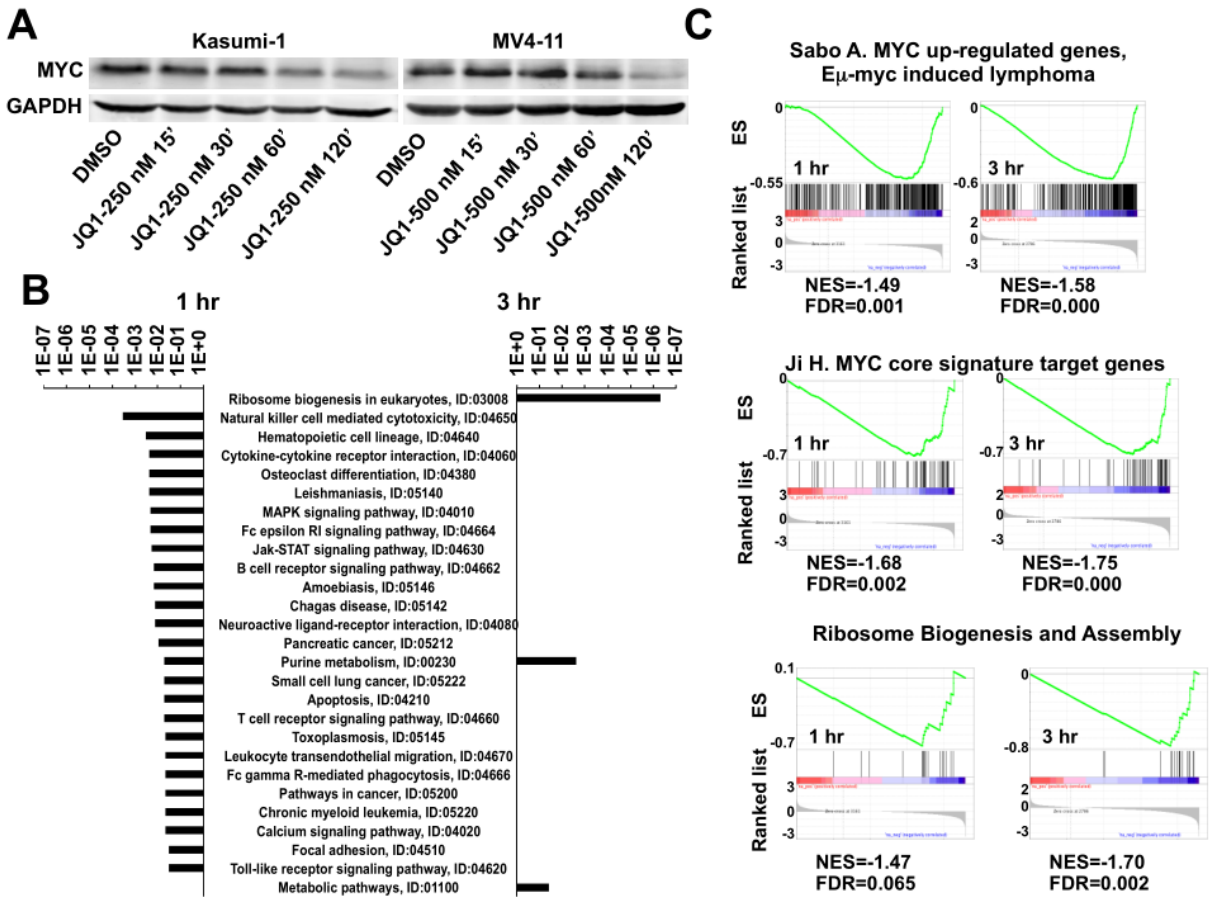

Figure 3.6. Meta-analysis of PRO-seq data of Kasumi-1 cells treated with JQ1 for 1 or 3 hr. (A) MYC levels drop rapidly upon BETi treatment. Western blot analysis of Kasumi-1 (left panel) and MV4–11 (right panel) cells treated with 250 or 500 nM JQ1 for the indicated times. (B) KEGG pathway analysis of PRO-seq data[31] showing genes in which promoter- proximal pausing was increased after 1 hr (left) and 3 hr (right) treatments. (C) Gene set enrichment analysis of PRO-seq data[31] showed decreased expression of MYC target genes including those genes regulating ribosomal biogenesis.

The role of BET inhibitors in reducing metabolism was further tested by directly examining bioenergetics in Kasumi-1, SKNO-1, and MOLM13 live cells by assessing the oxygen consumption rate (OCR) and extracellular acidification rates (ECAR) to track mitochondrial respiration and glycolysis using the Aligent Seahorse system (Figure 3.7). Cells were cultured in the absence or presence of BETi for 48 hr, and then assessed for

20 min to establish the basal respiration rates prior to injection of oligomycin to disrupt oxygen consumption and measure ATP production (Fig. 3.7, upper panels). BETi pretreatment reduced the basal respiration rate to essentially the level of control cells treated with oligomycin. Next, p-trifluoromethoxy carbonyl cyanide phenyl hydrazine (FCCP) was injected to uncouple the respiratory chain from phosphorylation and assess the maximal respiration rates. BETi-treated cells showed only a marginal response compared to a robust response from the untreated control cells. Finally, Rontenone and Antimycin A were injected to block respiration (Fig. 3.7, bottom panels). Overall, JQ1 dramatically impaired mitochondrial functions.

Cancer cells reprogram their metabolic pathways and are more dependent on glycolysis as an energy source. Therefore, we assessed glycolysis in the absence or presence of JQ1 (Fig. 3.7, upper panels). Cells were again treated with JQ1 for 48 hr prior to a 15 min assessment of the basal non-glycolytic media acidification. Glucose was then injected to assess glycolysis followed by an injection of oligomycin 20 min later to impair ATP production. Untreated control cells showed a rapid burst of glycolytic activity upon the addition of glucose, and oligomycin triggered a further step up in acidification indicating that control cells had a further glycolytic reserve (Fig. 3.7, bottom panels). In contrast, JQ1 treated AML cells showed a poor glycolytic burst with no further glycolysis upon oligomycin injection (Fig. 3.7, upper panels).

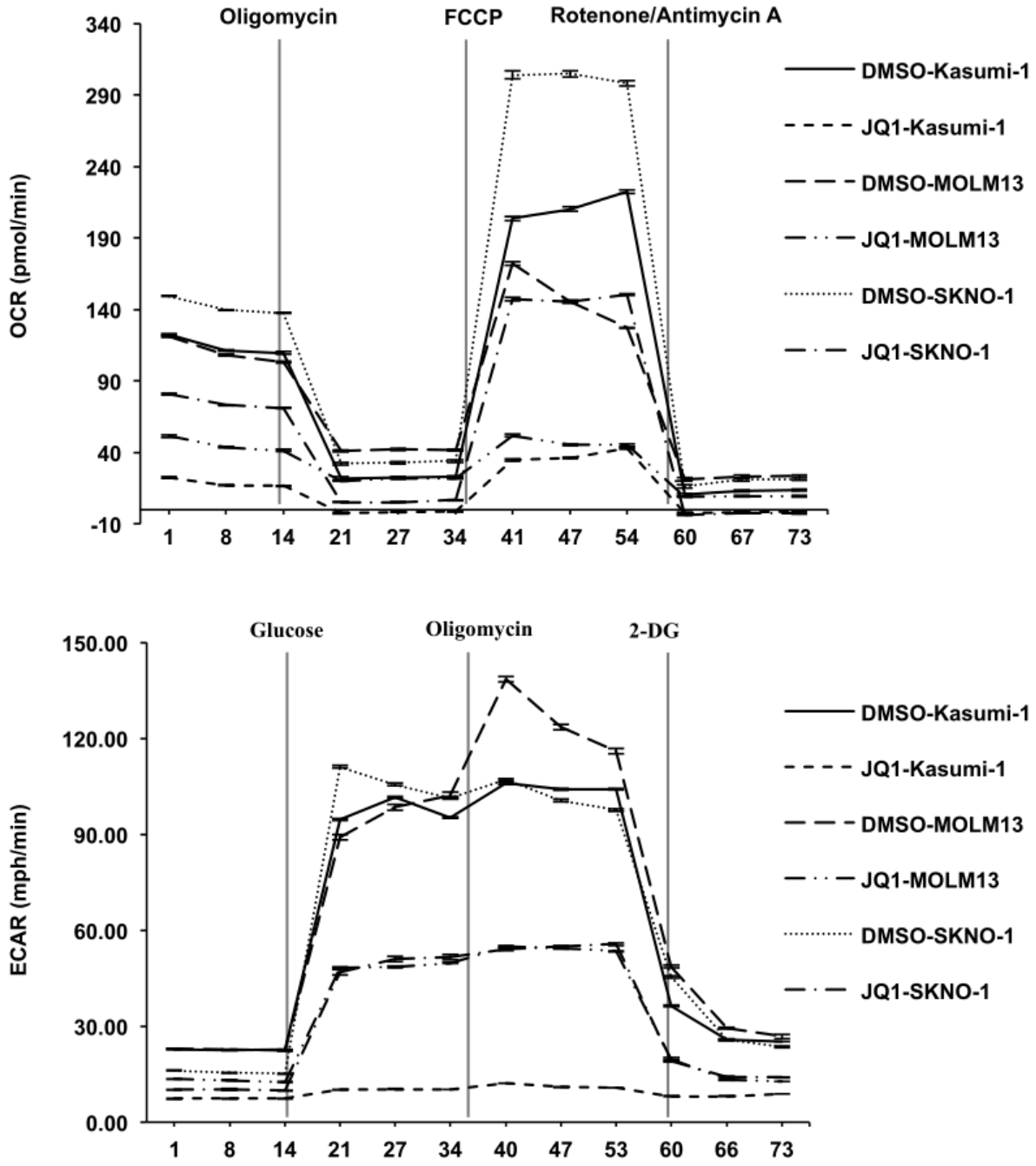

Figure 3.7. BET inhibitors reduce metabolic rate. (A) Oxygen consumption rate (OCR) and extracellular acidification rates (ECAR) were measured after JQ1 treatment for 2 days in Kasumi-1 cells, MOLM13 cells, and SKNO-1 (lower panels) cells. Decreased OCR and ECAR indicate repression of both mitochondrial dynamics and glycolytic function. For OCR, stage I injected oligomycin (5 mM), stage II injected FCCP (1 mM), and stage III injected Rotenone/Antimycin A (0.5 mM). For ECAR, stage I injected glucose (10 mM), stage II injected oligomycin (5 mM), and stage III injected 2-Deoxyglucose (50 mM).

3.2.4 BET inhibitor-induced cell cycle arrest is reversible

The rapid onset of cell cycle arrest without apoptosis for the first 24-48 hr after continuous drug treatment, suggested that even with daily dosing in patients the trough levels might allow survival of some AML cells (Odore et al., 2016). To assess whether JQ1-treated cells still possessed proliferative potential after drug removal, which could ultimately cause leukemic cell repopulation and resistance to BET inhibitor therapy, we treated Kasumi-1 cells for 24, 48, or 72 hr, washed out the drug, and then cultured them in fresh media and monitored cell growth. Consistent with these drugs inducing G_0/G_1 cell cycle arrest, but not senescence or cell death, Kasumi-1 cells treated for 24 or 48 hr were rescued to some degree by removing the drug (Fig. 3.8A, left and middle panels). However, longer treatments had a stronger effect on restricting cell proliferation, as the cells treated for 3 days grew much slower during the first 3 days after drug removal (Fig. 3.8A, right panel). The cells treated for 48 hr prior to rescue became more metabolically active three or five days after drug removal (RD3 and RD5; Fig. 3.8B) and returned to normal size within 3 days after being transferred to fresh media (Fig. 3.8C), and eventually began growing normally showing a rapid recovery of cell size and metabolism.

Next, we used optical metabolic imaging of single cells using two-photon microscopy and time-correlated single photon counting to measure the optical redox ratio (NADPH/FAD). This approach uses the autofluorescence of these co-enzymes within live cells and the ratio of NADPH to FAD yields a relative redox ratio that distinguishes apoptotic cells from proliferating, from G_0/G_1 cells (Heaster et al., 2018). JQ1 treated cells displayed a reduced redox ratio beginning at 24 hr after treatment, which was exacerbated by 72 hr (Fig. 3.8D). The use of single cell microscopy ensured that apoptotic cells did not confound this

analysis. Together, the combined effects of BET inhibitors on cell cycle arrest, cell size, and reduced metabolic rate suggested that the cells were not only being arrested in G_1, but were perhaps entering a $G_{0,}$ quiescent-like, state.

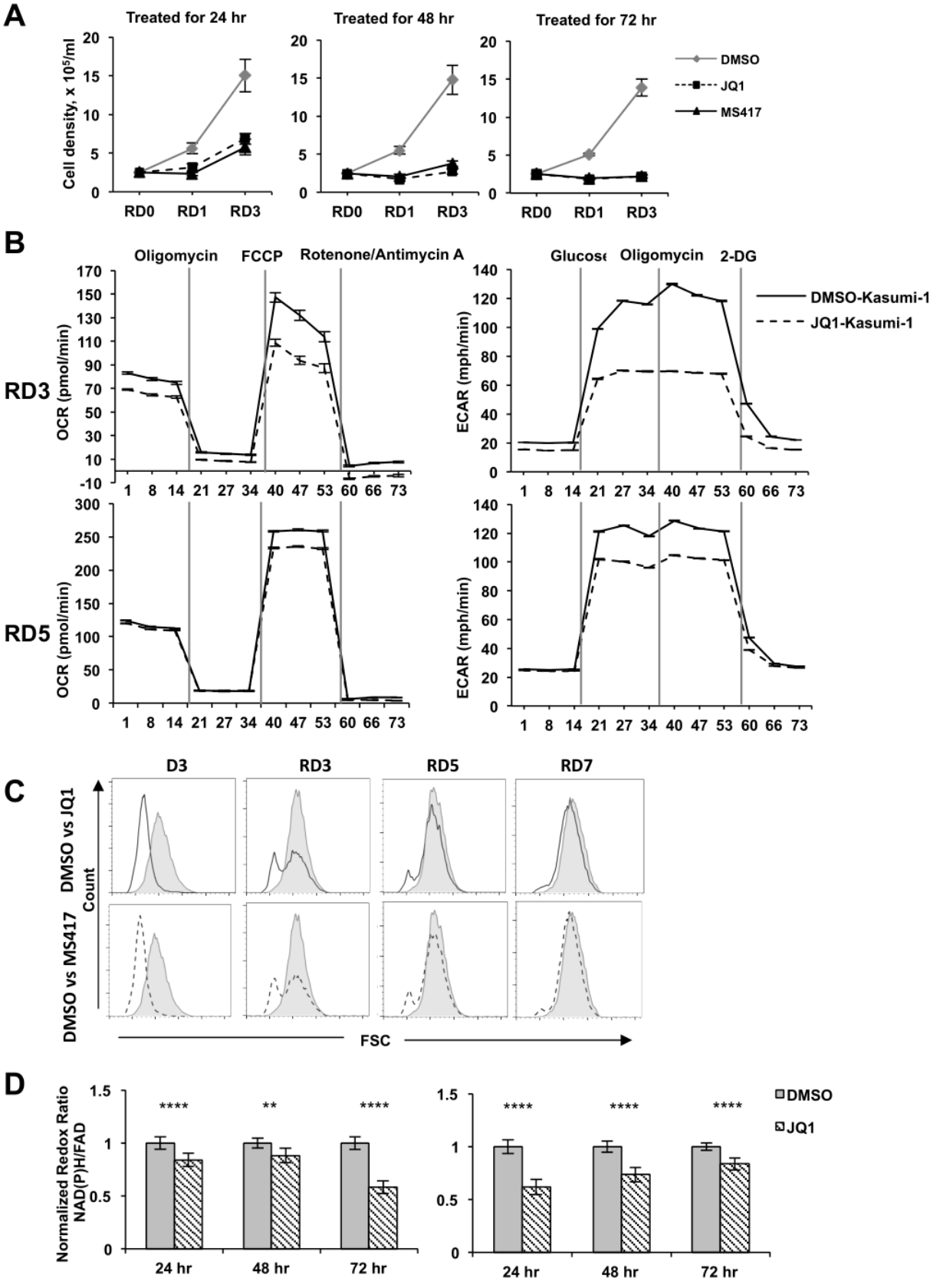
A
Treated for 24 hr
Treated for 48 hr
Treated for 72 hr
Cell density, x 10^5/ml
RD0
RD1
RD3
DMSO
JQ1
MS417
B
Oligomycin
FCCP
Rotenone/Antimycin A
Glucose
Oligomycin
2-DG
RD3
RD5
OCR (pmol/min)
ECAR (mph/min)
DMSO-Kasumi-1
JQ1-Kasumi-1
C
D3
RD3
RD5
RD7
DMSO vs JQ1
DMSO vs MS417
Count
FSC
D
Normalized Redox Ratio NAD(P)H/FAD
24 hr
48 hr
72 hr
DMSO
JQ1

Figure 3.8. Metabolic effects of BETi are reversible. (A) Kasumi-1 cells were treated with BETi for 24, 48 or 72 hr and the cells allowed to recover for 0, 1 or 3 days. Viable cell numbers were graphed over time. (B) Oxygen consumption rate (OCR) and extracellular acidification rates (ECAR) were measured after treatment of Kasumi-1 cells for 2 days and allowed to recover in the absence of JQ1 for 3 or 5 days. For OCR, stage I injected Oligomycin (5 mM), stage II injected FCCP (1 mM), and stage III injected Rotenone/Antimycin A (0.5 mM). For ECAR, stage I injected Glucose (10 mM), stage II injected Oligomycin (5 mM), and stage III injected 2-Deoxyglucose (50 mM) (C) Kasumi-1 cells treated with BETi for 3 days (D3) and then allowed to recover for 3, 5 or 7 days without BETi were tested for cell size using forward scatter in FACS. (D) Normalized optical redox ratio (NAD(P)H/FAD) was assessed using optical metabolic imaging. A minimum of 125 cells per sample in biological triplicates were measured for DMSO- and JQ1-treated Kasumi-1 cells at 24–72 hours before washout (left panel) or for the 24–72 hours after washout (recovery) of JQ1 (right panel). **, $p<0.01$; ****, $p<0.0001$; Mann-Whitney test.

Finally, we arrested cells with JQ1 for 72 hr (a time when the cells were beginning to die, Fig. 3.1 and 3.3), washed the cells to remove the compound, and cultured them in fresh media lacking JQ1 for 12-24 hr before quantifying the number of cells entering S-phase using BrdU incorporation. By 12 hr after drug removal, cells were beginning to re-enter the early S phase and this trend continued through 24 hr (Fig. 3.9A, JQ1 panels; and 2.9B, hashed bars). Intriguingly, it appears that some of the S phase-arrested cells began incorporating BrdU (note that cells already synthesizing DNA do not incorporate as much BrdU leading to a broadening of the band of cells in the 12, 18, and 24 hr samples, Fig. 3.9A, JQ1 panels). Conversely, some cells with between 2N and 4N DNA content did not incorporate BrdU (Fig. 3.9A, for example, see the oval in the 0 hr panel), suggesting that these cells were actually arrested in the S phase or were dying. Nevertheless, even after a 72 hr treatment with JQ1, there were cells that appeared to be quiescent, but still capable of re-entering the cell cycle after drug removal, indicating a potential mechanism of resistance to BETi.

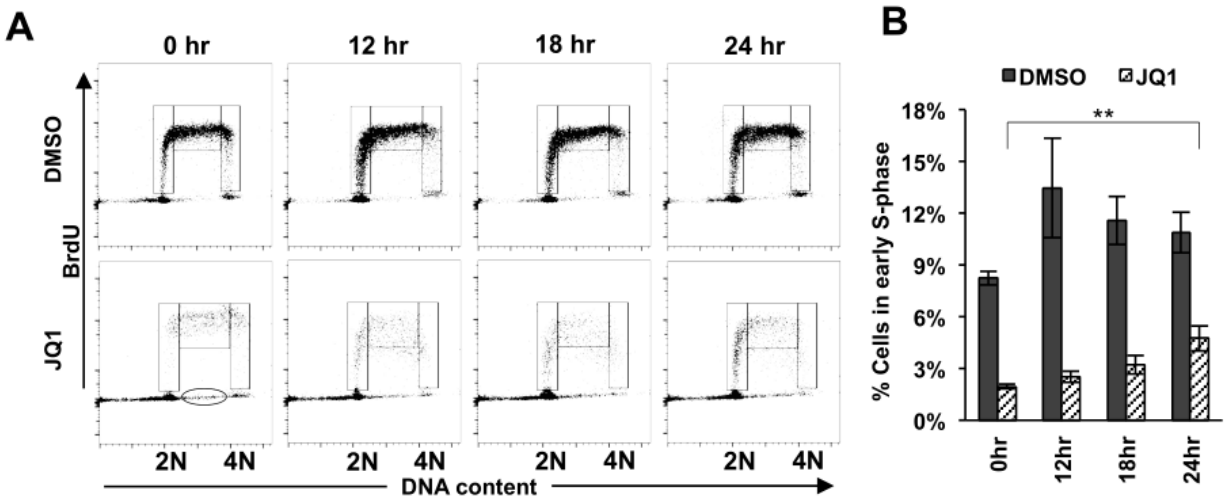

Figure 3.9. BETi induce reversible cell cycle arrest in Kasumi-1 cells. (A) Flow cytometry plots of incorporated BrdU versus propidium iodide show that Kasumi-1 cells treated with 250 nM JQ1 for 72 hr can recover and re-enter the cell cycle after drug removal for the indicated times. Cells were gated as early, middle, and late S phases from left to right. Oval indicates $BrdU^-$ cells in the S phase. (B) Bar graph displays the percentage of cells in the early S phase. Data are presented as mean ± SEM (n=4). ** $P < 0.001$ by two-sided Student's T-test when 0 hr and 24 hr levels were compared.

3.2.5 BET inhibitors sensitize cells to BCL2 inhibitors

The finding that BET inhibitors can arrest the cell cycle without dramatic AML cell killing suggested the need for combination therapy. The anti-apoptotic protein BCL2 is often expressed in leukemia cells and our earlier study showed that BET inhibitors caused promoter-proximal pausing of RNA polymerase II and reduced the rate of transcription of *BCL2* and *BCL-xL* in Kasumi-1 cells (Zhao et al., 2016). Therefore, we tested the combination of BET inhibitors and BCL2 inhibitors to target the residual BCL2. We pre-treated Kasumi-1 cells with JQ1 for 2 days to bring down the expression of *BCL2* and *BCL-xL* and found that the addition of BCL2/BCL-xL (ABT-263) or BCL2-selective (venetoclax; ABT-199) inhibitors quickly triggered apoptosis as measured by Annexin V and PI staining (Fig. 3.10A). We next extended this co-treatment analysis to other cell

lines (SKNO-1, MOLM13, and MOLT4) that also showed cell cycle arrest with little apoptosis and found that inhibiting BCL2 family proteins following BET inhibitor pre-treatment also induced cell death (Fig. 3.10B-D). This suggests that entering a reversible cell cycle arrest induced by BET inhibitors may protect leukemia cells from quick cell death and increase the chance of relapse, which necessitates a second drug (e.g. BCL2 inhibitor) to induce cell death for efficient killing of leukemia cells.

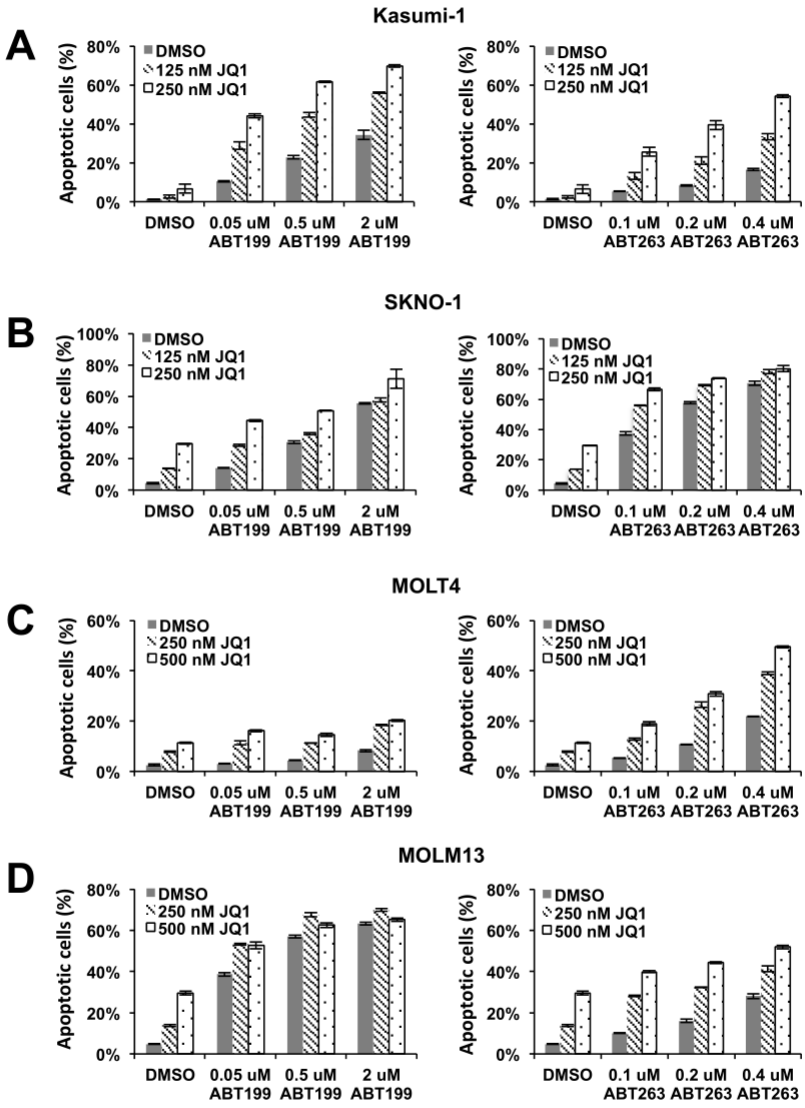

Figure 3.10. BET inhibitors sensitize AML cells to BCL2 inhibitor-induced cell death. AML cell lines were treated with BCL2 selective (ABT199) or BCL2/BCLxL (ABT263) inhibitors for 6 hours after pre-treating with BETi for 2 days. Apoptotic cell population was

detected by Annexin V positivity (AnnV+) and the absence of propidium iodide (PI) staining. Data are mean ± SEM (n=3). (A) Kasumi-1 cells and (B) SKNO-1 cells were incubated with 125 nM or 250 nM JQ1 before BCL2 inhibitor treatment. (C) MOLT4 cells, (D) MOLM13 cells were incubated with 250 nM or 500 nM JQ1 before BCL2 inhibitor treatment.

3.3 Discussion

While there is justifiable excitement about the therapeutic efficacy of BETi in AML, the therapeutic window appears to be due to the loss of *MYC* expression (Delmore et al., 2011; Ott et al., 2012). However, as observed in Kasumi-1 cells, the rapid loss of *MYC* was accompanied by a rapid cell cycle arrest, loss of metabolic activity, and reduced cell size, which is reminiscent of quiescence rather than cell death. In standard assays that use metabolism as a surrogate marker for cell viability, these compounds appear to work well, yet these cells recovered after BETi removal, suggesting that cell cycle arrest could be a mechanism of resistance to these compounds. The addition of a BCL2 inhibitor could provide the additional push toward apoptosis needed, and this could be an extremely safe and efficacious combination.

We identified this effect in t(8;21) containing Kasumi-1 cells, yet the effect was not limited to the t(8;21), as cells that express MLL fusion proteins were similarly slow to die in response to BETi. In addition, in a panel of diffuse large B cell lymphoma cell lines, JQ1 strongly induced G_1 cell cycle arrest, but only caused minor levels of apoptosis in several of these cell types (e.g. Ly7, Toledo, and Ly19) (Chapuy et al., 2014). Poor pharmacokinetic profile has been proposed as the cause of the much lower efficacy of BETi in mouse models compared to *in vitro* studies with cell lines, but reversible cell cycle arrest likely contributes. This may be a limiting factor for the usefulness of these compounds as *MYC* activation is a later event in myeloid leukemias that are not triggered

by a translocation or amplification directly affecting *MYC*. This is an important consideration because when *MYC* was not the only oncogene driving AML development, removal of *MYC* expression failed to prevent tumor recurrence (Rakhra et al., 2010; Choi et al., 2010).

Mechanistically, *MYC* is perhaps the best known transcriptional regulator of metabolism, cell cycle, and cell size (van Riggelen et al., 2010), as it controls the production of ribosomes that control translational outputs. Thus, it is most likely that suppression of MYC is the key event in the regulation of cell size in our studies. It is notable that our PRO-seq analysis did not identify RNA polymerase II promoter-proximal pausing associated with ribosomal genes or pathways linked to metabolism until 3 hr after JQ1 treatment (Fig. 3.6A), even though large numbers of genes were affected within 15-30 min after treatment, including *MYC* (Zhao et al., 2016). Thus, the loss of metabolic activity (Fig. 3.7-3.8) is likely a secondary consequence, which is consistent with the down regulation of *MYC* in the first hour followed by the loss of MYC targets beginning at1 hr and increasing 3 hr post drug treatment (Fig. 3.6). However, we also noted the loss of expression of cyclin D1 (*CCND1*) and D2 (*CCND2*), CDK4, and CDK6. In addition, we detected an “E2F/retinoblastoma (RB) signature” of increased pausing ratio with E2F2 and E2F8 being directly affected within the first hour of treatment with BETi (Zhao et al., 2016). Conversely, we noted a rapid up regulation of *CDKN1A* (*p21*^{CIP}), but this was not associated with DNA damage (Fig. 3.2). Given that RB family-dependent repression is associated with G_1 arrest and quiescence and E2F family members control nucleotide metabolism, these data suggest that the effects on metabolism and cell cycle control are multi-factorial in nature.

In addition to controlling cell size, MYC is a direct regulator of genes that control glycolysis and mitochondrial biogenesis (Fig.3.7-3.8). MYC stimulates the expression of glucose transporter-1 while also stimulating the genes that directly control glycolysis (Osthus et al., 2000; Kim et al., 2004; Hu et al., 2011). Therefore, the loss of *MYC* expression is consistent with the loss of glycolytic burst and glycolytic capacity in AML cells treated with JQ1 (Fig. 3.7). At the same time, JQ1 treatment induced a loss of mitochondrial functions including reductions in basal respiration, ATP-linked respiration, and maximal respiration capacity (Fig. 3.7). Analysis of transcription at the early time points suggested only defects in growth factor signal transduction, so these effects could also be traced to reduced MYC expression by three hours post BET inhibitor treatment.

Given the loss of MYC expression and the large effects on metabolism, it is somewhat surprising that AML cells survived and could re-enter the cell cycle (Figures 6-7). An intriguing hypothesis is that the cells have entered a quiescent-like state in which metabolic needs are greatly reduced. This possibility is consistent with the gene expression profiles, the reduced cell size, and the ability of these cells to begin cycling again after removal of JQ1. Nevertheless, the increased apoptosis upon addition of venetoclax, was more than an additive effect in Kasumi-1 cells, indicating that the suppression of BCL2 levels sets the stage for the induction of apoptosis. While the effects were not as dramatic in other cell types (Fig. 3.10), this could be due to induction of MCL1, whose levels increase after JQ1 treatment, possibly as a stress response. Given that venetoclax is beginning to gain traction as a component of the standard of care for AML (DiNardo et al., 2018; Konopleva et al., 2016), these data support a rational combination

approach to the utilization of BET inhibitors with venetoclax in the clinic to avoid the use of genotoxic agents such as hypomethylating agents or Cytarabine.

CHAPTER 4

Mechanism of PAX3-FOXO1 transcriptional control in alveolar rhabdomyosarcoma

4.1 Background

PAX3-FOXO1 is the critical driver of aRMS and an ideal therapeutic target. A thorough understanding of PAX3-FOXO1 function is critical to define aRMS etiology as well as to develop more innovative therapeutic strategies for this aggressive disease. Moreover, defining with high certainty exactly where in the genome a transcription factor acts allows a detailed dissection of its mechanism of action. A critical component of understanding how oncogenic transcription factors such as PAX3- FOXO1 drive disease is defining their direct transcriptional targets. However, the study of transcription factor functions has largely been limited to overexpression or genetic deletion approaches after days of altering transcription factor protein levels, while transcriptional control is a highly dynamic process which is changing within the first hours in response to external stimuli (Swift and Coruzzi, 2017).

Identification of direct targets can be further aided by assays of genome-wide transcription factor binding. However, these are only correlations, and ChIP-Seq for PAX3-FOXO1 identified many thousands of binding sites (Cao et al., 2010; Gryder et al., 2017; Sunkel et al., 2021). Thus, while it is clear from these studies that PAX3-FOXO1 overwhelmingly associates with distal enhancer elements, identifying which enhancer binding events drive changes in gene expression is a challenge. Therefore, accurate

identification of both direct gene targets as well as identification of regulated enhancers is critical for further elucidating the mechanism(s) by which PAX3-FOXO1 regulates gene expression.

We used PAX3-FOXO1 as a model of a potent transcriptional activator to define how an oncogenic transcription factor reorganizes transcriptional networks to cause cancer. We used CRISPR-based engineering to integrate a degron tag (FKBP12) into the endogenous *PAX3-FOXO1* locus (Nabet et al., 2018). This allowed us to rapidly degrade endogenous PAX3-FOXO1 to provide the temporal resolution required to identify direct gene targets. This study identified just over a hundred high-confidence PAX3-FOXO1 gene targets that exhibited rapid loss of expression and were associated with a nearby regulated enhancer.

4.2 Results

4.2.1 Model of endogenous PAX3-FOXO1 degradation

We used CRISPR-based genome editing to integrate a 2x*HA-FKBP12*^{F36V} degron tag into the last exon of the endogenous *PAX3-FOXO1* (Davis and Barr, 1997; Linardic, 2008; Missiaglia et al., 2012) locus of the Rh30 and Rh4 aRMS cell lines (Fig. 4.1A). This yielded a model for rapid PAX3-FOXO1 protein degradation following the addition of a small molecule proteolysis-targeting chimera (PROTAC), dTAG-47 (Fig. 4.1B) (Weintraub et al., 2017; Nabet et al., 2018). Western blot analysis confirmed that much of the endogenous PAX3-FOXO1 protein was degraded by 2 hours after adding dTAG47, although the protein did not completely disappear. To account for clonal variation, we generated four *PAX3-FOXO1-2xHA-FKBP12*^{F36V}-expressing clones in Rh30 cells and

two *PAX3-FOXO1-2xHA-FKBP12^{F36V}*-expressing clones in Rh4 cells (e.g., Fig. 4.1C). RNA-seq was performed from all four Rh30 PAX3-FOXO1-FKBP clones in the absence of dTAG-47, to demonstrate that the addition of the degron tag did not significantly alter gene expression patterns relative to unedited cells. Differential expression analysis shows that all clones clustered well with parental Rh30 with a high Pearson Correlation R-value from 0.9 to 1.0 (Fig. 4.1D). Furthermore, heatmaps generated using all the expressed genes showed that the PAX3-FOXO1-FKBP cell lines displayed similar transcriptional profiles with parental Rh30 cells (Fig. 4.1E). Thus, the global gene expression patterns from all clones were highly consistent, both with each other and with the parental Rh30 cell line.

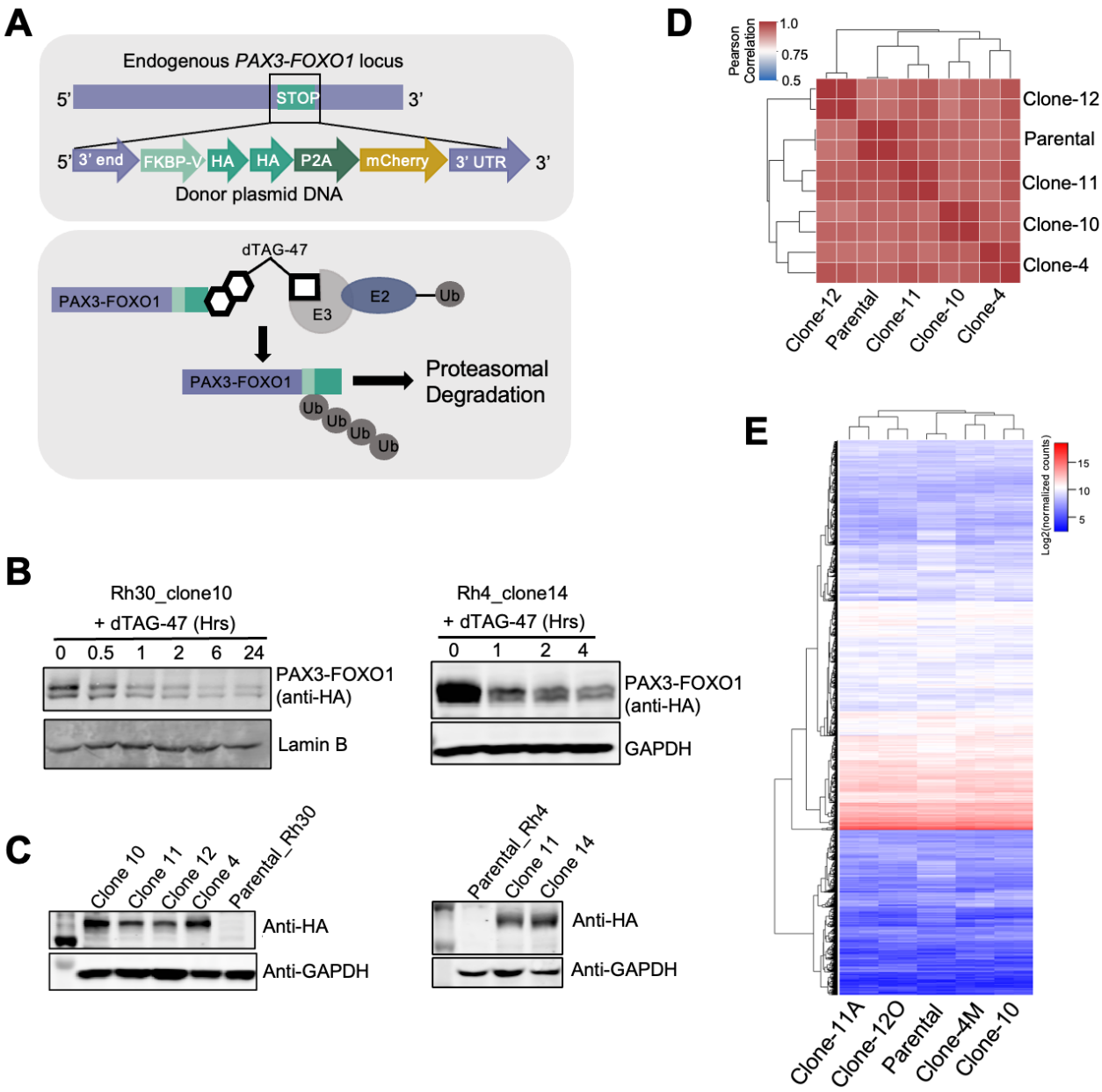

Figure 4.1. Analysis of PAX3-FOXO1-FKBP single cell clones. (A) Model of the plasmid DNA template used to insert FKBP12F36V-2XHA-P2A-mCherry into the endogenous *PAX3-FOXO1* allele (upper panel). Model showing the derivative of thalidomide (dTAG47) that binds to the FKBP module to link PAX3-FOXO1-FKBP to the cereblon E3 ligase to cause rapid degradation of PAX3-FOXO1-FKBP. (B) Rh30 and Rh4 PAX3-FOXO1-FKBP cell lines were treated with 500 nM dTAG47, and western blot analysis showing degradation of endogenous PAX3-FOXO1 in Rh30 and Rh4 cell clones. (C) Western blot analysis of four Rh30_PAX3-FOXO1-FKBP clones and two Rh4_PAX3-FOXO1-FKBP clones. (D) Cluster heatmap of Pearson correlations from RNA-seq of four different PAX3-FOXO-FKBP cell lines expanded from single cell clones and parental

Rh30 cells. Each cell line has two biological replicates and data was normalized to total counts. (E) Heatmap of log_2 normalized counts from RNA-seq across the four different PAX3-FOXO-FKBP clonal cell lines and parental Rh30 cell line using all the expressed genes. Each cell lines have two biological replicates.

4.2.2 PAX3-FOXO1 degradation triggers growth defect, cell differentiation, apoptosis, and reduced growth in soft agar

Since PAX3-FOXO1 is thought to be the main cause for aRMS harboring this translocation, we first examined how the loss of the fusion protein affected the cell viability and proliferation of aRMS cells (Shern et al., 2014). After three days of treatment, all Rh30 and Rh4 clones expressing PAX3-FOXO1-FKBP exhibited a similar growth inhibition following PAX3-FOXO1 degradation (Fig. 4.2A). This growth defect became even more apparent from Day 4 to Day 9. Given the high similarity between all FKBP clones, we chose Rh30 clone 10 and Rh4 clone 14 for further analysis.

Flow cytometry analysis after BrdU incorporation on day-3, 6, and 9 showed degradation of PAX3-FOXO1 caused a G_1-phase cell cycle arrest (Fig. 4.2B). Inconsistent with previous studies suggesting that apoptosis- or anti-apoptosis- related genes were regulated by PAX3-FOXO1 (Ahn et al., 2013, Marshall et al., 2013), Rh30-PAX3-FOXO1-FKBP cells showed an increase in cell death following PAX3-FOXO1 degradation as measured by annexin-V and 7-AAD (Fig. 4.2C). A hallmark of cellular transformation is anchorage-independent growth, characterized by the ability to grow independently of a solid surface. To determine if PAX3-FOXO1 is required for anchorage-independent growth, we performed soft agar colony formation assays. After degrading PAX3-FOXO1, soft agar colony formation was significantly reduced in the Rh30-PAX3-FOXO1-FKBP clone 10 (Fig. 4.2D).

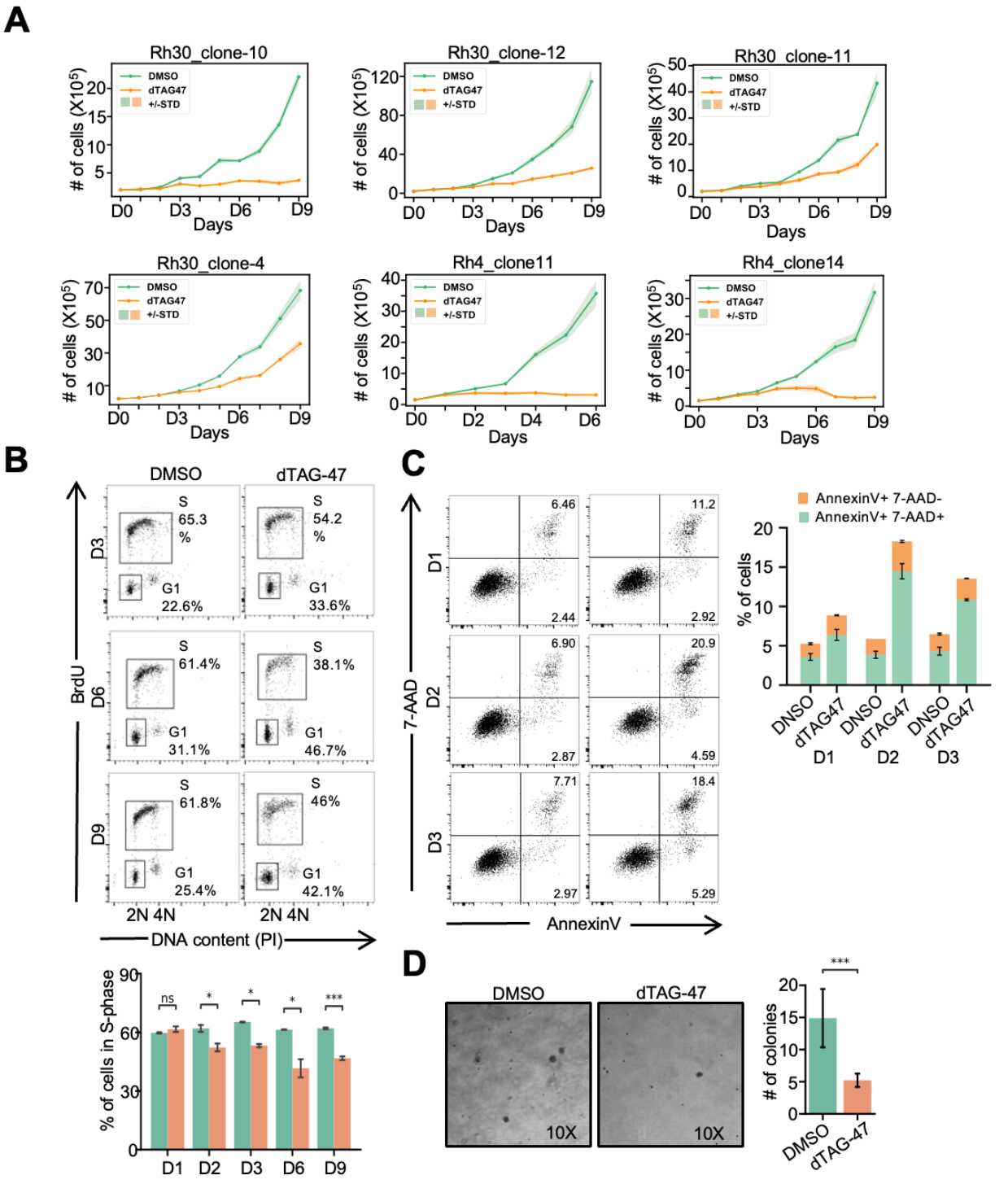

Figure 4.2. Degradation of PAX3-FOXO1 triggers cell death and differentiation. (A) Rh30 and Rh4 PAX3-FOXO1-FKBP clones were treated with 500 nM dTAG-47, and cell counts were determined using Trypan Blue dye exclusion. Data are mean ± STD (n=3). (B) Cell cycle analysis of Rh30 PAX3-FOXO1-FKBP cells. The cells were treated with

500 nM dTAG-47 for the indicated times before flow cytometry analysis for BrdU incorporation. Plots of BrdU versus propidium iodide (PI) show fewer cells in the S-phase and accumulation of cells in the G_1-phase after dTAG-47 treatment. The bottom bar graph showing statistical analysis of biological replicates of cells in S phase from the upper panel. Data are presented as mean ± STD (n=3). (C) Apoptosis analysis of Rh30 PAX3-FOXO1-FKBP cells. The cells were treated with 500 nM dTAG-47 for the indicated times before flow cytometry analysis for AnnexinV and 7-AAD staining. The bar graph on the right showing percentage of early and late apoptotic cells. Data are presented as mean ± STD (n=3). (D) Growth in soft agar. Rh30_PAX3-FOXO1-FKBP cells were pre-treated with 500 nM dTAG-47 for 6 days before being plated in soft agar. 4 weeks later the number of colonies was counted using microscopy. Representative images show colonies using an inverted microscope (10X). The bar graph displays colony counts with the bar the mean ± STD (n=9). (*p*, independent T test. *: *p* <= 5.0e-02, **: *p* <= 1.e-02, ***: *p* <= 1.0e-03, ****: *p* <= 1.0e-04).

The cell origin of aRMS is still obscure, but it is generally thought that aRMS development is connected to a differentiation defect of stem or early progenitor cells (Skrzypek et al., 2018; Keller et al., 2018). Consistent with these data, after PAX3-FOXO1 degradation for 3 days, cells showed morphological signs typical of myogenic differentiation, as they developed a more elongated morphology (Fig. 4.3A and C). In myogenic differentiation regulation, early and late regulators of normal myogenesis are temporally expressed (Khan et al., 1998). Myogenin (MYOG) is one of the factors responsible for terminal differentiation, and it was upregulated after PAX3-FOXO1 degradation (Fig. 4.3 B and D, right panel). In addition, the degradation of PAX3-FOXO1 caused increased expression of myosin heavy chain, which is involved in muscle differentiation (Fig. 4.3 B and D, left panel). Taken together, our data suggested that PAX3-FOXO1 fusion protein is required for aRMS cells to maintain a more stem cell-like state that is more proliferative.

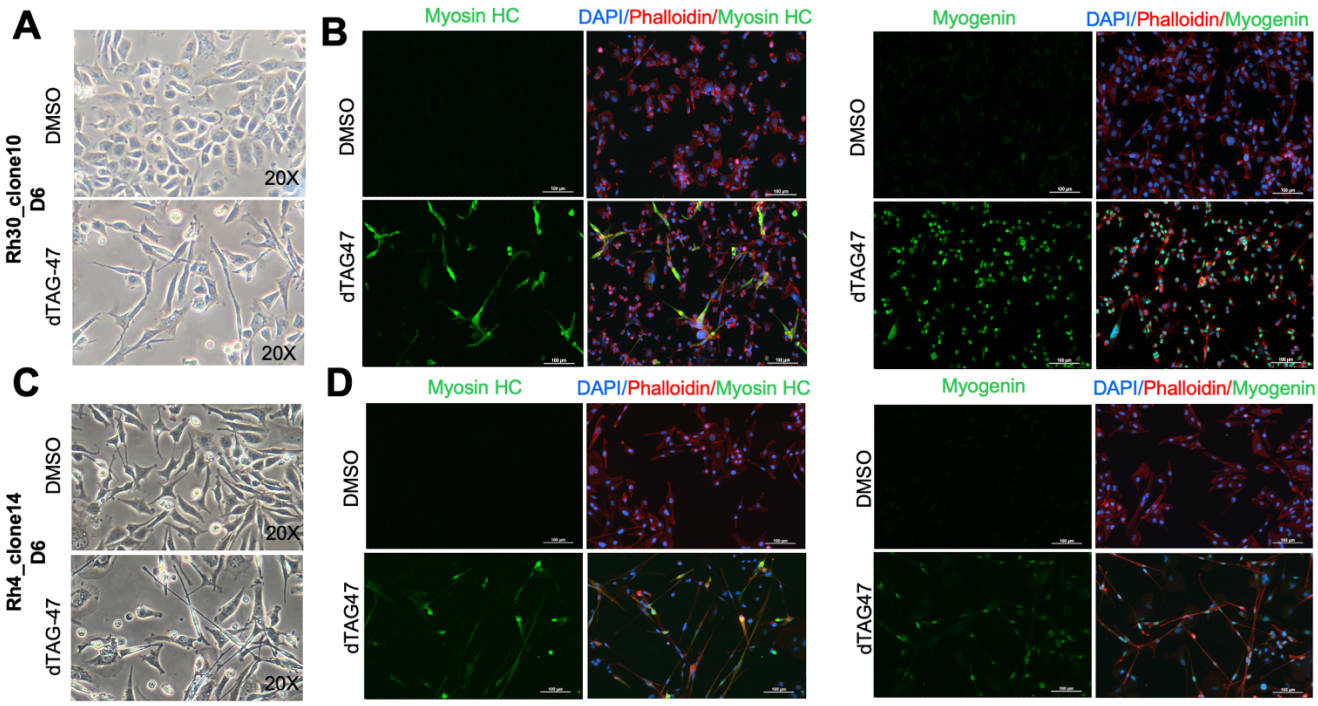

Figure 4.3. Degradation of PAX3-FOXO1 triggers cell differentiation. Morphological analysis of PAX3-FOXO1 cells after treatment with dTAG-47 for 6 days (20X). (A and C) Immunofluorescence analysis of Myosin Heavy Chain (left) and Myogenin (right) expression in Rh30 PAX3-FOXO1-FKBP clone 10 (B) and Rh4_PAX3-FOXO1-FKBP clone 14 (D). Rh30 PAX3-FOXO1-FKBP cells were treated with 500 nM dTAG-47 for 6 days. DAPI was used to label nuclei (blue). Alexa 568-labeled Phalloidin was used to mark actin filaments (red). Alexa 488 secondary antibody was used to visualize the primary antibody against skeletal muscle differentiation markers Myosin Heavy Chain and Myogenin (green; 20X).

4.2.3 Degradation of endogenous PAX3-FOXO1 triggers loss of expression of a small number of genes

In order to understand how PAX3-FOXO1 contributes to aRMS, it is necessary to identify its transcriptional targets. The inclusion of a 2xHA tag in the degron cassette allowed for the robust detection of PAX3-FOXO1 chromatin association by CUT&RUN (Skene and Henikoff, 2017). PAX3-FOXO1 binding was detected at 44,267 sites in Rh30 cells (Fig. 4.4A) and 27,635 sites in Rh4 cells (Fig. 4.4B). Levels of chromatin-bound

PAX3-FOXO1 were reduced at nearly all identified peaks within 2hr of dTAG-47 treatment, and maximal reduction of chromatin-bound PAX3-FOXO1 was observed after 4hr, while any unchanged peaks were considered background. A comparison of Rh30 and Rh4 CUT&RUN peaks indicated that there were 21,401 in common (Fig. 4.4C). We also compared our anti-HA CUT&RUN data with the previously published antibody-based ChIP-seq (Sunket et al., 2021) of PAX3-FOXO1 chromatin association, the Venn diagrams show a high degree of overlap (Fig. 4.4D). Also, the anti-HA CUT&RUN is more robust with less background than the previously published ChIP-seq data.

K means clustering identified the most robust peaks within clusters 1 and 2. PAX3-FOXO1 binds DNA through the combined action of the paired domain and the homeodomain, which yields a larger consensus DNA binding site that is unusually amenable to the motif analysis (Sunkel et al., 2021). *De novo* motif analysis indicated that cluster 3 did not select for regions with robust PAX3-FOXO1 DNA binding motifs and cluster 2 showed only a modest enrichment for this motif (e.g., 4.5% and 5.9%; Fig. 4.4E). In contrast, the most robust peaks (cluster 1) also showed the greatest enrichment for the PAX3-FOXO1 DNA-binding motif (Fig. 4.4E).

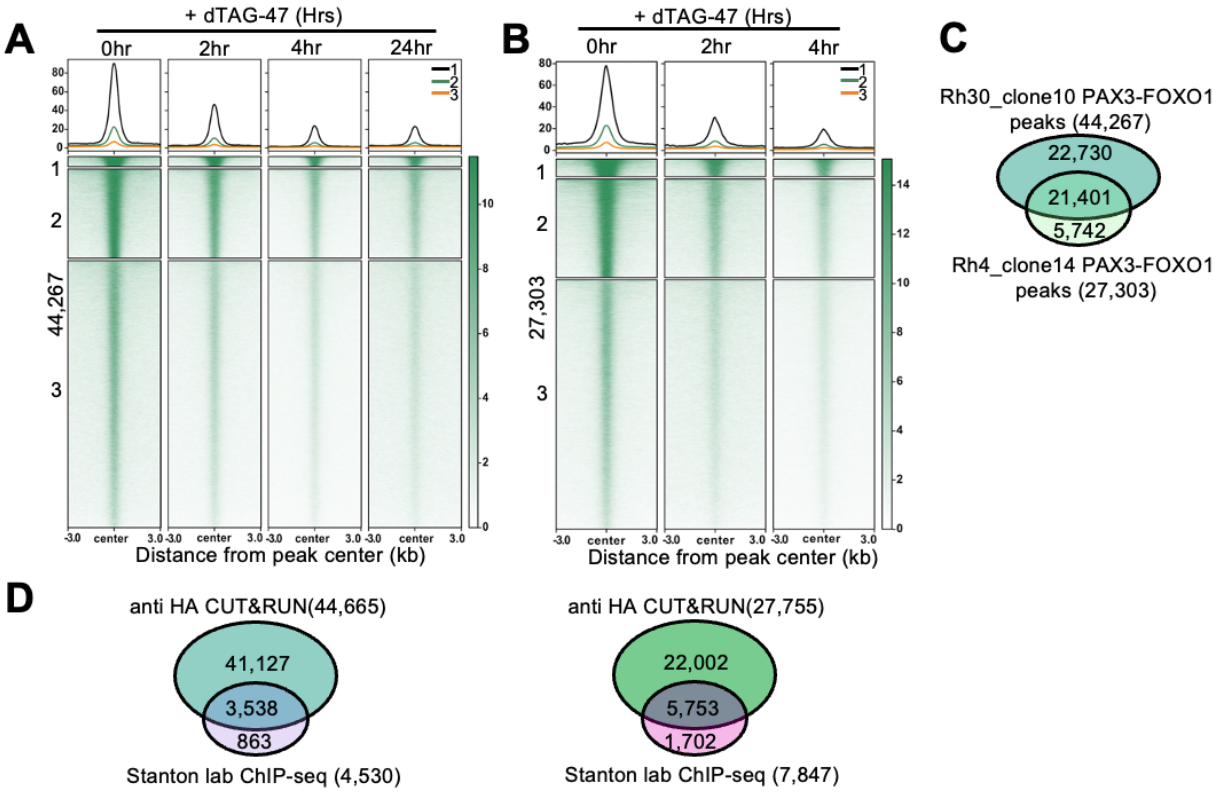

E

Motif	Name	% of Targets	p-value
	PAX3:FKHR	18.34	1e-185
	MYOG	16.95	1e-49
	HOXD10	5.74	1e-33
	PAX3	2.77	1e-28
	GSC2	41.26	1e-19

Motif	Name	% of Targets	p-value
	PAX3:FKHR	9.97	1e-130
	MYOG	19.13	1e-44
	PAX7	11.97	1e-22
	SMAD2	4.71	1e-18
	SOX10	2.09	1e-12

Motif	Name	% of Targets	p-value
	MYOG	23.62	1e-406
	PAX3:FKHR	4.51	1e-281
	RUNX	11.00	1e-98
	TEAD2	19.83	1e-83
	OTX2	7.63	1e-73

Motif	Name	% of Targets	p-value
	MYOG	15.61	1e-287
	PAX3:FKHR	5.85	1e-204
	OTX1	50.19	1e-86
	PAX2	7.13	1e-81
	RUNX	12.31	1e-43

Motif	Name	% of Targets	p-value
	BHLHA15	14.92	1e-666
	FRA1	7.05	1e-297
	SOX6	15.77	1e-191
	TEAD3	17.28	1e-167
	RUNX1	5.46	1e-140

Motif	Name	% of Targets	p-value
	MYOG	3.68	1e-343
	PAX3:FKHR	2.76	1e-283
	DLX5	48.62	1e-146
	NFY	56.19	1e-82
	ATF2	8.51	1e-72

Figure 4.4. PAX3-FOXO1 regulated sites are enriched for the best PAX3-FOXO1 binding sites. (A and B) K-means clustered heatmaps of PAX3-FOXO1 CUT&RUN peaks after treatment with dTAG47 in Rh30 clone 10 (A) and Rh4 clone 14 (B). (C) Venn diagram showing the overlap between PAX3-FOXO1 binding sites in Rh30 clone 10 and Rh4 clone 14 cells. (D) Venn diagrams showing the overlap between the peaks defined by ChIP-seq and CUT&RUN in each cell line. (E) Motif analysis (de novo) of transcription factors predicted to reside under the 3 clusters of PAX3-FOXO1 genomic peaks in Rh30 clone 10 and Rh4 clone 14.

Given the thousands of PAX3-FOXO1 binding sites that were identified, we next asked which transcripts require the presence of PAX3-FOXO1 binding to drive gene expression. Most previous studies have been done through expression profiling after knock-in or shRNA knockdown (Gryder et al., 2017, Walters et al., 2014). However, while knockdown or over-expression coupled with RNA-seq analysis can identify genes with altered expression, these approaches require days before transcriptional changes can be measured. Thus, many of these changes could be indirect or compensatory transcriptional changes resulting from chronic transcription factor loss or over-expression. Importantly, we have demonstrated that by 3-6 days following PAX3-FOXO1 degradation, cells are already undergoing cell cycle arrest and differentiation, highlighting the need to monitor transcription at hours rather than days following PAX3-FOXO1 protein degradation in order to define direct transcriptional events.

We performed precision nuclear run-on transcription sequencing (PRO-seq) in Rh30 cells at short time points following PAX3-FOXO1 degradation to determine how rapid loss of the PAX3-FOXO1 protein impacts gene expression. PRO-seq maps transcriptionally engaged RNA polymerase across the genome, and provides a readout of nascent transcription, as well as assessments of RNA polymerase pausing and elongation (Kwak et al., 2013; Mahat et al., 2016). Relative changes in gene body

transcription were quantified using the nascent RNA-sequencing analysis (NRSA) pipeline (Wang et al., 2018), which identified only 1 gene with increased transcription at 2hr and only 33 within 4hr of PAX3-FOXO1 degradation (Fig. 4.5A). In contrast, 158 genes exhibited decreased gene body transcription at 2hr following PAX3-FOXO1 degradation, and transcription of most of these genes remained reduced at 4 hours (Fig. 4.5A), which is consistent with the established role for PAX3-FOXO1 in transcriptional activation. Moreover, the vast majority of down-regulated genes were associated with nearby PAX3-FOXO1 CUT&RUN peaks (Fig. 4.5B; 149 genes at 2hr and 210 at 4hr).

Furthermore, the reduced polymerase activity detected by PRO-seq resulted in a reduction of mature mRNA as detected by RNA-seq (Fig. 4.5C), nominating these genes as direct PAX3-FOXO1 gene targets. CUT&RUN analysis found reduced H3K4me3 at regulated promoters, further confirming the loss of gene expression (Fig. 4.5D). It is notable that several transcription factors were turned off by degradation of PAX3-FOXO1, including oncogenes and “stemness” factors (e.g., *JUN, KLF4, RUNX2, ETS1*, *PRDM12,* and the co-repressor *RUNX1T1*), which likely trigger cascades of transcriptional changes. For example, within 6hr of dTAG-47 addition, there were 717 significant changes by RNA-seq with roughly 40% of these mRNAs increased rather than decreased (Fig. 4.5E). These results emphasize the need to use nascent transcript analysis at early time points after the inactivation of transcription factors to avoid the detection of secondary transcriptional changes found by RNA-seq at later times.

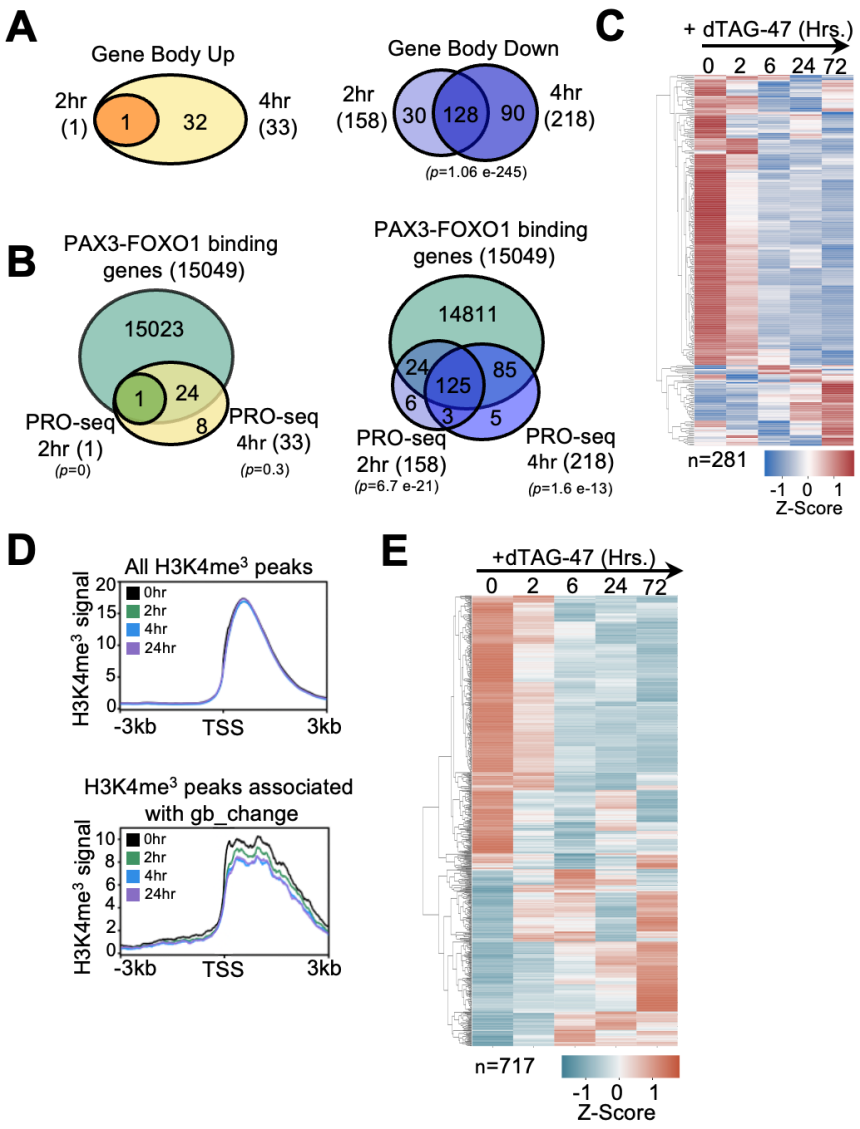

Figure 4.5. Transcription activation function of PAX3-FOXO1. (A and B) Venn diagrams showing the PRO-seq signal quantified within the gene body with changes over time, and the overlap between CUT&RUN and PRO-seq signal quantified within the gene body as increased over time (A), or decreased over time (B). (C) Heatmap visualizing the relative change of RNA-seq-detected mRNAs corresponding to the genes identified from the PRO-seq analysis with gene body changes in at least one time point. Heatmap is normalized by row Z-score to emphasize the changes in the RNA-seq data. (D) Histograms of all H3K4me3 CUT&RUN peaks (upper panel) and the H3K4me3 peaks annotated to genes showing transcriptional changes (lower panel) ±3Kb around the transcription start site (TSS). (E) Heatmap of RNA-seq plotted by the genes changed after 6hr of dTAG-47 treatment at indicated time points.

Next, we generated histograms depicting the PRO-seq signal across genes up-regulated (33, Fig. 4.6A, upper) or down-regulated (248, Fig. 4.6A, bottom) in at least one time point following PAX3-FOXO1 degradation. Interestingly, down-regulated genes exhibited a clear reduction in gene body polymerase density, but maintained high levels of paused polymerase just downstream of the transcription start site (Fig. 4.6A, bottom). This pattern is indicative of a reduction in RNA polymerase pause release rather than a significant change in transcription initiation.

In fact, most down-regulated genes showed an increase in RNA polymerase pausing index, which reached statistical significance at 106 of 248 down-regulated genes (Fig. 4.6B). Notably, those genes with a significant increase in pausing index were more highly down-regulated than genes without changes in pausing index (Fig. 4.6C). Examination of long genes such as *NELL1* further illustrates this phenomenon (Fig. 4.6D). By 2hr following PAX3-FOXO1 degradation, there was a specific reduction of elongating RNA polymerase at the 5'end of the gene, and by 4hr the elongating polymerase had reached the 3' end and the locus was maximally silenced (Fig. 4.6D, arrows). During this time, levels of paused polymerase downstream of the TSS remained relatively unchanged for both sense and antisense transcripts (Fig. 4.6D, shaded box).

In addition, we further mapped the total Pol II, Pol II-S2, and Pol II-S5 at the genes with decreased transcription and increased pausing index. The S2 phosphorylated Pol II was dramatically reduced, while the S5 phosphorylated Pol II was increased at the TSS (Fig. 4.6E). Thus, PAX3-FOXO1-regulated the transcription of many target genes by promoting RNA pol II pause release and transcription elongation. Taken together, these results suggest that PAX3-FOXO1 functions mainly to activate transcription.

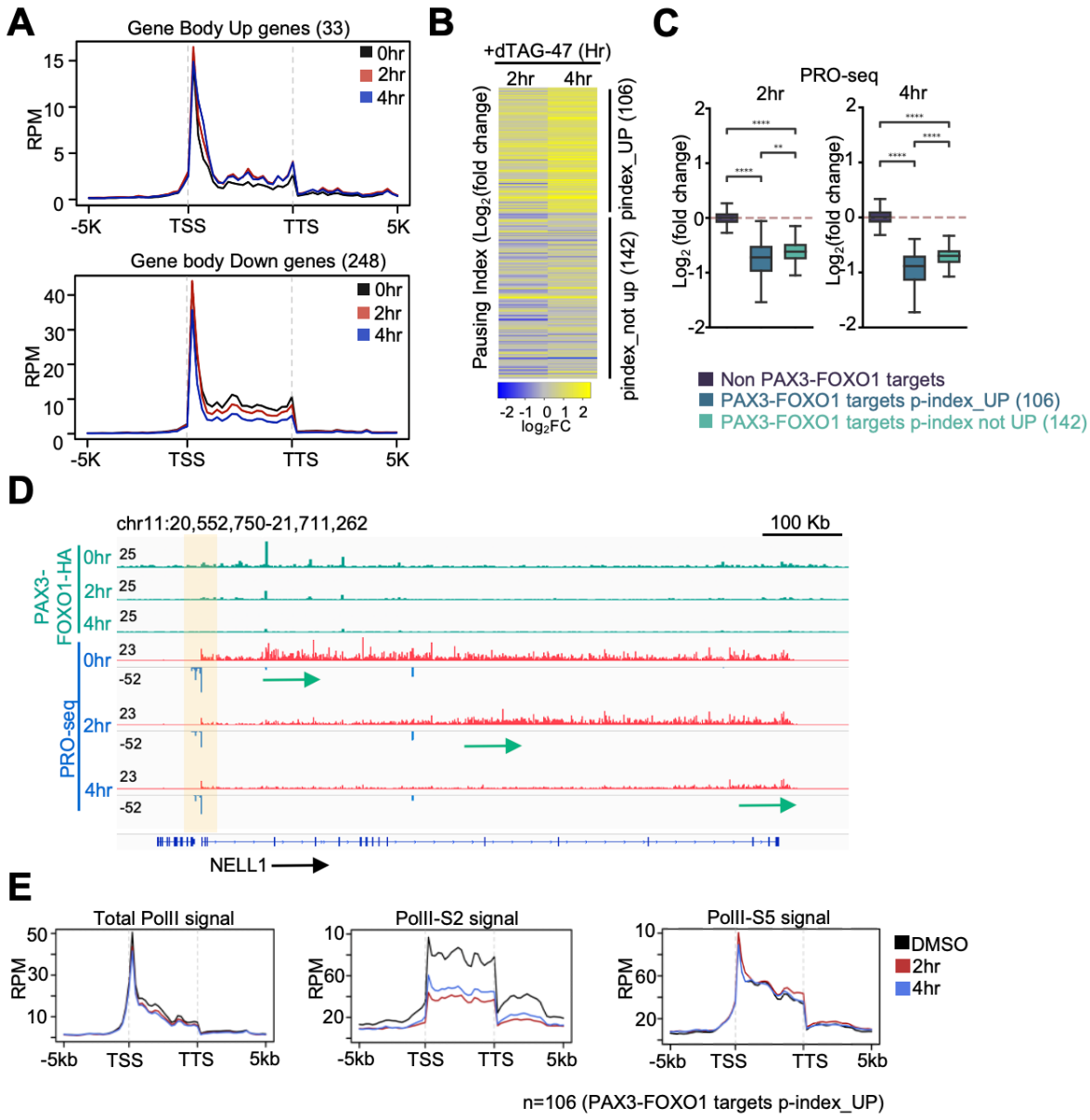

Figure 4.6. PAX3-FOXO1 function to regulate transcription elongation. (A) Metagene plots of PRO-seq reads of all genes with increased (upper) or decreased (bottom) transcription. (B) Heatmap of Log_2 transformed fold change (log_2FC) values of pausing indices of all the genes with down-regulated transcription in at least one time point. (C) Box plots displays the Log_2 transformed fold change (log_2FC) values of PRO-seq at indicated time points (Mann-Whitney U test, *: p <= 5.0e-02, **: p <= 1.0e-02, ***: p <= 1.0e-03, ****: p <= 1.00e-04). (D) Genome browser view of the *NELL1* gene locus showing RNA polymerase pausing and the polymerase moving down the gene (arrows). Green tracks are the CUT&RUN signal before and after degradation of PAX3-FOXO1, which shows a peak at an enhancer within the 1st intron. (E) Metagene plots of ChIP-seq signal

of Pol II, Pol II-S2, Pol II-S5 of all genes with decreased transcription and increased pausing index.

4.2.4 PAX3-FOXO1 maintains active enhancers

Greater than 80% of PAX3-FOXO1 CUT&RUN peaks were localized to intergenic or intronic regions (Fig. 4.7A), suggesting that PAX3-FOXO1 functions at enhancers to regulate gene expression. PRO-seq also detects non-coding nascent transcripts, therefore, NRSA was used to quantify intergenic enhancer RNA (eRNA) transcription following PAX3-FOXO1 degradation (Fig. 4.7B). Within the first 4hr of PAX3-FOXO1 degradation, 305 eRNAs were significantly down-regulated and 289 (96%) of these overlapped with PAX3-FOXO1 binding sites identified by CUT&RUN (Fig. 4.7C). To begin to address the mechanism of regulation at PAX3-FOXO1-regulated enhancers, we performed ChIP-seq for histone H3K27ac (Fig. 4.7D), CUT&RUN for BRD4 (Fig. 3.7E), and ATAC-seq to identify accessible regions (Fig. 4.7F), all of which are hallmarks of active enhancers (Chapuy et al., 2013).

When examining all 44,267 PAX3-FOXO1 bound regions, there was no change in H3K27ac levels, BRD4 occupancy, or chromatin accessibility (Fig. 4.7G, left). However, when we focused on PAX3-FOXO1 peaks associated with changes in eRNA production, we observed a rapid and dramatic reduction in H3K27ac, BRD4 binding, and chromatin accessibility following PAX3-FOXO1 degradation (Fig. 4.7G, right panels). This was despite a similar reduction of PAX3-FOXO1 binding at all sites (Fig. 4.7G, upper panels). This indicated that while PAX3-FOXO1 associates with chromatin at many sites throughout the genome, only a small number of those sites were associated with changes in enhancer function following PAX3-FOXO1 degradation.

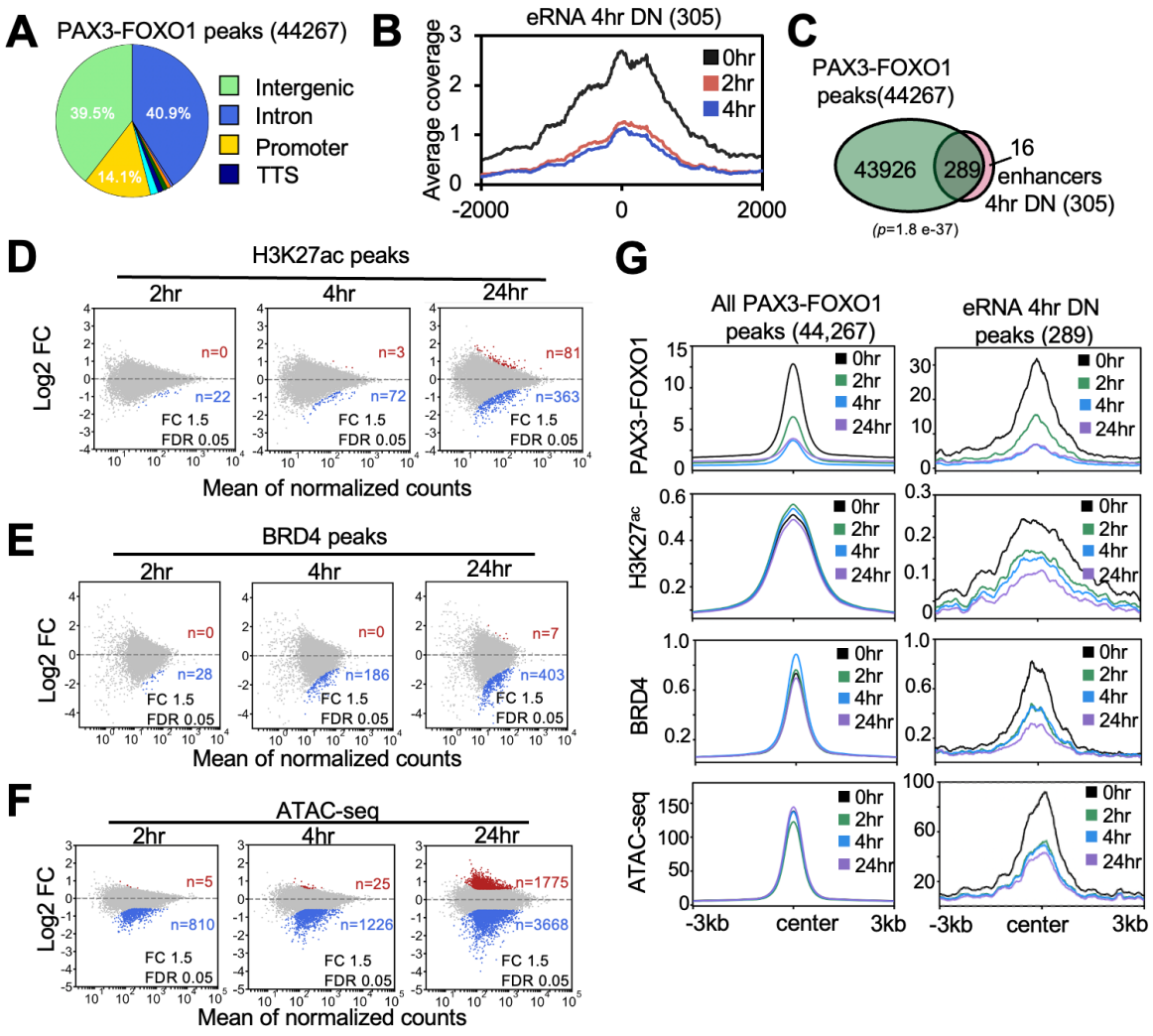

Figure 4.7. PAX3-FOXO1 maintains active enhancers. (A) Pie chart showing annotation of PAX3-FOXO1 peaks with genomic features using HOMER. (B) PRO-seq reads around enhancer centers after PAX3-FOXO1 degradation. (C) Venn diagram showing the overlap between PAX3-FOXO1 peaks and the down-regulated eRNA peaks at 4hr. (D and E) MA-plots of H3K27ac (D) and BRD4 (E) peak changes from 2hr to 24hr after degrading PAX3-FOXO1. (F) MA plots showing ATAC-seq peak changes; red (up) or blue (down) (dTAG-47/DMSO, n = 2). (G) Average signal of PAX3-FOXO1, H3K27ac, BRD4, and ATAC-seq over a 24hr time course of dTAG47 treatment over the regions encompassing all P3F bound sites, those peaks associated with changes in eRNA transcription.

It is notable that changes in eRNA transcription likely underestimate the number of enhancers regulated by PAX3-FOXO1, because it does not include intronic enhancers

that confound the eRNA analysis due to the gene body transcription (Wang et al., 2018). Therefore, given the rapid and robust reduction in chromatin accessibility observed upon PAX3-FOXO1 degradation, we turned to ATAC-Seq to define enhancers regulated by PAX3-FOXO1. At 2 hours following PAX3-FOXO1 degradation in Rh30 cells, loss of chromatin accessibility was observed at 810 regulatory elements, while only 5 elements exhibited an increase in accessibility (Fig. 4.7F). We obtained similar results in Rh4 cells where 1100 sites lost accessibility following degradation of the fusion protein (Fig. 4.8A).

These 810 sites were nearly evenly split between intergenic and intronic sequences (Fig. 4.8B) and showed a rapid and sustained change in accessibility over the 24hr time course of PAX3-FOXO1 degradation (Fig. 4.8C, right panel). Moreover, these 810 ATAC-seq peaks were predominately associated with the most robust PAX3-FOXO1 binding sites located within cluster 1 and cluster 2 (Fig. 4.8D&E). We then annotated these sites to genes that were down-regulated upon PAX3-FOXO1 degradation and found that 163 of the 810 ATAC-seq peaks showed a reduced signal (Fig. 4.8F). Thus, we defined these 163 sites as high-confidence PAX3-FOXO1-regulated enhancers and could associate them with 147 high-confidence PAX3-FOXO1 gene targets. Moreover, these 163 PAX3-FOXO1-regulated enhancers were even further enriched for some of the most robust PAX3-FOXO1 binding sites (Fig. 4.8E), and they highly overlapped with enhancers showing loss of accessibility in Rh4 cells (Fig. 4.8G).

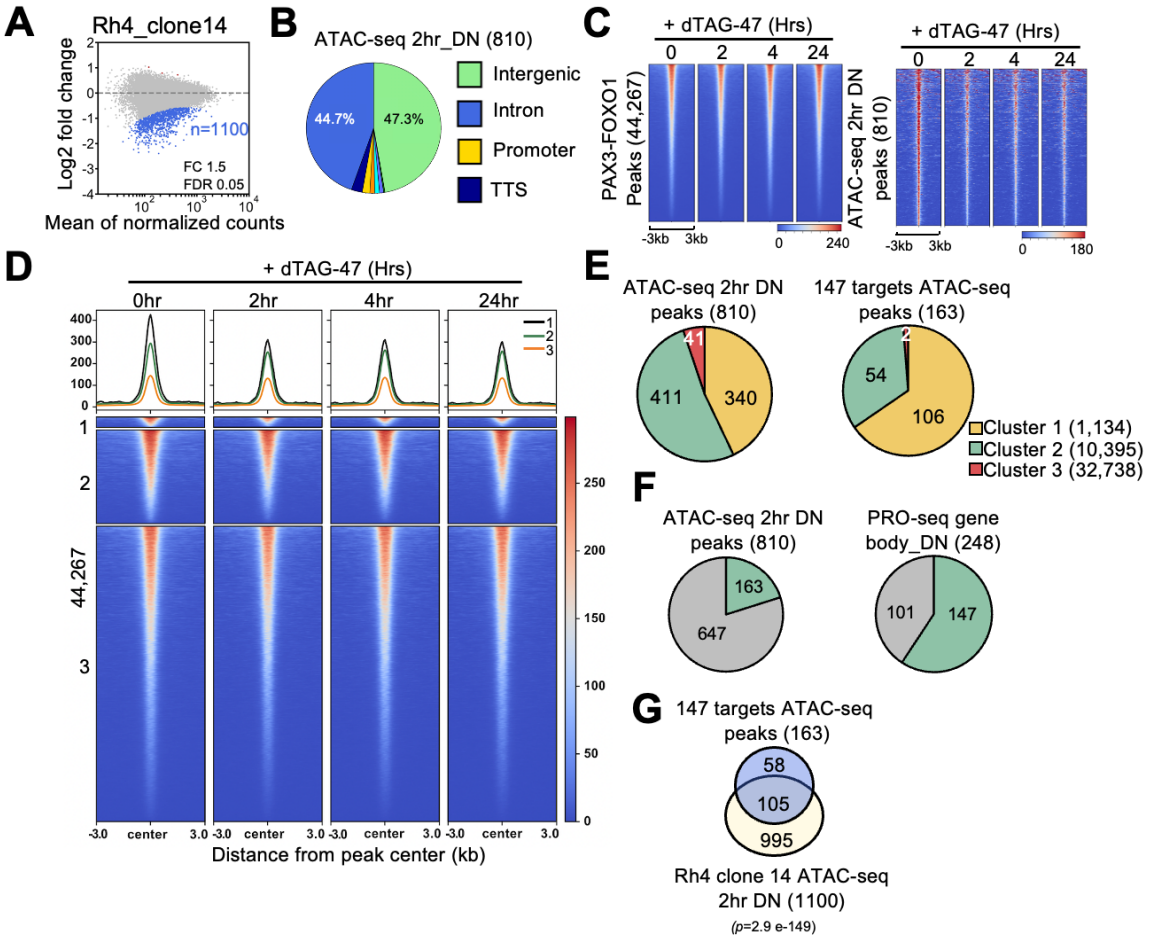

Figure 4.8. Annotation of PAX3-FOXO1regulated elements. (A) MA-plot of ATAC-seq changes in Rh4 clone 14 cells treated with dTAG-47 for 2hr. (B) Pie chart showing the annotation of ATAC-seq peaks that change upon degradation of PAX3-FOXO1 to genomic features in Rh30 cells. (C) Heatmaps of ATAC-seq signal over all PAX3-FOXO1 peaks in 10 bp bins ± 3 Kb from the peak center over the 24hr time course after degrading PAX3-FOXO1. (D) Heat map of the ATAC-seq changes over time from Rh30 cells plotted with respect to the K means clustered PAX3-FOXO1 binding sites from Fig. 3.4A. (E) Pie charts showing the ATAC- seq peaks down-regulated at 2hr after degradation of PAX3-FOXO1 in Rh30 cells (left panel) or associated with the 147 gene changes (right panel) segmented based on K means clustered PAX3-FOXO1 binding sites from Fig. 3.4A. (F) Pie chart showing annotation of down-regulated ATAC-seq peaks with down-regulated genes in PRO-seq. (G) Venn diagram showing the overlap between the 163 ATAC-seq peaks associated with changed genes from Rh30 cells with ATAC-seq changes from Rh4 cells.

PAX3-FOXO1 has been suggested to establish super-enhancers to drive myogenic transcription networks (Gryder et al., 2020; Gryder et al., 2019b; Sunkel et al., 2021). Therefore, we identified super-enhancers based on the BRD4 enrichment (Chapuy et al., 2013; Loven et al., 2013; Pott and Lieb, 2015; Whyte et al., 2013) and asked whether continued PAX3-FOXO1 expression was required to maintain these regulatory structures (Fig. 4.9A). Our analysis identified many of the super-enhancers previously associated with PAX3-FOXO1 function, but the degradation of PAX3-FOXO1 did not affect the eRNA production or ATAC-seq peaks at the super-enhancers of *MYOD1, MYOG*, and *MYCN* which were previously reported to be regulated by PAX3-FOXO1 (Gryder et al., 2017; Gryder et al., 2019b). Moreover, while we did observe PAX3-FOXO1 binding at all three of these super-enhancers (Fig. 4.9B-D), we observed no change in *MYCN* transcription, an increase in *MYOG* transcription, and only a minimal decrease in *MYOD1* transcription at 4 hours, which did not result in altered *MYOD1* mRNA levels by RNA-seq. Moreover, the *MYOD1*, *MYOG* and *MYCN* super-enhancers persisted even 24 hours after PAX3-FOXO1 degradation (Fig. 4.9A), suggesting that PAX3-FOXO1 was not required for their maintenance.

In contrast, we identified super-enhancers whose associated genes were rapidly down-regulated following PAX3-FOXO1 degradation, including *RUNX2*, *KLF4*, *FGGY*, and *PRDM12* (Fig. 4.9A). Interestingly, these super-enhancers fell lower on the BRD4-defined super-enhancer list over time, indicating reductions in BRD4 signal. Manual inspection of each of these super-enhancers showed that they were bound by PAX3-FOXO1, but rather than a complete collapse of the super-enhancer, there was a disruption of select PAX3-FOXO1-bound enhancer elements upon degradation of PAX3-

FOXO1. For instance, the region upstream of *KLF4* and the intronic regions of *FGGY* contained multiple enhancers marked by eRNA production, chromatin accessibility, H3K27ac, and BRD4 binding. However, only one of the enhancer elements (box, Fig. 4.9E for *FGGY* and Fig. 4.9F for *KLF4*) showed a rapid reduction in H3K27ac and BRD4 binding upon PAX3-FOXO1 degradation.

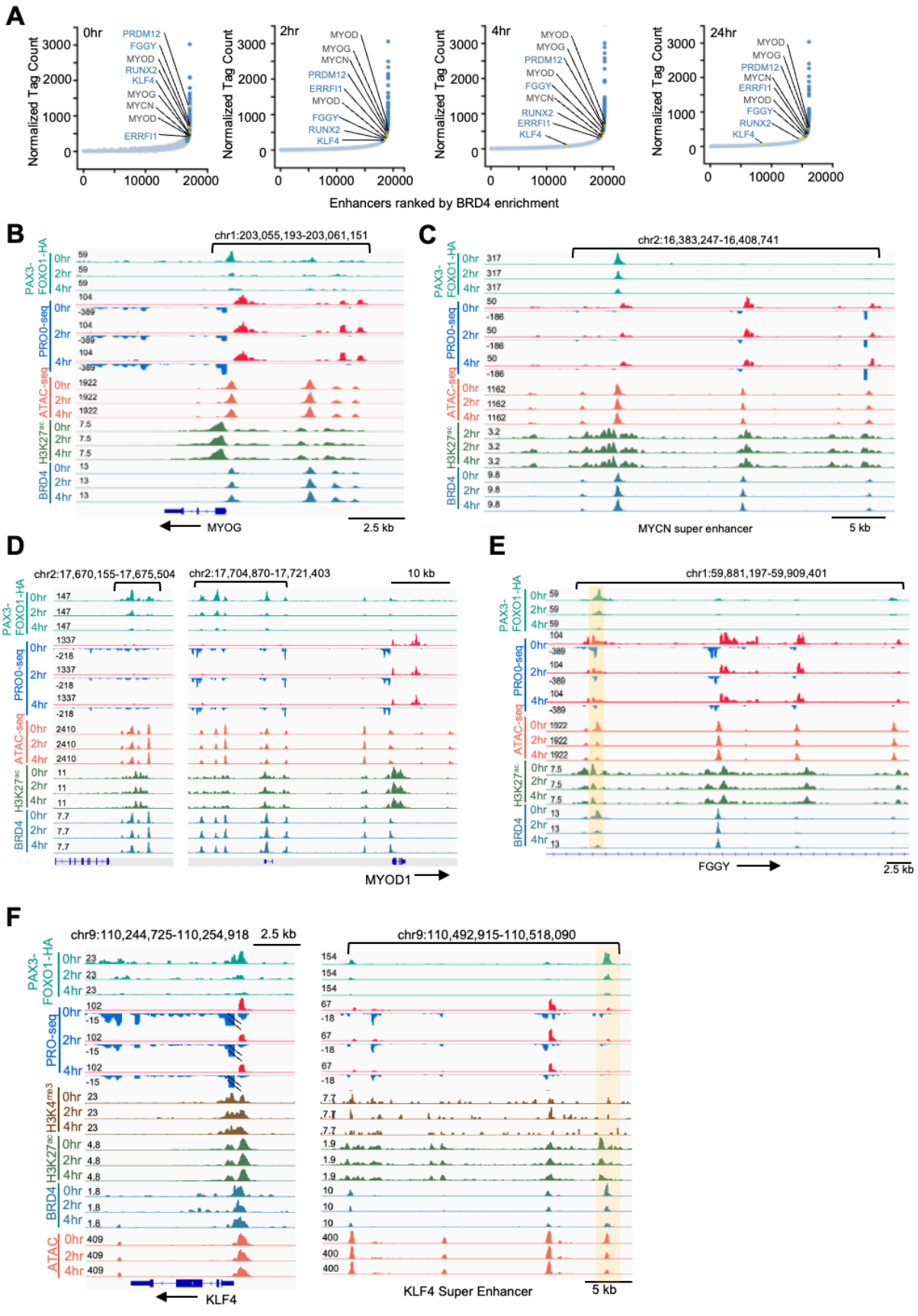
A
0hr
2hr
4hr
24hr
Normalized Tag Count
Enhancers ranked by BRD4 enrichment
PRDM12
FGGY
MYOD
RUNX2
KLF4
MYOG
MYCN
ERRFI1
B
chr1:203,055,193-203,061,151
MYOG
2.5 kb
C
chr2:16,383,247-16,408,741
MYCN super enhancer
5 kb
D
chr2:17,670,155-17,675,504
chr2:17,704,870-17,721,403
10 kb
MYOD1
E
chr1:59,881,197-59,909,401
FGGY
2.5 kb
F
chr9:110,244,725-110,254,918
2.5 kb
KLF4
chr9:110,492,915-110,518,090
KLF4 Super Enhancer
5 kb
PAX3-FOXO1-HA
PRO-seq
ATAC-seq
H3K27ac
BRD4
H3K4me3
ATAC

Figure 4.9. PAX3-FOXO1 is required to maintain super-enhancer structure of its targets. (A) The putative typical-enhancers (light blue) and super-enhancers (dark blue) in Rh30 cells were marked by BRD4 binding at 2, 4, and 24 hrs following P3F degradation. Gold asterisks mark the examples of super-enhancers that are regulated by PAX3-FOXO1, and black + marks the examples of previously identified super-enhancers that were not regulated by PAX3-FOXO1 in our system. (B-F) IGV gene tracks showing the PAX3-FOXO1 CUT&RUN, PRO-seq, ATAC-seq, H3K27ac ChIP-seq, and BRD4 CUR&RUN at the super-enhancers associated with the MYOG (B), MYCN (C), MYOD1 (D), FGGY (E), and KLF4 (F).

Furthermore, we disrupted the enhancers with or without loss of ATAC signal to investigate if individual enhancers within a super-enhancer cluster contribute to target gene expression. Our PRO-seq data indicates that the eRNA synthesis of each enhancer within the super-enhancer cluster is down-regulated (Fig. 4.10A&B, PRO-seq track, comparing enhancer_A and enhancer_B). We next used CRISPR/cas9 to delete a 200 bp-600 bp binding region of the indicated enhancer (Fig. 4.10A&B, enhancer_A and enhancer_B), and verified the deletion by genomic PCR (Fig. 4.10C). After 72hrs of deletion, qPCR was performed to examine the mRNA level of the target gene KLF4 and RUNX2. Interestingly, we see that deletion of both types of enhancers affects the expression of the associated gene (Fig. 4.10D). Meanwhile, the expression of KLF4 and RUNX2 after enhancer deletion is comparable to PAX3-FOXO1 degradation. Further indicating these genes are PAX3-FOXO1 transcriptional targets.

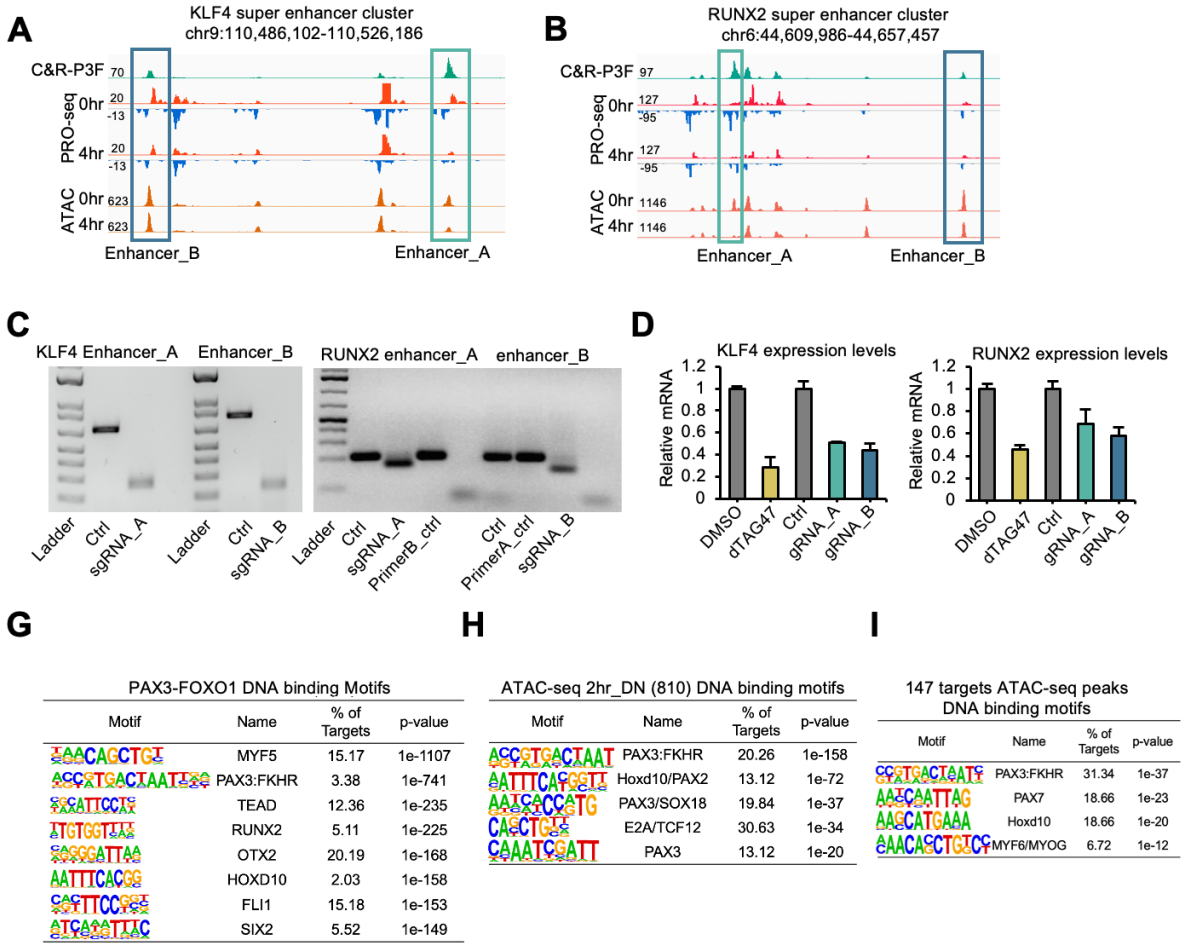

Figure 4.10. Verification of PAX3-FOXO1 regulated enhancer. (A&B) IGV gene tracks showing the PAX3-FOXO1 CUT&RUN, PRO-seq and ATAC-seq at the super-enhancers of KLF4 and RUNX2. (C) Genomic PCR flanking the deleted enhancer region indicated in A and B. Successful deletion generates a smaller PCR product. (D) The bar graph reveals the relative mRNA expression of KLF4 and RUNX2 genes with indicated treatment. Data are mean ± SEM (n=3). (G-I) Motif analysis (de novo) of transcription factors predicted to reside under all PAX3-FOXO1 binding sited from the CUT&RUN data. (G), ATAC-seq peaks that were changed upon PAX3-FOXO1 degradation (H), or at the 147 putative direct targets in Rh30 cells (I).

The fact that we could only confidently assign a function to 163 out of greater than 44,000 PAX3-FOXO1 binding events was surprising. In order to address what might confer functionality to PAX3-FOXO1 chromatin associations, we revisited the motif

analysis and compared all PAX3-FOXO1 bound loci (44,267), those bound loci that showed a reduction in chromatin accessibility (810), or those changes in chromatin accessibility that annotated to PAX3-FOXO1-regulated gene targets (163). While the PAX3-FOXO1 binding motif was only detected at 3% of total PAX3-FOXO1-bound loci, that number increased to 20% at sites that showed reduced accessibility within 2hr of fusion protein degradation, and climbed to 31% at the high-confidence enhancers (a 10-fold enrichment over all binding sites; Fig. 4.10G-I). Thus, PAX3-FOXO1-regulated enhancers were enriched for the best PAX3-FOXO1 binding sites. Moreover, using functional assays for PAX3-FOXO1 (nascent transcription and accessibility) greatly refined the genomic localization data and defined high confidence binding sites at which PAX3-FOXO1 likely acts.

4.2.5 PAX3-FOXO1 recruits complexes involved in transcription

Having identified PAX3-FOXO1-regulated enhancers and target genes, we next sought to define protein complexes that contribute to PAX3-FOXO1-mediated transcription activation at these loci. Previous proteomic analyses of PAX3-FOXO1 relied on overexpression of the fusion protein (Bohm et al., 2016). Therefore, we modified our CRISPR homology-directed repair vector to generate an endogenous PAX3-FOXO1-APEX2 protein fusion. APEX2 is an engineered peroxidase, which creates biotin-phenoxyl radicals that covalently modify nearby proteins (<20 nm)(Hung et al., 2016; Lam et al., 2015; Martell et al., 2012). Thus, proteins in close proximity to PAX3-FOXO1 were purified using streptavidin beads and identified by liquid chromatography coupled with mass spectrometry (LC-MS).

We identified over 500 significantly enriched proteins including components of multiple transcriptional complexes, such as FACT and SWI/SNF, transcription elongation factors (e.g. CDK9, CCNT1, NELFB), and components of a Mediator subcomplex that is associated with transcriptional elongation (Donner et al., 2010) (MED12 and CDK8, Fig. 4.11A-B). Interestingly, while we did not identify an association with BRD4 (Gryder et al., 2017), which was surprising given the colocalization observed at enhancers, we did identify histone acetyltransferases that might place the marks bound by BRD4 (e.g., EP400) (Dey et al., 2003). We also identified other sequence-specific transcription factors, which may cooperate with PAX3-FOXO1 to regulate gene expression, including MYOD, HEB (TCF12), and RUNX1/CBFB (Fig. 4.11A-B). We also used CRISPR/Cas9 to integrate a 3xFLAG tag into the endogenous *PAX3-FOXO1* locus and confirmed a number of these associations by affinity purification using the 3xFLAG tag and LC-MS (Fig. 4.11C-D).

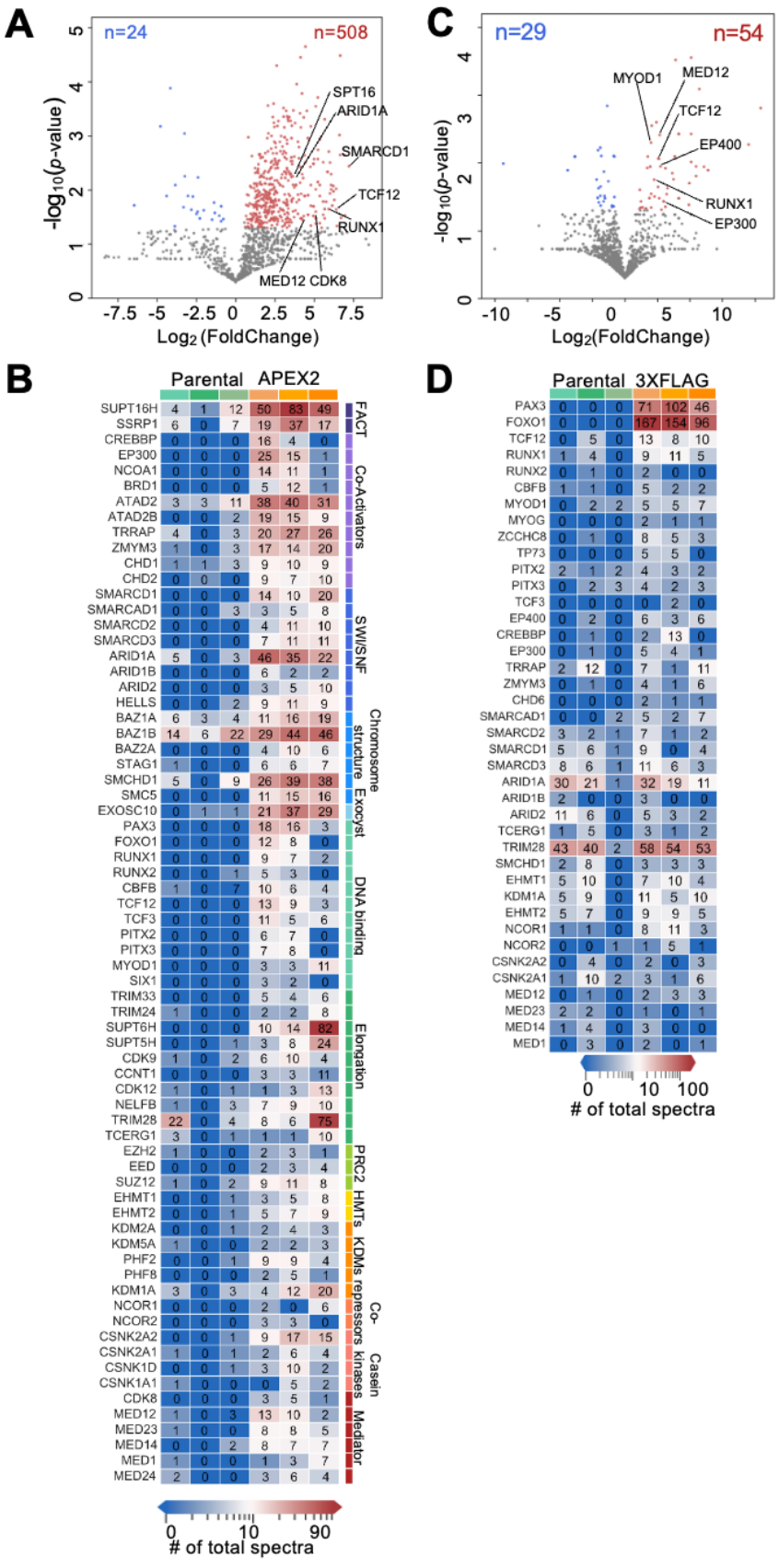
A
n=24
n=508
SPT16
ARID1A
SMARCD1
TCF12
RUNX1
MED12 CDK8
-log10(p-value)
Log2 (FoldChange)
C
n=29
n=54
MYOD1
MED12
TCF12
EP400
RUNX1
EP300
-log10(p-value)
Log2(FoldChange)
B
Parental APEX2
FACT
Co-Activators
SWI/SNF
Chromosome structure
Exocyst
DNA binding
Elongation
PRC2
HMTs
KDMs
repressors
Co-kinases
Casein
Mediator
# of total spectra
D
Parental 3XFLAG
# of total spectra

Figure 4.11. PAX3-FOXO1 recruits complexes involved in transcription. (A) Volcano plot showing log2-fold change (PAX3-FOXO1-APEX2/Parental) vs. -log10 of the p-value generated from the mass spectrometry results of PAX3-FOXO1-APEX2-mediated biotinylation (n=3, one-tail unpaired T-test). Blue dots, enriched in parental samples; red dots, enriched in PAX3-FOXO1-APEX2 samples. (B) Heatmaps of selected PAX3-FOXO1-APEX2 biotinylated proteins from the APEX2-mass spectrometry analysis. Total spectral count is shown within each box. (A) Volcano plot generated from the mass spectrometry results of PAX3-FOXO1-3XFLAG immunoprecipitation/mass spectrometry. Proteins that purified with FLAG-M2 beads were plotted as log2 fold change (PAX3-FOXO1-3xFLAG/Parental) vs. -log10 of the p-value. The absolute 1.5-fold change and p-value 0.05 was used as the threshold (n = 3 biological replicates, *p* calculated using one-tail unpaired T-test). Significant hits are depicted in blue and red to reflect proteins that are enriched in parental samples and PAX3-FOXO1-APEX2 samples, respectively. (B) Heatmaps of selected PAX3-FOXO1-associated proteins from the 3XFLAG analysis. Spectral counts are shown within each box.

Next, we performed CUT&RUN for MYOD1, HEB (TCF12), RUNX1, ARID1A (a SWI/SNF component), SPT16 (FACT component), and CDK8 (Mediator). There was an enrichment of all of these factors at PAX3-FOXO1 binding sites confirming our proteomic analysis (Fig. 4.12A). Therefore, we performed CUT&RUN analysis before and after PAX3-FOXO1 degradation to determine if PAX3-FOXO1 was required to maintain the APEX2-identified complexes at regulated enhancers. While we did not see a global reduction of any of these factors from PAX3-FOXO1 binding sites following PAX3-FOXO1 degradation, we did observe the synchronous loss of all factors from specific PAX3-FOXO1 binding sites associated with the 810 ATAC-seq peaks that were lost upon PAX3-FOXO1 degradation (Fig. 4.12B). These effects were even more pronounced when examining the 163 PAX3-FOXO1-regulated enhancers (Fig. 4.12C, right panels). The enrichment of MYOD1, HEB (TCF12), RUNX1, SPT16, and CDK8 has also been verified

by CUT&RUN in the Rh4 cell line, and there is a decent overlap of each factor in two cell lines (Fig. 4.12D).

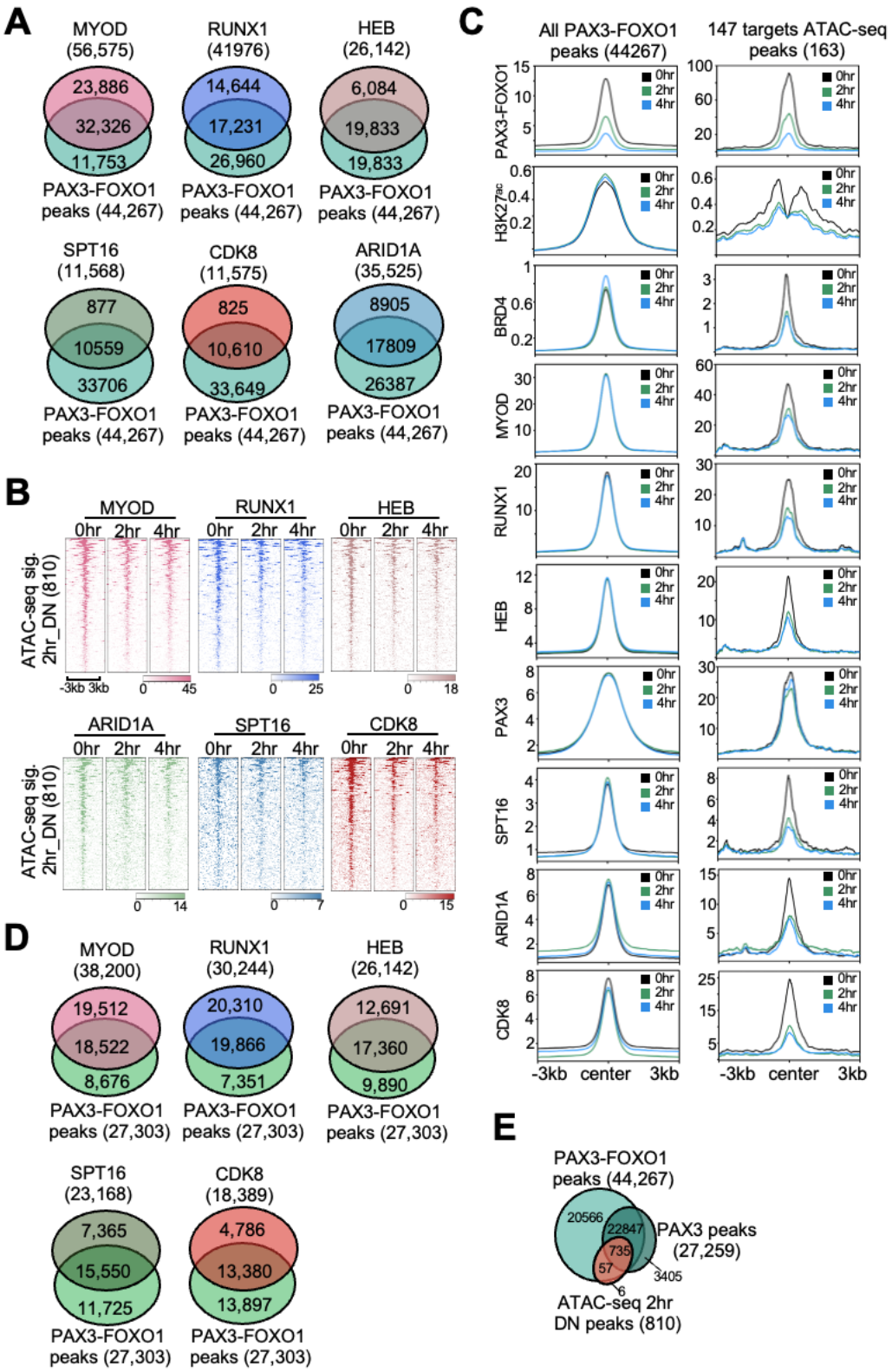
A
MYOD (56,575)
23,886
32,326
11,753
PAX3-FOXO1 peaks (44,267)
RUNX1 (41976)
14,644
17,231
26,960
PAX3-FOXO1 peaks (44,267)
HEB (26,142)
6,084
19,833
19,833
PAX3-FOXO1 peaks (44,267)
SPT16 (11,568)
877
10559
33706
PAX3-FOXO1 peaks (44,267)
CDK8 (11,575)
825
10,610
33,649
PAX3-FOXO1 peaks (44,267)
ARID1A (35,525)
8905
17809
26387
PAX3-FOXO1 peaks (44,267)
B
MYOD
RUNX1
HEB
ARID1A
SPT16
CDK8
0hr 2hr 4hr
ATAC-seq sig. 2hr_DN (810)
-3kb 3kb
0 45
0 25
0 18
0 14
0 7
0 15
C
All PAX3-FOXO1 peaks (44267)
147 targets ATAC-seq peaks (163)
PAX3-FOXO1
H3K27ac
BRD4
MYOD
RUNX1
HEB
PAX3
SPT16
ARID1A
CDK8
0hr
2hr
4hr
-3kb center 3kb
D
MYOD (38,200)
19,512
18,522
8,676
PAX3-FOXO1 peaks (27,303)
RUNX1 (30,244)
20,310
19,866
7,351
PAX3-FOXO1 peaks (27,303)
HEB (26,142)
12,691
17,360
9,890
PAX3-FOXO1 peaks (27,303)
SPT16 (23,168)
7,365
15,550
11,725
PAX3-FOXO1 peaks (27,303)
CDK8 (18,389)
4,786
13,380
13,897
PAX3-FOXO1 peaks (27,303)
E
PAX3-FOXO1 peaks (44,267)
20566
22847
735
57
6
3405
PAX3 peaks (27,259)
ATAC-seq 2hr DN peaks (810)

Figure 4.12. CUT&RUN analysis of factors defined from proteomic data. (A) Venn diagrams display the overlap of MACS2 identified peaks from CUT&RUN analysis between PAX3-FOXO1 and the indicated factor in Rh30 cells. (B) Heatmaps of CUT&RUN signal of the indicated factors around all the 810 changed ATAC-seq peaks from Rh30 cells. (C) Histograms of the CUT&RUN signal of the indicated factors around all PAX3-FOXO1 peaks and the regulated ATAC-seq peaks. (D) Venn diagrams display the overlap of MACS2 identified peaks from CUT&RUN analysis between PAX3-FOXO1 and the indicated factor in Rh4 cells. (E) Venn diagram showing the overlap of PAX3-FOXO1 peaks, PAX3 peaks, and down-regulated ATAC-seq peaks.

Given that the fusion protein binds to the same consensus motif as PAX3, we also asked whether degradation of PAX3-FOXO1 affected DNA binding by PAX3. CUT&RUN analysis using an antibody to the C-terminus of PAX3 showed that PAX3 bound to the same sites as the fusion protein, including those enhancers that showed a decrease in accessibility following PAX3-FOXO1 degradation (Fig. 4.12E). These data suggest that unlike PAX3-FOXO1, PAX3 was not sufficient to maintain chromatin accessibility at these enhancers (Fig. 4.12C). It is also worth noting that, compared with other transcriptional complexes, PAX3 binding was only minimally affected by PAX3-FOXO1 degradation (Fig. 4.12C).

We were surprised to note that enhancer accessibility was so quickly affected at regulated enhancers following dTAG-47 treatment. Therefore, we performed an even shorter ATAC-seq and PRO-seq time course to precisely define how quickly loss of PAX3-FOXO1 affected chromatin accessibility and enhancer activation (eRNA production). While only modest changes in chromatin accessibility were observed 30 min after dTAG-47 treatment, by 1hr chromatin accessibility was reduced at 272 sites and by 2hr the changes mirrored our previous ATAC experiment (909 vs. 810, compare Fig. 4.13A and Fig. 4.7F). In fact, when the sites affected at 2hr were plotted as a heat map

alongside the 30min and 1hr timepoints (Fig. 4.13B), one can see that many of the 909 down-regulated peaks were losing accessibility within the first 30min, but had not reached our significance cut offs (Fig. 4.13B). Similar to the ATAC-seq analysis, PRO-seq analysis identified few changes in gene body transcription in the first 30min after dTAG-47 treatment, but by 1hr, significant changes in gene body transcription were observed (Fig. 4.13C). Combined, the proteomic and genomic data indicate that chromatin was rapidly remodeled following PAX3-FOXO1 degradation, leading to the synchronous loss of transcriptional complexes and the collapse of a small number of discrete enhancer elements, such as that at the *RUNX2* super-enhancer (Fig. 4.13D, shaded box) that ultimately resulted in the loss of transcriptional elongation at PAX3-FOXO1 target genes.

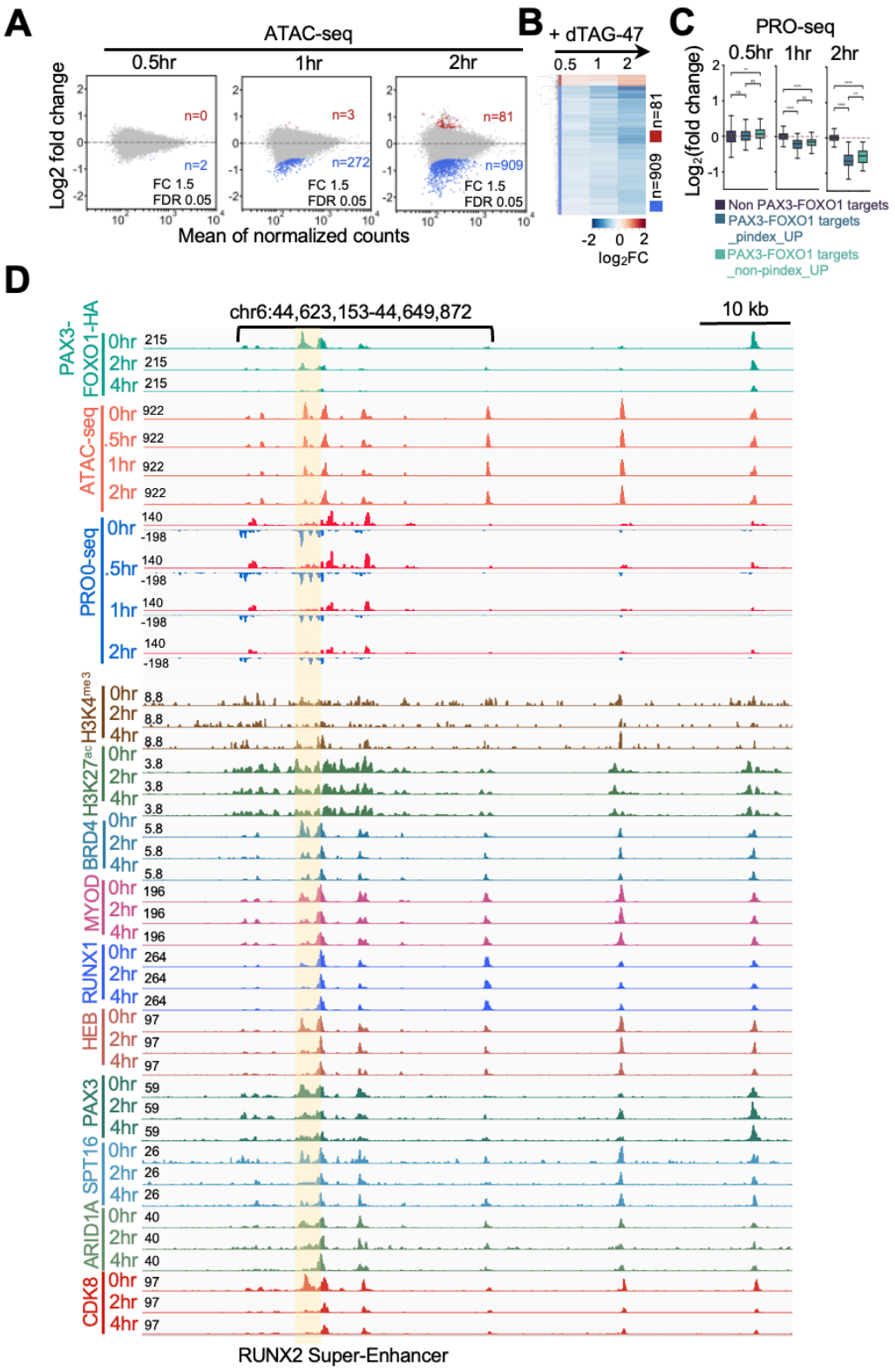

Figure 4.13. PAX3-FOXO1 is required for maintaining open chromatin structure at the regulated enhancers. (A) MA plots showing ATAC-seq peak changes; red (up) or

blue (down) (dTAG-47/DMSO, n = 2). . (B) Heatmap of significant changes in ATAC-seq peaks after a time course of PAX3-FOXO1 degradation. Heatmap is plotted using the peaks significantly changed after a 2hr dTAG-47 treatment. (C) Box plots display the Log_2 transformed fold change (log_2FC) values of PRO-seq at indicated time points (Mann-Whitney U test, *: p <= 5.0e-02, **: p <= 1.0e-02, ***: p <= 1.0e- 03, ****: p <= 1.00e-04). (D) Model integrating the proteomic and genomic data into a hypothetical model by which PAX3-FOXO1 regulates transcription of its target genes. Created with BioRender.com.

4.3 Discussion

Given that transcriptional changes occur rapidly, traditional genetic approaches have failed to effectively define the direct targets of sequence-specific transcription factors, and therefore, have inadequately defined mechanisms of transcriptional control by these proteins (Jaeger and Winter, 2021; Prozzillo et al., 2020). In addition, these slow approaches might miss interpret the activation or repression function of transcription factor action. The RNA-seq shows more than 1,000 genes changed after 24hr of PAX3-FOXO1 degradation, and the changed genes include both up-regulated and down-regulated genes with similar numbers. Thus, CRISPR-based addition of degron tags to endogenous transcription factors has provided a technological breakthrough that is greatly aiding the study of the transcription factor function (Luan et al., 2021; Muhar et al., 2018; Nora et al., 2017; Stengel et al., 2021).

We have applied this approach to an oncogenic fusion transcription factor, PAX3-FOXO1. While we identified over 40,000 PAX3-FOXO1 binding sites throughout the genome, by combining rapid protein degradation with nascent transcript analysis by PRO-seq and enhancer accessibility by ATAC-seq, we determined that PAX3-FOXO1 only activates the transcription of approximately 147 high-confidence gene targets. Among the high-confidence gene targets, there are several key targets that are important for the cell phenotypes after PAX3-FOXO1 degradation. NELL1, RUNX1T1, and FGFR2 is

associated with differentiation. FGF8 supports anchorage independent growth, and FGF8 is reported to be necessary and sufficient to induce PAX3-FOXO1-independent tumor growth through an autocrine mechanism, and also contribute to proliferation and transformation (Boudjadi et al., 2021). The cell cycle inhibition is at least due to the downregulation of RUNX2 and KLF4.

Furthermore, we find that many of the PAX3-FOXO1 targets are regulated at the level of RNA polymerase pause release rather than at the stage of transcription initiation, which defines a new mechanism of PAX3-FOXO1 action. Both of the PRO-seq and Pol II ChIP-seq data show the increasing of paused Pol II at near the transcription started site, and loss of elongated Pol II along the gene body. How PAX3-FOXO1 facilitates Pol II pause release, and the key factors that contribute to PAX3-FOXO1 mediated pause release mechanism is still need to be defined.

Previous studies have postulated that PAX3-FOXO1 possesses pioneer activity, facilitating the establishment of *de novo* enhancer elements that drive myogenic transcriptional programs (Gryder et al., 2017; Sunkel et al., 2021). Indeed, we observed the rapid loss of chromatin accessibility at regulated enhancers following PAX3-FOXO1 degradation. However, these regulated enhancers represented less than 3% of the PAX3-FOXO1 binding sites. Given the high degree of overlap between ATAC-seq peaks and PAX3-FOXO1 binding sites, it appears that PAX3-FOXO1 binds to nucleosome free regions (NFR) throughout the genome, but that the vast majority of these sites do not rely on continued PAX3-FOXO1 expression to maintain accessibility. This could be indicative of a “hit and run” mechanism by which PAX3-FOXO1 establishes the accessible site and then other factors maintain the accessibility, but such a hypothesis is difficult to test.

Another possibility is that genome-wide methods for identifying binding sites for transcription factors are too sensitive and pick up weak sites that are not regulatory. In fact, motif analysis of the CUT&RUN data suggested that most of the binding sites were of poor quality. Alternatively, it is possible that PAX3-FOXO1 works in an alternative manner to open enhancers, possibly binding DNA in concert with other factors such as RUNX1/2, HEB, and MYOD to recruit the SWI/SNF complex in a very selective manner.

We also detected the binding of PAX3-FOXO1 at super-enhancers (Fig. 4.9. However, we did not observe the broad collapse of these super-enhancers following PAX3-FOXO1 degradation, but rather a rapid loss of accessibility at specific enhancer elements within the enhancer cluster. Surprisingly, disruption of a single enhancer at PAX3-FOXO1-bound super-enhancers resulted in a significant loss of gene transcription from the associated promoter (e.g., *RUNX2, KLF4, PRDM12*). In addition, in the same super-enhancer cluster, the deletion of the enhancers without loss of accessibility also results in a loss of gene transcription. We also detected down-regulation of eRNA synthesis at each enhancer within the super-enhancer cluster. These findings are consistent with CRISPR-mediated deletion of individual elements in super-enhancers that identified a hierarchical organization of super-enhancers in which a “hub” enhancer was the major determinant of super-enhancer function (Huang et al., 2018). Having identified a cohort of genes directly regulated by PAX3-FOXO1, we are poised to further define whether the fusion protein triggers the formation of higher order complexes (e.g., nuclear condensates or transcription factories) or acts through individual enhancer elements.

By engineering the endogenous PAX3-FOXO1 for proximity labeling, we identified DNA binding factors and transcriptional complexes that are associated with PAX3-FOXO1 (Fig. 4.11). Among the identified interacting proteins was ARID1A, which could suggest that the continued recruitment of SWI/SNF may be required to maintain the NFR at enhancers to allow full transcriptional complex assembly. Our data also suggests that PAX3, which was bound at these same loci, was not sufficient to maintain open chromatin at these regulatory elements. This raises the possibility that PAX3-FOXO1, and not PAX3, possesses pioneer activity; however, future studies are needed to more rigorously test this hypothesis.

Finally, these data indicate that PAX3-FOXO1 is continuously required to maintain the expression of genes critical for blocking terminal differentiation and to maintain cell viability such as *RUNX2*, *KLF4*, *PRDM12*, *FGF8*, and *FGFR2* and further emphasize the utility of PAX3-FOXO1 as a therapeutic target in rhabdomyosarcoma (Fig. 4.14).

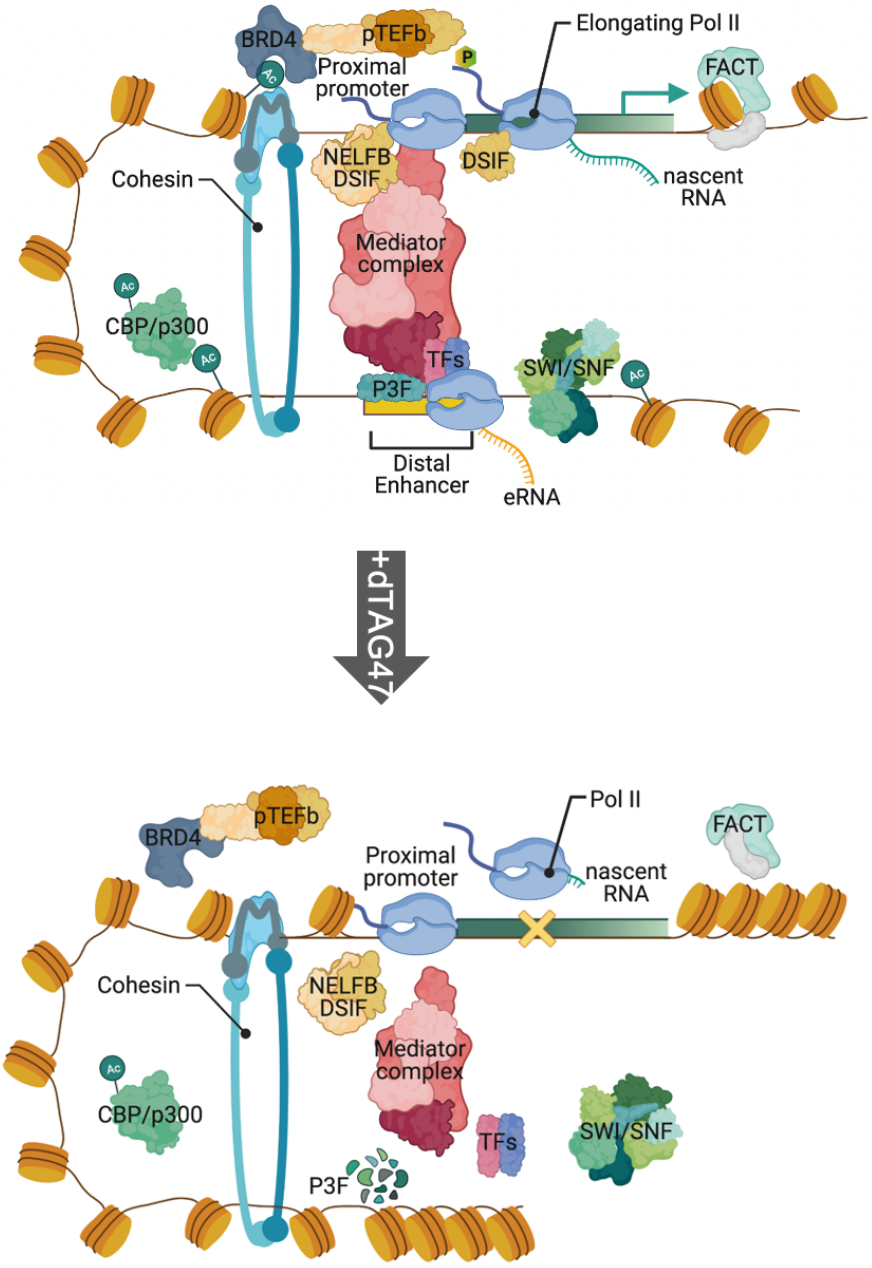

Figure 4.14. Model of PAX3-FOXO1 function at the regulated enhancers. Model integrating the proteomic and genomic data into a hypothetical model by which PAX3-FOXO1 regulates transcription of its target genes. Created with BioRender.com.

CHAPTER 5

Conclusions and future directions

Transcription deregulation is a hallmark of cancer (Bradner et al., 2017). Sequence-specific transcription factors are the essential regulators that recruit different complexes to cause the assembly of the transcription machinery at a gene. In addition, for certain types of cancer, such as aRMS driven by PAX3-FOXO1, the aberrant transcription factor is the main driver, thus making PAX3-FOXO1 the most promising therapeutic target for drug development. Due to the challenge of inhibition of transcription factor, the alternative inhibitory strategies have focused on the transcriptional targets and associated partners of the transcription factor. However, traditional genetic approaches failed to effectively define the direct targets of transcription factors and the mechanism of transcription regulation. This dissertation mainly focuses on a transcription activator, PAX3-FOXO1, to define the mechanism by which it disrupts gene expression programs.

With a specific inhibition of endogenous PAX3-FOXO1 protein, we show that PAX3-FOXO1 degradation triggers growth defect, cell differentiation, apoptosis, and reduced growth in soft agar. These results suggest the development of therapeutic proteolysis targeting chimera molecules of PAX3-FOXO1 for aRMS. In addition, many of the transcriptional target genes defined by our system are associated with these phenotype changes. For example, *NELL1* (neural EGFL like 1), *RUNX1T1* (RUNX1 partner transcriptional co-repressor 1), *FGFR2* (fibroblast growth factor receptor 2) are related to cell differentiation, *KLF4* (kruppel-like factor 4) and *RUNX2* (runt-related

transcription factor 2) is responsible for cell cycle control, and *FGF8* (fibroblast growth factor 8) supports anchorage-independent growth of tumor cells (Mattila et al., 2001; Hasebe et al., 2012; Zou et al., 2015; Choi et al., 2018; Tiwari et al., 2019; Zhai et al., 2019; Han et al., 2019; Zou et al., 2020; Lee et al., 2021; Maehara et al., 2021).

RUNX1 is a transcription factor that is critical for the G1 to S cell cycle transition (Bernardin et al., 2002; Bernardin-Fried et al., 2004), As a member of the same runt family DNA-binding transcription factor with RUNX1, RUNX2 may also have an important role during cell cycle regulation. In addition, RUNX2 is related to the gene associated with phenotype changes mentioned above. NELL1 induces the phosphorylation of RUNX2 by activating the MAPK (mitogen-activated protein kinase) signaling cascade (Bokui et al., 2008). RUNX2 binds the *FGFR2* promoter to regulate FGFR2 expression, while the FGF/FGFR, such as FGFR2 and FGF8, can induce RUNX2 expression in turn (Kim et al., 2003; Guenou et al., 2005; Omoteyama et al., 2009; Kawane et al., 2018). KLF4 is reported to bind with the RUNX2 motif and a direct interaction between KLF4 and RUNX2 is detected (Kim et al., 2014). Therefore, RUNX2 can be a promising target of PAX3-FOXO1 in the future investigation of its function in aRMS.

It is surprising that there are only around 200 genes that are regulated by PAX3-FOXO1, rather than the thousands of genes previously reported, even though it binds over 44,000 genomic sites (Fig. 4.4 and 4.5). In addition, after PAX3-FOXO1 degradation, there are only ~800 regulatory elements that show a loss of chromatin accessibility, and among these peaks, 163 sites are annotated to 147 genes with high confidence. For the rest of ~ 600 regulatory elements that are defined by ATAC-seq and cannot be assigned, their associated genes and how they contribute to target gene regulation are still unclear

and need further investigation. One possible way might be that they regulated the associated genes by 3D chromatin interaction which needs to be measured by Hi-C to identify promoter-enhancer interactions.

The identification of 147 target genes from 43,000 genome binding sites, which are annotated to 15,000 genes, suggests the importance of using functional assays to study transcription factor regulatory mechanisms. On the other hand, the function of the other 44,000 PAX3-FOXO1 binding sites is still unknown. It is possible that these PAX3-FOXO1 binding sites are sensitively detected due to indirect effects such as enhancer-promoter contacts. Since some of these sites are very robust (Fig. 4.4, cluster 1 and cluster 2), it is also possible that they are involved in other regulatory mechanisms other than transcription. It would be helpful if there is a way to distinguish the functional sites by the DNA sequences. Therefore, statistical and machine learning-based methods might be a great tool to predict the functional regulatory element of a transcription factor (Mochida et al., 2018; Razaghi-Moghadam et al., 2020).

While PAX3-FOXO1 binds to multiple enhancer elements within super-enhancer cluster, its continued presence was only required at individual enhancer elements (Fig. 4.9). In addition, the deletion of enhancers with or without loss of accessibility both results in a loss of gene transcription (Fig. 4.10). The mechanisms of how individual enhancers within super-enhancer affect each other, and how they function as a group to regulate transcription need further studies to uncover how they act. A more detailed investigation to delete every enhancer in the same cluster or outside the cluster, even a non-regulatory element nearby would provide some hints for this question.

There are ~500 more proteins that are associated with PAX3-FOXO1 in addition to the DNA binding factors and transcriptional complexes reported in Chapter 4. Therefore, more work is necessary to further narrow down the key partners that contribute to PAX3-FOXO1-mediated transcriptional control. CRISPR-Cas9-mediated deletion could be used to rapidly screen the key partners to identify of additional therapeutic targets. Aligning the proteomic data with the RMS Dependency map (Dharia et al., 2021) has already provided some clues for combination targeting, such as deleting several genes in the same complex or genes in several different complexes according to the dependency scores. Also, the identified PAX3-FOXO1 core target genes can be a group of reporter genes to evaluate the effects of inhibiting therapeutic targets, as an alternative to examining the cell growth defect or differentiation after days.

In conclusion, the endogenous PAX3-FOXO1 degradation using dTAG system provides a system to study the detailed transcriptional regulation mechanism of almost every transcription factor. With the identification of direct transcriptional targets of the transcription factor, one can use these loci to define the molecular mechanism of action of the factor. For fusion-positive aRMS, my data supports the idea that PAX3-FOXO1 contributes to aRMS tumor development, and that PAX3-FOXO1 is a critical regulator of cell proliferation and impairs myogenic differentiation. It is primarily an activator of transcription that works by recruiting SWI/SNF, mediator and elongation machinery to tigger the expression of a small cohort of genes critical for tumor development. Most importantly, my work establishes that PAX3-FOXO1 is a promising therapeutic target for PROTAC development.

References

Adachi M, Osawa Y, Uchinami H, Kitamura T, Accili D, Brenner DA. The forkhead transcription factor FoxO1 regulates proliferation and transdifferentiation of hepatic stellate cells. Gastroenterology. 2007 Apr;132(4):1434-46. doi: 10.1053/j.gastro.2007.01.033. Epub 2007 Jan 25. PMID: 17408630.

Adelman K, Lis JT. Promoter-proximal pausing of RNA polymerase II: emerging roles in metazoans. Nat Rev Genet. 2012 Oct;13(10):720-31. doi: 10.1038/nrg3293. PMID: 22986266; PMCID: PMC3552498.

Affer M, Chesi M, Chen WG, Keats JJ, Demchenko YN, Roschke AV, Van Wier S, Fonseca R, Bergsagel PL, Kuehl WM. Promiscuous MYC locus rearrangements hijack enhancers but mostly super-enhancers to dysregulate MYC expression in multiple myeloma. Leukemia. 2014 Aug;28(8):1725-1735. doi: 10.1038/leu.2014.70. Epub 2014 Feb 12. PMID: 24518206; PMCID: PMC4126852.

Ahn EH, Mercado GE, Laé M, Ladanyi M. Identification of target genes of PAX3-FOXO1 in alveolar rhabdomyosarcoma. Oncol Rep. 2013 Aug;30(2):968-78. doi: 10.3892/or.2013.2513. Epub 2013 Jun 3. PMID: 23733015; PMCID: PMC3776721.

Akaike K, Suehara Y, Kohsaka S, Hayashi T, Tanabe Y, Kazuno S, Mukaihara K, Toda-Ishii M, Kurihara T, Kim Y, Okubo T, Hayashi Y, Takamochi K, Takahashi F, Kaneko K, Ladanyi M, Saito T. *PPP2R1A* regulated by PAX3/FOXO1 fusion contributes to the acquisition of aggressive behavior in PAX3/FOXO1-positive alveolar rhabdomyosarcoma. Oncotarget. 2018 May 18;9(38):25206-25215. doi: 10.18632/oncotarget.25392. PMID: 29861864; PMCID: PMC5982774.

Amann JM, Nip J, Strom DK, Lutterbach B, Harada H, Lenny N, Downing JR, Meyers S, Hiebert SW. ETO, a target of t(8;21) in acute leukemia, makes distinct contacts with multiple histone deacetylases and binds mSin3A through its oligomerization domain. Mol Cell Biol. 2001 Oct;21(19):6470-83. doi: 10.1128/MCB.21.19.6470-6483.2001. PMID: 11533236; PMCID: PMC99794.

Anderson J, Ramsay A, Gould S, Pritchard-Jones K. PAX3-FKHR induces morphological change and enhances cellular proliferation and invasion in rhabdomyosarcoma. Am J Pathol. 2001 Sep;159(3):1089-96. doi: 10.1016/S0002-9440(10)61784-1. PMID: 11549601; PMCID: PMC1850440.

Bai L, Zhou H, Xu R, Zhao Y, Chinnaswamy K, McEachern D, Chen J, Yang CY, Liu Z, Wang M, Liu L, Jiang H, Wen B, Kumar P, Meagher JL, Sun D, Stuckey JA, Wang S. A Potent and Selective Small-Molecule Degrader of STAT3 Achieves Complete Tumor Regression In Vivo. Cancer Cell. 2019 Nov 11;36(5):498-511.e17. doi: 10.1016/j.ccell.2019.10.002. PMID: 31715132; PMCID: PMC6880868.

Barger CJ, Branick C, Chee L, Karpf AR. Pan-Cancer Analyses Reveal Genomic Features of FOXM1 Overexpression in Cancer. Cancers (Basel). 2019 Feb 21;11(2):251. doi: 10.3390/cancers11020251. PMID: 30795624; PMCID: PMC6406812.

Barr FG, Galili N, Holick J, Biegel JA, Rovera G, Emanuel BS. Rearrangement of the PAX3 paired box gene in the paediatric solid tumour alveolar rhabdomyosarcoma. Nat Genet. 1993 Feb;3(2):113-7. doi: 10.1038/ng0293-113. PMID: 8098985.

Bartholomeeusen K, Fujinaga K, Xiang Y, Peterlin BM. Histone deacetylase inhibitors (HDACis) that release the positive transcription elongation factor b (P-TEFb) from its inhibitory complex also activate HIV transcription. J Biol Chem. 2013 May 17;288(20):14400-14407. doi: 10.1074/jbc.M113.464834. Epub 2013 Mar 28. PMID: 23539624; PMCID: PMC3656295.

Bartkowiak B, Liu P, Phatnani HP, Fuda NJ, Cooper JJ, Price DH, Adelman K, Lis JT, Greenleaf AL. CDK12 is a transcription elongation-associated CTD kinase, the metazoan ortholog of yeast Ctk1. Genes Dev. 2010 Oct 15;24(20):2303-16. doi: 10.1101/gad.1968210. PMID: 20952539; PMCID: PMC2956209.

Batt DB, Luo Y, Carmichael GG. Polyadenylation and transcription termination in gene constructs containing multiple tandem polyadenylation signals. Nucleic Acids Res. 1994 Jul 25;22(14):2811-6. doi: 10.1093/nar/22.14.2811. PMID: 7519768; PMCID: PMC308251.

Battiprolu PK, Hojayev B, Jiang N, Wang ZV, Luo X, Iglewski M, Shelton JM, Gerard RD, Rothermel BA, Gillette TG, Lavandero S, Hill JA. Metabolic stress-induced activation of FoxO1 triggers diabetic cardiomyopathy in mice. J Clin Invest. 2012 Mar;122(3):1109-18. doi: 10.1172/JCI60329. Epub 2012 Feb 13. PMID: 22326951; PMCID: PMC3287230.

Bejerano G, Lowe CB, Ahituv N, King B, Siepel A, Salama SR, Rubin EM, Kent WJ, Haussler D. A distal enhancer and an ultraconserved exon are derived from a novel retroposon. Nature. 2006 May 4;441(7089):87-90. doi: 10.1038/nature04696. Epub 2006 Apr 16. PMID: 16625209.

Belotserkovskaya R, Oh S, Bondarenko VA, Orphanides G, Studitsky VM, Reinberg D. FACT facilitates transcription-dependent nucleosome alteration. Science. 2003 Aug 22;301(5636):1090-3. doi: 10.1126/science.1085703. PMID: 12934006.

Bennicelli JL, Advani S, Schäfer BW, Barr FG. PAX3 and PAX7 exhibit conserved cis-acting transcription repression domains and utilize a common gain of function mechanism in alveolar rhabdomyosarcoma. Oncogene. 1999 Jul 29;18(30):4348-56. doi: 10.1038/sj.onc.1202812. PMID: 10439042.

Bennicelli JL, Fredericks WJ, Wilson RB, Rauscher FJ 3rd, Barr FG. Wild type PAX3 protein and the PAX3-FKHR fusion protein of alveolar rhabdomyosarcoma contain potent, structurally distinct transcriptional activation domains. Oncogene. 1995 Jul 6;11(1):119-30. PMID: 7624119.

Benveniste D, Sonntag HJ, Sanguinetti G, Sproul D. Transcription factor binding predicts histone modifications in human cell lines. Proc Natl Acad Sci U S A. 2014 Sep 16;111(37):13367-72. doi: 10.1073/pnas.1412081111. Epub 2014 Sep 3. PMID: 25187560; PMCID: PMC4169916.

Berg T, Fliegauf M, Burger J, Staege MS, Liu S, Martinez N, Heidenreich O, Burdach S, Haferlach T, Werner MH, Lübbert M. Transcriptional upregulation of p21/WAF/Cip1 in myeloid leukemic blasts expressing AML1-ETO. Haematologica. 2008 Nov;93(11):1728-33. doi: 10.3324/haematol.13044. Epub 2008 Sep 11. PMID: 18790797.

Bernardin F, Friedman AD. AML1 stimulates G1 to S progression via its transactivation domain. Oncogene. 2002 May 9;21(20):3247-52. doi: 10.1038/sj.onc.1205447. PMID: 12082641.

Bernardin-Fried F, Kummalue T, Leijen S, Collector MI, Ravid K, Friedman AD. AML1/RUNX1 increases during G1 to S cell cycle progression independent of cytokine-dependent phosphorylation and induces cyclin D3 gene expression. J Biol Chem. 2004 Apr 9;279(15):15678-87. doi: 10.1074/jbc.M310023200. Epub 2004 Jan 27. PMID: 14747476.

Blackwell TK, Kretzner L, Blackwood EM, Eisenman RN, Weintraub H. Sequence-specific DNA binding by the c-Myc protein. Science. 1990 Nov 23;250(4984):1149-51. doi: 10.1126/science.2251503. PMID: 2251503.

Blazek D, Kohoutek J, Bartholomeeusen K, Johansen E, Hulinkova P, Luo Z, Cimermancic P, Ule J, Peterlin BM. The Cyclin K/Cdk12 complex maintains genomic stability via regulation of expression of DNA damage response genes. Genes Dev. 2011 Oct 15;25(20):2158-72. doi: 10.1101/gad.16962311. PMID: 22012619; PMCID: PMC3205586.

Blümli S, Wiechens N, Wu MY, Singh V, Gierlinski M, Schweikert G, Gilbert N, Naughton C, Sundaramoorthy R, Varghese J, Gourlay R, Soares R, Clark D, Owen-Hughes T. Acute depletion of the ARID1A subunit of SWI/SNF complexes reveals distinct pathways for activation and repression of transcription. Cell Rep. 2021 Nov 2;37(5):109943. doi: 10.1016/j.celrep.2021.109943. PMID: 34731603; PMCID: PMC8578704.

Böhm M, Wachtel M, Marques JG, Streiff N, Laubscher D, Nanni P, Mamchaoui K, Santoro R, Schäfer BW. Helicase CHD4 is an epigenetic coregulator of PAX3-FOXO1 in alveolar rhabdomyosarcoma. J Clin Invest. 2016 Nov 1;126(11):4237-4249. doi: 10.1172/JCI85057. Epub 2016 Oct 17. PMID: 27760049; PMCID: PMC5096911.

Bokui N, Otani T, Igarashi K, Kaku J, Oda M, Nagaoka T, Seno M, Tatematsu K, Okajima T, Matsuzaki T, Ting K, Tanizawa K, Kuroda S. Involvement of MAPK signaling molecules and Runx2 in the NELL1-induced osteoblastic differentiation. FEBS Lett. 2008 Jan 23;582(2):365-71. doi: 10.1016/j.febslet.2007.12.006. Epub 2007 Dec 17. PMID: 18082140; PMCID: PMC2959102.

Borsari B, Villegas-Mirón P, Pérez-Lluch S, Turpin I, Laayouni H, Segarra-Casas A, Bertranpetit J, Guigó R, Acosta S. Enhancers with tissue-specific activity are enriched in intronic regions. Genome Res. 2021 Aug;31(8):1325-1336. doi: 10.1101/gr.270371.120. Epub 2021 Jul 21. PMID: 34290042; PMCID: PMC8327915.

Boudjadi S, Pandey PR, Chatterjee B, Nguyen TH, Sun W, Barr FG. A Fusion Transcription Factor-Driven Cancer Progresses to a Fusion-Independent Relapse via Constitutive Activation of a Downstream Transcriptional Target. Cancer Res. 2021 Jun 1;81(11):2930-2942. doi: 10.1158/0008-5472.CAN-20-1613. Epub 2021 Feb 15. PMID: 33589519; PMCID: PMC8178207.

Bourbon HM. Comparative genomics supports a deep evolutionary origin for the large, four-module transcriptional mediator complex. Nucleic Acids Res. 2008 Jul;36(12):3993-4008. doi: 10.1093/nar/gkn349. Epub 2008 May 31. PMID: 18515835; PMCID: PMC2475620.

Boveri, Theodor. *Zur frage der entstehung maligner tumoren*. Fischer, 1914.

Bradner JE, Hnisz D, Young RA. Transcriptional Addiction in Cancer. Cell. 2017 Feb 9;168(4):629-643. doi: 10.1016/j.cell.2016.12.013. PMID: 28187285; PMCID: PMC5308559.

Brunet A, Sweeney LB, Sturgill JF, Chua KF, Greer PL, Lin Y, Tran H, Ross SE, Mostoslavsky R, Cohen HY, Hu LS, Cheng HL, Jedrychowski MP, Gygi SP, Sinclair DA, Alt FW, Greenberg ME. Stress-dependent regulation of FOXO transcription factors by the SIRT1 deacetylase. Science. 2004 Mar 26;303(5666):2011-5. doi: 10.1126/science.1094637. Epub 2004 Feb 19. PMID: 14976264.

Budry L, Balsalobre A, Gauthier Y, Khetchoumian K, L'honoré A, Vallette S, Brue T, Figarella-Branger D, Meij B, Drouin J. The selector gene Pax7 dictates alternate pituitary cell fates through its pioneer action on chromatin remodeling. Genes Dev. 2012 Oct 15;26(20):2299-310. doi: 10.1101/gad.200436.112. PMID: 23070814; PMCID: PMC3475802.

Buenrostro JD, Wu B, Chang HY, Greenleaf WJ. ATAC-seq: A Method for Assaying Chromatin Accessibility Genome-Wide. Curr Protoc Mol Biol. 2015 Jan 5;109:21.29.1-21.29.9. doi: 10.1002/0471142727.mb2129s109. PMID: 25559105; PMCID: PMC4374986.

Burslem GM, Crews CM. Proteolysis-Targeting Chimeras as Therapeutics and Tools for Biological Discovery. Cell. 2020 Apr 2;181(1):102-114. doi: 10.1016/j.cell.2019.11.031. Epub 2020 Jan 16. PMID: 31955850; PMCID: PMC7319047.

Bushweller JH. Targeting transcription factors in cancer - from undruggable to reality. Nat Rev Cancer. 2019 Nov;19(11):611-624. doi: 10.1038/s41568-019-0196-7. Epub 2019 Sep 11. PMID: 31511663; PMCID: PMC8820243.

Cai Y, Zhang Y, Loh YP, Tng JQ, Lim MC, Cao Z, Raju A, Lieberman Aiden E, Li S, Manikandan L, Tergaonkar V, Tucker-Kellogg G, Fullwood MJ. H3K27me3-rich genomic regions can function as silencers to repress gene expression via chromatin interactions. Nat Commun. 2021 Jan 29;12(1):719. doi: 10.1038/s41467-021-20940-y. PMID: 33514712; PMCID: PMC7846766.

Calhoun VC, Stathopoulos A, Levine M. Promoter-proximal tethering elements regulate enhancer-promoter specificity in the Drosophila Antennapedia complex. Proc Natl Acad Sci U S A. 2002 Jul 9;99(14):9243-7. doi: 10.1073/pnas.142291299. Epub 2002 Jul 1. PMID: 12093913; PMCID: PMC123125.

Calo E, Wysocka J. Modification of enhancer chromatin: what, how, and why? Mol Cell. 2013 Mar 7;49(5):825-37. doi: 10.1016/j.molcel.2013.01.038. PMID: 23473601; PMCID: PMC3857148.

Cao L, Yu Y, Bilke S, Walker RL, Mayeenuddin LH, Azorsa DO, Yang F, Pineda M, Helman LJ, Meltzer PS. Genome-wide identification of PAX3-FKHR binding sites in rhabdomyosarcoma reveals candidate target genes important for development and cancer. Cancer Res. 2010 Aug 15;70(16):6497-508. doi: 10.1158/0008-5472.CAN-10-0582. Epub 2010 Jul 27. PMID: 20663909; PMCID: PMC2922412.

Carroll M, Tomasson MH, Barker GF, Golub TR, Gilliland DG. The TEL/platelet-derived growth factor beta receptor (PDGF beta R) fusion in chronic myelomonocytic leukemia is a transforming protein that self-associates and activates PDGF beta R kinase-dependent signaling pathways. Proc Natl Acad Sci U S A. 1996 Dec

10;93(25):14845-50. doi: 10.1073/pnas.93.25.14845. PMID: 8962143; PMCID: PMC26224.

Chalepakis G, Jones FS, Edelman GM, Gruss P. Pax-3 contains domains for transcription activation and transcription inhibition. Proc Natl Acad Sci U S A. 1994 Dec 20;91(26):12745-9. doi: 10.1073/pnas.91.26.12745. PMID: 7809114; PMCID: PMC45516.

Chapuy B, McKeown MR, Lin CY, Monti S, Roemer MG, Qi J, Rahl PB, Sun HH, Yeda KT, Doench JG, Reichert E, Kung AL, Rodig SJ, Young RA, Shipp MA, Bradner JE. Discovery and characterization of super-enhancer-associated dependencies in diffuse large B cell lymphoma. Cancer Cell. 2013 Dec 9;24(6):777-90. doi: 10.1016/j.ccr.2013.11.003. Erratum in: Cancer Cell. 2014 Apr 14;25(4):545-6. PMID: 24332044; PMCID: PMC4018722.

Charles Richard JL, Shukla MS, Menoni H, Ouararhni K, Lone IN, Roulland Y, Papin C, Ben Simon E, Kundu T, Hamiche A, Angelov D, Dimitrov S. FACT Assists Base Excision Repair by Boosting the Remodeling Activity of RSC. PLoS Genet. 2016 Jul 28;12(7):e1006221. doi: 10.1371/journal.pgen.1006221. PMID: 27467129; PMCID: PMC4965029.

Chen JL, Attardi LD, Verrijzer CP, Yokomori K, Tjian R. Assembly of recombinant TFIID reveals differential coactivator requirements for distinct transcriptional activators. Cell. 1994 Oct 7;79(1):93-105. doi: 10.1016/0092-8674(94)90403-0. PMID: 7923382.

Choi H, Roh J. Role of *Klf4* in the Regulation of Apoptosis and Cell Cycle in Rat Granulosa Cells during the Periovulatory Period. Int J Mol Sci. 2018 Dec 26;20(1):87. doi: 10.3390/ijms20010087. PMID: 30587813; PMCID: PMC6337711.

Choi PS, Li Y, Felsher DW. Addiction to multiple oncogenes can be exploited to prevent the emergence of therapeutic resistance. Proc Natl Acad Sci U S A. 2014 Aug 12;111(32):E3316-24. doi: 10.1073/pnas.1406123111. Epub 2014 Jul 28. PMID: 25071175; PMCID: PMC4136575.

Cirillo LA, Lin FR, Cuesta I, Friedman D, Jarnik M, Zaret KS. Opening of compacted chromatin by early developmental transcription factors HNF3 (FoxA) and GATA-4. Mol Cell. 2002 Feb;9(2):279-89. doi: 10.1016/s1097-2765(02)00459-8. PMID: 11864602.

Clark VE, Harmancı AS, Bai H, Youngblood MW, Lee TI, Baranoski JF, Ercan-Sencicek AG, Abraham BJ, Weintraub AS, Hnisz D, Simon M, Krischek B, Erson-Omay EZ, Henegariu O, Carrión-Grant G, Mishra-Gorur K, Durán D, Goldmann JE, Schramm J, Goldbrunner R, Piepmeier JM, Vortmeyer AO, Günel JM, Bilgüvar K, Yasuno K, Young RA, Günel M. Recurrent somatic mutations in POLR2A define a distinct subset of meningiomas. Nat Genet. 2016 Oct;48(10):1253-9. doi: 10.1038/ng.3651. Epub 2016 Aug 22. PMID: 27548314; PMCID: PMC5114141.

Collins MH, Zhao H, Womer RB, Barr FG. Proliferative and apoptotic differences between alveolar rhabdomyosarcoma subtypes: a comparative study of tumors containing PAX3-FKHR or PAX7-FKHR gene fusions. Med Pediatr Oncol. 2001 Aug;37(2):83-9. doi: 10.1002/mpo.1174. PMID: 11496344.

Collins SJ, Groudine MT. Rearrangement and amplification of c-abl sequences in the human chronic myelogenous leukemia cell line K-562. Proc Natl Acad Sci U S A.

1983 Aug;80(15):4813-7. doi: 10.1073/pnas.80.15.4813. PMID: 6308652; PMCID: PMC384135.

Connelly S, Manley JL. A functional mRNA polyadenylation signal is required for transcription termination by RNA polymerase II. Genes Dev. 1988 Apr;2(4):440-52. doi: 10.1101/gad.2.4.440. PMID: 2836265.

Costa IG, Roider HG, do Rego TG, de Carvalho Fde A. Predicting gene expression in T cell differentiation from histone modifications and transcription factor binding affinities by linear mixture models. BMC Bioinformatics. 2011 Feb 15;12 Suppl 1(Suppl 1):S29. doi: 10.1186/1471-2105-12-S1-S29. PMID: 21342559; PMCID: PMC3044284.

Côté J, Quinn J, Workman JL, Peterson CL. Stimulation of GAL4 derivative binding to nucleosomal DNA by the yeast SWI/SNF complex. Science. 1994 Jul 1;265(5168):53-60. doi: 10.1126/science.8016655. PMID: 8016655.

Creyghton MP, Cheng AW, Welstead GG, Kooistra T, Carey BW, Steine EJ, Hanna J, Lodato MA, Frampton GM, Sharp PA, Boyer LA, Young RA, Jaenisch R. Histone H3K27ac separates active from poised enhancers and predicts developmental state. Proc Natl Acad Sci U S A. 2010 Dec 14;107(50):21931-6. doi: 10.1073/pnas.1016071107. Epub 2010 Nov 24. PMID: 21106759; PMCID: PMC3003124.

Dagher R, Helman L. Rhabdomyosarcoma: an overview. Oncologist. 1999;4(1):34-44. PMID: 10337369.

Dalla-Favera R, Bregni M, Erikson J, Patterson D, Gallo RC, Croce CM. Human c-myc onc gene is located on the region of chromosome 8 that is translocated in Burkitt lymphoma cells. Proc Natl Acad Sci U S A. 1982 Dec;79(24):7824-7. doi: 10.1073/pnas.79.24.7824. PMID: 6961453; PMCID: PMC347441.

Danino YM, Even D, Ideses D, Juven-Gershon T. The core promoter: At the heart of gene expression. Biochim Biophys Acta. 2015 Aug;1849(8):1116-31. doi: 10.1016/j.bbagrm.2015.04.003. Epub 2015 Apr 28. PMID: 25934543.

Davis RJ, Barr FG. Fusion genes resulting from alternative chromosomal translocations are overexpressed by gene-specific mechanisms in alveolar rhabdomyosarcoma. Proc Natl Acad Sci U S A. 1997 Jul 22;94(15):8047-51. doi: 10.1073/pnas.94.15.8047. PMID: 9223312; PMCID: PMC21554.

de Almeida SF, Carmo-Fonseca M. The CTD role in cotranscriptional RNA processing and surveillance. FEBS Lett. 2008 Jun 18;582(14):1971-6. doi: 10.1016/j.febslet.2008.04.019. Epub 2008 Apr 22. PMID: 18435923.

De Souza C, Chatterji BP. HDAC Inhibitors as Novel Anti-Cancer Therapeutics. Recent Pat Anticancer Drug Discov. 2015;10(2):145-62. doi: 10.2174/1574892810666150317144511. PMID: 25782916.

de Souza RR, Oliveira ID, Caran EM, Alves MT, Abib S, Toledo SR. Investigation of PAX3/7-FKHR fusion genes and IGF2 gene expression in rhabdomyosarcoma tumors. Growth Horm IGF Res. 2012 Dec;22(6):245-9. doi: 10.1016/j.ghir.2012.07.003. Epub 2012 Oct 16. PMID: 23079386.

Delattre O, Zucman J, Plougastel B, Desmaze C, Melot T, Peter M, Kovar H, Joubert I, de Jong P, Rouleau G, et al. Gene fusion with an ETS DNA-binding domain caused by chromosome translocation in human tumours. Nature. 1992 Sep 10;359(6391):162-5. doi: 10.1038/359162a0. PMID: 1522903.

Delmore JE, Issa GC, Lemieux ME, Rahl PB, Shi J, Jacobs HM, Kastritis E, Gilpatrick T, Paranal RM, Qi J, Chesi M, Schinzel AC, McKeown MR, Heffernan TP, Vakoc CR, Bergsagel PL, Ghobrial IM, Richardson PG, Young RA, Hahn WC, Anderson KC, Kung AL, Bradner JE, Mitsiades CS. BET bromodomain inhibition as a therapeutic strategy to target c-Myc. Cell. 2011 Sep 16;146(6):904-17. doi: 10.1016/j.cell.2011.08.017. Epub 2011 Sep 1. PMID: 21889194; PMCID: PMC3187920.

Demizu Y, Shibata N, Hattori T, Ohoka N, Motoi H, Misawa T, Shoda T, Naito M, Kurihara M. Development of BCR-ABL degradation inducers via the conjugation of an imatinib derivative and a cIAP1 ligand. Bioorg Med Chem Lett. 2016 Oct 15;26(20):4865-4869. doi: 10.1016/j.bmcl.2016.09.041. Epub 2016 Sep 15. PMID: 27666635.

Dey A, Chitsaz F, Abbasi A, Misteli T, Ozato K. The double bromodomain protein Brd4 binds to acetylated chromatin during interphase and mitosis. Proc Natl Acad Sci U S A. 2003 Jul 22;100(15):8758-63. doi: 10.1073/pnas.1433065100. Epub 2003 Jul 2. PMID: 12840145; PMCID: PMC166386.

Dharia NV, Kugener G, Guenther LM, Malone CF, Durbin AD, Hong AL, Howard TP, Bandopadhayay P, Wechsler CS, Fung I, Warren AC, Dempster JM, Krill-Burger JM, Paolella BR, Moh P, Jha N, Tang A, Montgomery P, Boehm JS, Hahn WC, Roberts CWM, McFarland JM, Tsherniak A, Golub TR, Vazquez F, Stegmaier K. A first-generation pediatric cancer dependency map. Nat Genet. 2021 Apr;53(4):529-538. doi: 10.1038/s41588-021-00819-w. Epub 2021 Mar 22. PMID: 33753930; PMCID: PMC8049517.

Di Micco R, Fontanals-Cirera B, Low V, Ntziachristos P, Yuen SK, Lovell CD, Dolgalev I, Yonekubo Y, Zhang G, Rusinova E, Gerona-Navarro G, Cañamero M, Ohlmeyer M, Aifantis I, Zhou MM, Tsirigos A, Hernando E. Control of embryonic stem cell identity by BRD4-dependent transcriptional elongation of super-enhancer-associated pluripotency genes. Cell Rep. 2014 Oct 9;9(1):234-247. doi: 10.1016/j.celrep.2014.08.055. Epub 2014 Sep 26. PMID: 25263550; PMCID: PMC4317728.

DiNardo CD, Pratz KW, Letai A, Jonas BA, Wei AH, Thirman M, Arellano M, Frattini MG, Kantarjian H, Popovic R, Chyla B, Xu T, Dunbar M, Agarwal SK, Humerickhouse R, Mabry M, Potluri J, Konopleva M, Pollyea DA. Safety and preliminary efficacy of venetoclax with decitabine or azacitidine in elderly patients with previously untreated acute myeloid leukaemia: a non-randomised, open-label, phase 1b study. Lancet Oncol. 2018 Feb;19(2):216-228. doi: 10.1016/S1470-2045(18)30010-X. Epub 2018 Jan 12. PMID: 29339097.

Donner AJ, Ebmeier CC, Taatjes DJ, Espinosa JM. CDK8 is a positive regulator of transcriptional elongation within the serum response network. Nat Struct Mol Biol. 2010 Feb;17(2):194-201. doi: 10.1038/nsmb.1752. Epub 2010 Jan 24. PMID: 20098423; PMCID: PMC2920286.

Dowell P, Otto TC, Adi S, Lane MD. Convergence of peroxisome proliferator-activated receptor gamma and Foxo1 signaling pathways. J Biol Chem. 2003 Nov 14;278(46):45485-91. doi: 10.1074/jbc.M309069200. Epub 2003 Sep 9. PMID: 12966085.

Dyson HJ, Wright PE. Intrinsically unstructured proteins and their functions. Nat Rev Mol Cell Biol. 2005 Mar;6(3):197-208. doi: 10.1038/nrm1589. PMID: 15738986.

Eberharter A, Becker PB. Histone acetylation: a switch between repressive and permissive chromatin. Second in review series on chromatin dynamics. EMBO Rep. 2002 Mar;3(3):224-9. doi: 10.1093/embo-reports/kvf053. PMID: 11882541; PMCID: PMC1084017.

Eijkelenboom A, Burgering BM. FOXOs: signalling integrators for homeostasis maintenance. Nat Rev Mol Cell Biol. 2013 Feb;14(2):83-97. doi: 10.1038/nrm3507. Epub 2013 Jan 17. PMID: 23325358.

Epstein JA, Lam P, Jepeal L, Maas RL, Shapiro DN. Pax3 inhibits myogenic differentiation of cultured myoblast cells. J Biol Chem. 1995 May 19;270(20):11719-22. doi: 10.1074/jbc.270.20.11719. PMID: 7744814.

Erb MA, Scott TG, Li BE, Xie H, Paulk J, Seo HS, Souza A, Roberts JM, Dastjerdi S, Buckley DL, Sanjana NE, Shalem O, Nabet B, Zeid R, Offei-Addo NK, Dhe-Paganon S, Zhang F, Orkin SH, Winter GE, Bradner JE. Transcription control by the ENL YEATS domain in acute leukaemia. Nature. 2017 Mar 9;543(7644):270-274. doi: 10.1038/nature21688. Epub 2017 Mar 1. PMID: 28241139; PMCID: PMC5497220.

Esnault C, Ghavi-Helm Y, Brun S, Soutourina J, Van Berkum N, Boschiero C, Holstege F, Werner M. Mediator-dependent recruitment of TFIIH modules in preinitiation complex. Mol Cell. 2008 Aug 8;31(3):337-46. doi: 10.1016/j.molcel.2008.06.021. PMID: 18691966.

Filippakopoulos P, Qi J, Picaud S, Shen Y, Smith WB, Fedorov O, Morse EM, Keates T, Hickman TT, Felletar I, Philpott M, Munro S, McKeown MR, Wang Y, Christie AL, West N, Cameron MJ, Schwartz B, Heightman TD, La Thangue N, French CA, Wiest O, Kung AL, Knapp S, Bradner JE. Selective inhibition of BET bromodomains. Nature. 2010 Dec 23;468(7327):1067-73. doi: 10.1038/nature09504. Epub 2010 Sep 24. PMID: 20871596; PMCID: PMC3010259.

Frascella E, Toffolatti L, Rosolen A. Normal and rearranged PAX3 expression in human rhabdomyosarcoma. Cancer Genet Cytogenet. 1998 Apr 15;102(2):104-9. doi: 10.1016/s0165-4608(97)00352-x. PMID: 9546061.

Fredericks WJ, Galili N, Mukhopadhyay S, Rovera G, Bennicelli J, Barr FG, Rauscher FJ 3rd. The PAX3-FKHR fusion protein created by the t(2;13) translocation in alveolar rhabdomyosarcomas is a more potent transcriptional activator than PAX3. Mol Cell Biol. 1995 Mar;15(3):1522-35. doi: 10.1128/MCB.15.3.1522. PMID: 7862145; PMCID: PMC230376.

Fredericks WJ, Galili N, Mukhopadhyay S, Rovera G, Bennicelli J, Barr FG, Rauscher FJ 3rd. The PAX3-FKHR fusion protein created by the t(2;13) translocation in alveolar rhabdomyosarcomas is a more potent transcriptional activator than PAX3. Mol Cell Biol. 1995 Mar;15(3):1522-35. doi: 10.1128/MCB.15.3.1522. PMID: 7862145; PMCID: PMC230376.

Galili N, Davis RJ, Fredericks WJ, Mukhopadhyay S, Rauscher FJ 3rd, Emanuel BS, Rovera G, Barr FG. Fusion of a fork head domain gene to PAX3 in the solid tumour alveolar rhabdomyosarcoma. Nat Genet. 1993 Nov;5(3):230-5. doi: 10.1038/ng1193-230. Erratum in: Nat Genet 1994 Feb;6(2):214. PMID: 8275086.

Gao Q, Liang WW, Foltz SM, Mutharasu G, Jayasinghe RG, Cao S, Liao WW, Reynolds SM, Wyczalkowski MA, Yao L, Yu L, Sun SQ; Fusion Analysis Working Group; Cancer Genome Atlas Research Network, Chen K, Lazar AJ, Fields RC, Wendl MC, Van Tine BA, Vij R, Chen F, Nykter M, Shmulevich I, Ding L. Driver Fusions and Their Implications in the Development and Treatment of Human Cancers. Cell Rep. 2018 Apr 3;23(1):227-238.e3. doi: 10.1016/j.celrep.2018.03.050. PMID: 29617662; PMCID: PMC5916809.

Gershon TR, Oppenheimer O, Chin SS, Gerald WL. Temporally regulated neural crest transcription factors distinguish neuroectodermal tumors of varying malignancy and differentiation. Neoplasia. 2005 Jun;7(6):575-84. doi: 10.1593/neo.04637. PMID: 16036108; PMCID: PMC1501286.

Girardi T, Vicente C, Cools J, De Keersmaecker K. The genetics and molecular biology of T-ALL. Blood. 2017 Mar 2;129(9):1113-1123. doi: 10.1182/blood-2016-10-706465. Epub 2017 Jan 23. PMID: 28115373; PMCID: PMC5363819.

Golub TR, Barker GF, Lovett M, Gilliland DG. Fusion of PDGF receptor beta to a novel ets-like gene, tel, in chronic myelomonocytic leukemia with t(5;12) chromosomal translocation. Cell. 1994 Apr 22;77(2):307-16. doi: 10.1016/0092-8674(94)90322-0. PMID: 8168137.

Grandori C, Eisenman RN. Myc target genes. Trends Biochem Sci. 1997 May;22(5):177-81. doi: 10.1016/s0968-0004(97)01025-6. PMID: 9175477.

Graves JA, Wang Y, Sims-Lucas S, Cherok E, Rothermund K, Branca MF, Elster J, Beer-Stolz D, Van Houten B, Vockley J, Prochownik EV. Mitochondrial structure, function and dynamics are temporally controlled by c-Myc. PLoS One. 2012;7(5):e37699. doi: 10.1371/journal.pone.0037699. Epub 2012 May 21. PMID: 22629444; PMCID: PMC3357432.

Grewal SS, Li L, Orian A, Eisenman RN, Edgar BA. Myc-dependent regulation of ribosomal RNA synthesis during Drosophila development. Nat Cell Biol. 2005 Mar;7(3):295-302. doi: 10.1038/ncb1223. Epub 2005 Feb 20. PMID: 15723055.

Grignani F, Fagioli M, Ferrucci PF, Alcalay M, Pelicci PG. The molecular genetics of acute promyelocytic leukemia. Blood Rev. 1993 Jun;7(2):87-93. doi: 10.1016/s0268-960x(05)80018-9. PMID: 8396481.

Gryder BE, Pomella S, Sayers C, Wu XS, Song Y, Chiarella AM, Bagchi S, Chou HC, Sinniah RS, Walton A, Wen X, Rota R, Hathaway NA, Zhao K, Chen J, Vakoc CR, Shern JF, Stanton BZ, Khan J. Histone hyperacetylation disrupts core gene regulatory architecture in rhabdomyosarcoma. Nat Genet. 2019 Dec;51(12):1714-1722. doi: 10.1038/s41588-019-0534-4. Epub 2019 Nov 29. PMID: 31784732; PMCID: PMC6886578.

Gryder BE, Wachtel M, Chang K, El Demerdash O, Aboreden NG, Mohammed W, Ewert W, Pomella S, Rota R, Wei JS, Song Y, Stanton BZ, Schäfer B, Vakoc CR, Khan J. Miswired Enhancer Logic Drives a Cancer of the Muscle Lineage. iScience. 2020 May 22;23(5):101103. doi: 10.1016/j.isci.2020.101103. Epub 2020 Apr 29. PMID: 32416589; PMCID: PMC7226896.

Gryder BE, Wu L, Woldemichael GM, Pomella S, Quinn TR, Park PMC, Cleveland A, Stanton BZ, Song Y, Rota R, Wiest O, Yohe ME, Shern JF, Qi J, Khan J. Chemical genomics reveals histone deacetylases are required for core regulatory

transcription. Nat Commun. 2019 Jul 8;10(1):3004. doi: 10.1038/s41467-019-11046-7. PMID: 31285436; PMCID: PMC6614369.

Gryder BE, Yohe ME, Chou HC, Zhang X, Marques J, Wachtel M, Schaefer B, Sen N, Song Y, Gualtieri A, Pomella S, Rota R, Cleveland A, Wen X, Sindiri S, Wei JS, Barr FG, Das S, Andresson T, Guha R, Lal-Nag M, Ferrer M, Shern JF, Zhao K, Thomas CJ, Khan J. PAX3-FOXO1 Establishes Myogenic Super Enhancers and Confers BET Bromodomain Vulnerability. Cancer Discov. 2017 Aug;7(8):884-899. doi: 10.1158/2159-8290.CD-16-1297. Epub 2017 Apr 26. PMID: 28446439; PMCID: PMC7802885.

Guenou H, Kaabeche K, Mée SL, Marie PJ. A role for fibroblast growth factor receptor-2 in the altered osteoblast phenotype induced by Twist haploinsufficiency in the Saethre-Chotzen syndrome. Hum Mol Genet. 2005 Jun 1;14(11):1429-39. doi: 10.1093/hmg/ddi152. Epub 2005 Apr 13. PMID: 15829502.

Gui Y, Guo G, Huang Y, Hu X, Tang A, Gao S, Wu R, Chen C, Li X, Zhou L, He M, Li Z, Sun X, Jia W, Chen J, Yang S, Zhou F, Zhao X, Wan S, Ye R, Liang C, Liu Z, Huang P, Liu C, Jiang H, Wang Y, Zheng H, Sun L, Liu X, Jiang Z, Feng D, Chen J, Wu S, Zou J, Zhang Z, Yang R, Zhao J, Xu C, Yin W, Guan Z, Ye J, Zhang H, Li J, Kristiansen K, Nickerson ML, Theodorescu D, Li Y, Zhang X, Li S, Wang J, Yang H, Wang J, Cai Z. Frequent mutations of chromatin remodeling genes in transitional cell carcinoma of the bladder. Nat Genet. 2011 Aug 7;43(9):875-8. doi: 10.1038/ng.907. PMID: 21822268; PMCID: PMC5373841.

Guo S, Rena G, Cichy S, He X, Cohen P, Unterman T. Phosphorylation of serine 256 by protein kinase B disrupts transactivation by FKHR and mediates effects of insulin on insulin-like growth factor-binding protein-1 promoter activity through a conserved insulin response sequence. J Biol Chem. 1999 Jun 11;274(24):17184-92. doi: 10.1074/jbc.274.24.17184. PMID: 10358076.

Haberle V, Stark A. Eukaryotic core promoters and the functional basis of transcription initiation. Nat Rev Mol Cell Biol. 2018 Oct;19(10):621-637. doi: 10.1038/s41580-018-0028-8. PMID: 29946135; PMCID: PMC6205604.

Hagenbuchner J, Ausserlechner MJ. Targeting transcription factors by small compounds--Current strategies and future implications. Biochem Pharmacol. 2016 May 1;107:1-13. doi: 10.1016/j.bcp.2015.12.006. Epub 2015 Dec 11. PMID: 26686579.

Hahn S. Structure and mechanism of the RNA polymerase II transcription machinery. Nat Struct Mol Biol. 2004 May;11(5):394-403. doi: 10.1038/nsmb763. PMID: 15114340; PMCID: PMC1189732.

Han Q, Wang Q, Wu J, Li M, Fang Y, Zhu H, Wang X. Nell-1 promotes the neural-like differentiation of dental pulp cells. Biochem Biophys Res Commun. 2019 May 28;513(2):515-521. doi: 10.1016/j.bbrc.2019.04.028. Epub 2019 Apr 9. PMID: 30979495.

Hasebe A, Nakamura Y, Tashima H, Takahashi K, Iijima M, Yoshimoto N, Ting K, Kuroda S, Niimi T. The C-terminal region of NELL1 mediates osteoblastic cell adhesion through integrin α3β1. FEBS Lett. 2012 Jul 30;586(16):2500-6. doi: 10.1016/j.febslet.2012.06.014. Epub 2012 Jun 20. PMID: 22728432.

Hatley ME, Tang W, Garcia MR, Finkelstein D, Millay DP, Liu N, Graff J, Galindo RL, Olson EN. A mouse model of rhabdomyosarcoma originating from the adipocyte

lineage. Cancer Cell. 2012 Oct 16;22(4):536-46. doi: 10.1016/j.ccr.2012.09.004. PMID: 23079662; PMCID: PMC3479681.

Hatta M, Cirillo LA. Chromatin opening and stable perturbation of core histone:DNA contacts by FoxO1. J Biol Chem. 2007 Dec 7;282(49):35583-93. doi: 10.1074/jbc.M704735200. Epub 2007 Oct 8. PMID: 17923482.

Hayday AC, Gillies SD, Saito H, Wood C, Wiman K, Hayward WS, Tonegawa S. Activation of a translocated human c-myc gene by an enhancer in the immunoglobulin heavy-chain locus. Nature. 1984 Jan 26-Feb 1;307(5949):334-40. doi: 10.1038/307334a0. PMID: 6420706.

He S, Yoon HS, Suh BJ, Eccles MR. PAX3 Is extensively expressed in benign and malignant tissues of the melanocytic lineage in humans. J Invest Dermatol. 2010 May;130(5):1465-8. doi: 10.1038/jid.2009.434. Epub 2010 Jan 28. PMID: 20107488.

Heaster TM, Walsh AJ, Zhao Y, Hiebert SW, Skala MC. Autofluorescence imaging identifies tumor cell-cycle status on a single-cell level. J Biophotonics. 2018 Jan;11(1):10.1002/jbio.201600276. doi: 10.1002/jbio.201600276. Epub 2017 May 9. PMID: 28485124; PMCID: PMC5680147.

Heintzman ND, Stuart RK, Hon G, Fu Y, Ching CW, Hawkins RD, Barrera LO, Van Calcar S, Qu C, Ching KA, Wang W, Weng Z, Green RD, Crawford GE, Ren B. Distinct and predictive chromatin signatures of transcriptional promoters and enhancers in the human genome. Nat Genet. 2007 Mar;39(3):311-8. doi: 10.1038/ng1966. Epub 2007 Feb 4. PMID: 17277777.

Hibbitts E, Chi YY, Hawkins DS, Barr FG, Bradley JA, Dasgupta R, Meyer WH, Rodeberg DA, Rudzinski ER, Spunt SL, Skapek SX, Wolden SL, Arndt CAS. Refinement of risk stratification for childhood rhabdomyosarcoma using FOXO1 fusion status in addition to established clinical outcome predictors: A report from the Children's Oncology Group. Cancer Med. 2019 Oct;8(14):6437-6448. doi: 10.1002/cam4.2504. Epub 2019 Aug 27. PMID: 31456361; PMCID: PMC6797586.

Hnisz D, Abraham BJ, Lee TI, Lau A, Saint-André V, Sigova AA, Hoke HA, Young RA. Super-enhancers in the control of cell identity and disease. Cell. 2013 Nov 7;155(4):934-47. doi: 10.1016/j.cell.2013.09.053. Epub 2013 Oct 10. PMID: 24119843; PMCID: PMC3841062.

Hoth CF, Milunsky A, Lipsky N, Sheffer R, Clarren SK, Baldwin CT. Mutations in the paired domain of the human PAX3 gene cause Klein-Waardenburg syndrome (WS-III) as well as Waardenburg syndrome type I (WS-I). Am J Hum Genet. 1993 Mar;52(3):455-62. PMID: 8447316; PMCID: PMC1682157.

Hu S, Balakrishnan A, Bok RA, Anderton B, Larson PE, Nelson SJ, Kurhanewicz J, Vigneron DB, Goga A. 13C-pyruvate imaging reveals alterations in glycolysis that precede c-Myc-induced tumor formation and regression. Cell Metab. 2011 Jul 6;14(1):131-42. doi: 10.1016/j.cmet.2011.04.012. PMID: 21723511; PMCID: PMC3858338.

Huang H, Tindall DJ. CDK2 and FOXO1: a fork in the road for cell fate decisions. Cell Cycle. 2007 Apr 15;6(8):902-6. doi: 10.4161/cc.6.8.4122. Epub 2007 Apr 5. PMID: 17457058.

Huang J, Li K, Cai W, Liu X, Zhang Y, Orkin SH, Xu J, Yuan GC. Dissecting super-enhancer hierarchy based on chromatin interactions. Nat Commun. 2018 Mar

5;9(1):943. doi: 10.1038/s41467-018-03279-9. PMID: 29507293; PMCID: PMC5838163.

Hung V, Udeshi ND, Lam SS, Loh KH, Cox KJ, Pedram K, Carr SA, Ting AY. Spatially resolved proteomic mapping in living cells with the engineered peroxidase APEX2. Nat Protoc. 2016 Mar;11(3):456-75. doi: 10.1038/nprot.2016.018. Epub 2016 Feb 11. PMID: 26866790; PMCID: PMC4863649.

Itzen F, Greifenberg AK, Bösken CA, Geyer M. Brd4 activates P-TEFb for RNA polymerase II CTD phosphorylation. Nucleic Acids Res. 2014 Jul;42(12):7577-90. doi: 10.1093/nar/gku449. Epub 2014 May 23. PMID: 24860166; PMCID: PMC4081074.

Jaeger MG, Winter GE. Fast-acting chemical tools to delineate causality in transcriptional control. Mol Cell. 2021 Apr 15;81(8):1617-1630. doi: 10.1016/j.molcel.2021.02.015.

Jeanne M, Lallemand-Breitenbach V, Ferhi O, Koken M, Le Bras M, Duffort S, Peres L, Berthier C, Soilihi H, Raught B, de Thé H. PML/RARA oxidation and arsenic binding initiate the antileukemia response of As2O3. Cancer Cell. 2010 Jul 13;18(1):88-98. doi: 10.1016/j.ccr.2010.06.003. PMID: 20609355.

Ji H, Wu G, Zhan X, Nolan A, Koh C, De Marzo A, Doan HM, Fan J, Cheadle C, Fallahi M, Cleveland JL, Dang CV, Zeller KI. Cell-type independent MYC target genes reveal a primordial signature involved in biomass accumulation. PLoS One. 2011;6(10):e26057. doi: 10.1371/journal.pone.0026057. Epub 2011 Oct 19. PMID: 22039435; PMCID: PMC3198433.

Jin F, Li Y, Dixon JR, Selvaraj S, Ye Z, Lee AY, Yen CA, Schmitt AD, Espinoza CA, Ren B. A high-resolution map of the three-dimensional chromatin interactome in human cells. Nature. 2013 Nov 14;503(7475):290-4. doi: 10.1038/nature12644. Epub 2013 Oct 20. PMID: 24141950; PMCID: PMC3838900.

Johnston G, Ramsey HE, Liu Q, Wang J, Stengel KR, Sampathi S, Acharya P, Arrate M, Stubbs MC, Burn T, Savona MR, Hiebert SW. Nascent transcript and single-cell RNA-seq analysis defines the mechanism of action of the LSD1 inhibitor INCB059872 in myeloid leukemia. Gene. 2020 Aug 20;752:144758. doi: 10.1016/j.gene.2020.144758. Epub 2020 May 15. PMID: 32422235; PMCID: PMC7401316.

Jones S, Wang TL, Shih IeM, Mao TL, Nakayama K, Roden R, Glas R, Slamon D, Diaz LA Jr, Vogelstein B, Kinzler KW, Velculescu VE, Papadopoulos N. Frequent mutations of chromatin remodeling gene ARID1A in ovarian clear cell carcinoma. Science. 2010 Oct 8;330(6001):228-31. doi: 10.1126/science.1196333. Epub 2010 Sep 8. PMID: 20826764; PMCID: PMC3076894.

Kämpjärvi K, Kim NH, Keskitalo S, Clark AD, von Nandelstadh P, Turunen M, Heikkinen T, Park MJ, Mäkinen N, Kivinummi K, Lintula S, Hotakainen K, Nevanlinna H, Hokland P, Böhling T, Bützow R, Böhm J, Mecklin JP, Järvinen H, Kontro M, Visakorpi T, Taipale J, Varjosalo M, Boyer TG, Vahteristo P. Somatic MED12 mutations in prostate cancer and uterine leiomyomas promote tumorigenesis through distinct mechanisms. Prostate. 2016 Jan;76(1):22-31. doi: 10.1002/pros.23092. Epub 2015 Sep 18. PMID: 26383637.

Kassabov SR, Zhang B, Persinger J, Bartholomew B. SWI/SNF unwraps, slides, and rewraps the nucleosome. Mol Cell. 2003 Feb;11(2):391-403. doi: 10.1016/s1097-2765(03)00039-x. PMID: 12620227.

Kawamura-Saito M, Yamazaki Y, Kaneko K, Kawaguchi N, Kanda H, Mukai H, Gotoh T, Motoi T, Fukayama M, Aburatani H, Takizawa T, Nakamura T. Fusion between CIC and DUX4 up-regulates PEA3 family genes in Ewing-like sarcomas with t(4;19)(q35;q13) translocation. Hum Mol Genet. 2006 Jul 1;15(13):2125-37. doi: 10.1093/hmg/ddl136. Epub 2006 May 22. PMID: 16717057.

Kawane T, Qin X, Jiang Q, Miyazaki T, Komori H, Yoshida CA, Matsuura-Kawata VKDS, Sakane C, Matsuo Y, Nagai K, Maeno T, Date Y, Nishimura R, Komori T. Runx2 is required for the proliferation of osteoblast progenitors and induces proliferation by regulating Fgfr2 and Fgfr3. Sci Rep. 2018 Sep 10;8(1):13551. doi: 10.1038/s41598-018-31853-0. PMID: 30202094; PMCID: PMC6131145.

Keller A, Dziedzicka D, Zambelli F, Markouli C, Sermon K, Spits C, Geens M. Genetic and epigenetic factors which modulate differentiation propensity in human pluripotent stem cells. Hum Reprod Update. 2018 Mar 1;24(2):162-175. doi: 10.1093/humupd/dmx042. PMID: 29377992.

Kendall GC, Watson S, Xu L, LaVigne CA, Murchison W, Rakheja D, Skapek SX, Tirode F, Delattre O, Amatruda JF. *PAX3-FOXO1*transgenic zebrafish models identify *HES3* as a mediator of rhabdomyosarcoma tumorigenesis. Elife. 2018 Jun 5;7:e33800. doi: 10.7554/eLife.33800. PMID: 29869612; PMCID: PMC5988421.

Khan J, Simon R, Bittner M, Chen Y, Leighton SB, Pohida T, Smith PD, Jiang Y, Gooden GC, Trent JM, Meltzer PS. Gene expression profiling of alveolar rhabdomyosarcoma with cDNA microarrays. Cancer Res. 1998 Nov 15;58(22):5009-13. PMID: 9823299.

Kikuchi K, Tsuchiya K, Otabe O, Gotoh T, Tamura S, Katsumi Y, Yagyu S, Tsubai-Shimizu S, Miyachi M, Iehara T, Hosoi H. Effects of PAX3-FKHR on malignant phenotypes in alveolar rhabdomyosarcoma. Biochem Biophys Res Commun. 2008 Jan 18;365(3):568-74. doi: 10.1016/j.bbrc.2007.11.017. Epub 2007 Nov 20. PMID: 18022385.

Kim HJ, Kim JH, Bae SC, Choi JY, Kim HJ, Ryoo HM. The protein kinase C pathway plays a central role in the fibroblast growth factor-stimulated expression and transactivation activity of Runx2. J Biol Chem. 2003 Jan 3;278(1):319-26. doi: 10.1074/jbc.M203750200. Epub 2002 Oct 25. PMID: 12403780.

Kim JH, Kim K, Youn BU, Lee J, Kim I, Shin HI, Akiyama H, Choi Y, Kim N. Kruppel-like factor 4 attenuates osteoblast formation, function, and cross talk with osteoclasts. J Cell Biol. 2014 Mar 17;204(6):1063-74. doi: 10.1083/jcb.201308102. Epub 2014 Mar 10. PMID: 24616223; PMCID: PMC3998795.

Kim JW, Zeller KI, Wang Y, Jegga AG, Aronow BJ, O'Donnell KA, Dang CV. Evaluation of myc E-box phylogenetic footprints in glycolytic genes by chromatin immunoprecipitation assays. Mol Cell Biol. 2004 Jul;24(13):5923-36. doi: 10.1128/MCB.24.13.5923-5936.2004. PMID: 15199147; PMCID: PMC480875.

Knezevich SR, McFadden DE, Tao W, Lim JF, Sorensen PH. A novel ETV6-NTRK3 gene fusion in congenital fibrosarcoma. Nat Genet. 1998 Feb;18(2):184-7. doi: 10.1038/ng0298-184. PMID: 9462753.

Kohsaka S, Shukla N, Ameur N, Ito T, Ng CK, Wang L, Lim D, Marchetti A, Viale A, Pirun M, Socci ND, Qin LX, Sciot R, Bridge J, Singer S, Meyers P, Wexler LH, Barr FG, Dogan S, Fletcher JA, Reis-Filho JS, Ladanyi M. A recurrent neomorphic mutation in MYOD1 defines a clinically aggressive subset of embryonal rhabdomyosarcoma

associated with PI3K-AKT pathway mutations. Nat Genet. 2014 Jun;46(6):595-600. doi: 10.1038/ng.2969. Epub 2014 May 4. PMID: 24793135; PMCID: PMC4231202.

Konopleva M, Pollyea DA, Potluri J, Chyla B, Hogdal L, Busman T, McKeegan E, Salem AH, Zhu M, Ricker JL, Blum W, DiNardo CD, Kadia T, Dunbar M, Kirby R, Falotico N, Leverson J, Humerickhouse R, Mabry M, Stone R, Kantarjian H, Letai A. Efficacy and Biological Correlates of Response in a Phase II Study of Venetoclax Monotherapy in Patients with Acute Myelogenous Leukemia. Cancer Discov. 2016 Oct;6(10):1106-1117. doi: 10.1158/2159-8290.CD-16-0313. Epub 2016 Aug 12. PMID: 27520294; PMCID: PMC5436271.

Krivega I, Dean A. Enhancer and promoter interactions-long distance calls. Curr Opin Genet Dev. 2012 Apr;22(2):79-85. doi: 10.1016/j.gde.2011.11.001. Epub 2011 Dec 12. PMID: 22169023; PMCID: PMC3342482.

Kubo T, Shimose S, Fujimori J, Furuta T, Ochi M. Prognostic value of PAX3/7-FOXO1 fusion status in alveolar rhabdomyosarcoma: Systematic review and meta-analysis. Crit Rev Oncol Hematol. 2015 Oct;96(1):46-53. doi: 10.1016/j.critrevonc.2015.04.012. Epub 2015 May 14. PMID: 26008753.

Kurzrock R, Gutterman JU, Talpaz M. The molecular genetics of Philadelphia chromosome-positive leukemias. N Engl J Med. 1988 Oct 13;319(15):990-8. doi: 10.1056/NEJM198810133191506. PMID: 3047582.

Kwak H, Fuda NJ, Core LJ, Lis JT. Precise maps of RNA polymerase reveal how promoters direct initiation and pausing. Science. 2013 Feb 22;339(6122):950-3. doi: 10.1126/science.1229386. PMID: 23430654; PMCID: PMC3974810.

Kwiatkowski N, Zhang T, Rahl PB, Abraham BJ, Reddy J, Ficarro SB, Dastur A, Amzallag A, Ramaswamy S, Tesar B, Jenkins CE, Hannett NM, McMillin D, Sanda T, Sim T, Kim ND, Look T, Mitsiades CS, Weng AP, Brown JR, Benes CH, Marto JA, Young RA, Gray NS. Targeting transcription regulation in cancer with a covalent CDK7 inhibitor. Nature. 2014 Jul 31;511(7511):616-20. doi: 10.1038/nature13393. Epub 2014 Jun 22. PMID: 25043025; PMCID: PMC4244910.

Kwon H, Imbalzano AN, Khavari PA, Kingston RE, Green MR. Nucleosome disruption and enhancement of activator binding by a human SW1/SNF complex. Nature. 1994 Aug 11;370(6489):477-81. doi: 10.1038/370477a0. PMID: 8047169.

Lai WKM, Pugh BF. Understanding nucleosome dynamics and their links to gene expression and DNA replication. Nat Rev Mol Cell Biol. 2017 Sep;18(9):548-562. doi: 10.1038/nrm.2017.47. Epub 2017 May 24. PMID: 28537572; PMCID: PMC5831138.

Lam SS, Martell JD, Kamer KJ, Deerinck TJ, Ellisman MH, Mootha VK, Ting AY. Directed evolution of APEX2 for electron microscopy and proximity labeling. Nat Methods. 2015 Jan;12(1):51-4. doi: 10.1038/nmeth.3179. Epub 2014 Nov 24. PMID: 25419960; PMCID: PMC4296904.

Langmead B, Salzberg SL. Fast gapped-read alignment with Bowtie 2. Nat Methods. 2012 Mar 4;9(4):357-9. doi: 10.1038/nmeth.1923. PMID: 22388286; PMCID: PMC3322381.

Layden HM, Eleuteri NA, Hiebert SW, Stengel KR. A protocol for rapid degradation of endogenous transcription factors in mammalian cells and identification of direct regulatory targets. STAR Protoc. 2021 May 19;2(2):100530. doi: 10.1016/j.xpro.2021.100530. PMID: 34041503; PMCID: PMC8142277.

Lee JH, Song YM, Min SK, Lee HJ, Lee HL, Kim MJ, Park YH, Park JU, Park JB. NELL-1 Increased the Osteogenic Differentiation and mRNA Expression of Spheroids Composed of Stem Cells. Medicina (Kaunas). 2021 Jun 8;57(6):586. doi: 10.3390/medicina57060586. PMID: 34201046; PMCID: PMC8229008.

Levine M, Tjian R. Transcription regulation and animal diversity. Nature. 2003 Jul 10;424(6945):147-51. doi: 10.1038/nature01763. PMID: 12853946.

Levine M. Transcriptional enhancers in animal development and evolution. Curr Biol. 2010 Sep 14;20(17):R754-63. doi: 10.1016/j.cub.2010.06.070. PMID: 20833320; PMCID: PMC4280268.

Li G, Ruan X, Auerbach RK, Sandhu KS, Zheng M, Wang P, Poh HM, Goh Y, Lim J, Zhang J, Sim HS, Peh SQ, Mulawadi FH, Ong CT, Orlov YL, Hong S, Zhang Z, Landt S, Raha D, Euskirchen G, Wei CL, Ge W, Wang H, Davis C, Fisher-Aylor KI, Mortazavi A, Gerstein M, Gingeras T, Wold B, Sun Y, Fullwood MJ, Cheung E, Liu E, Sung WK, Snyder M, Ruan Y. Extensive promoter-centered chromatin interactions provide a topological basis for transcription regulation. Cell. 2012 Jan 20;148(1-2):84-98. doi: 10.1016/j.cell.2011.12.014. PMID: 22265404; PMCID: PMC3339270.

Li S, Ilaria RL Jr, Million RP, Daley GQ, Van Etten RA. The P190, P210, and P230 forms of the BCR/ABL oncogene induce a similar chronic myeloid leukemia-like syndrome in mice but have different lymphoid leukemogenic activity. J Exp Med. 1999 May 3;189(9):1399-412. doi: 10.1084/jem.189.9.1399. PMID: 10224280; PMCID: PMC2193055.

Li Y, Hu M, Shen Y. Gene regulation in the 3D genome. Hum Mol Genet. 2018 Aug 1;27(R2):R228-R233. doi: 10.1093/hmg/ddy164. PMID: 29767704; PMCID: PMC6061806.

Liao GB, Li XZ, Zeng S, Liu C, Yang SM, Yang L, Hu CJ, Bai JY. Regulation of the master regulator FOXM1 in cancer. Cell Commun Signal. 2018 Sep 12;16(1):57. doi: 10.1186/s12964-018-0266-6. PMID: 30208972; PMCID: PMC6134757.

Lin K, Hsin H, Libina N, Kenyon C. Regulation of the Caenorhabditis elegans longevity protein DAF-16 by insulin/IGF-1 and germline signaling. Nat Genet. 2001 Jun;28(2):139-45. doi: 10.1038/88850. PMID: 11381260.

Linardic CM. PAX3-FOXO1 fusion gene in rhabdomyosarcoma. Cancer Lett. 2008 Oct 18;270(1):10-8. doi: 10.1016/j.canlet.2008.03.035. Epub 2008 May 23. PMID: 18457914; PMCID: PMC2575376.

Linggi B, Müller-Tidow C, van de Locht L, Hu M, Nip J, Serve H, Berdel WE, van der Reijden B, Quelle DE, Rowley JD, Cleveland J, Jansen JH, Pandolfi PP, Hiebert SW. The t(8;21) fusion protein, AML1 ETO, specifically represses the transcription of the p14(ARF) tumor suppressor in acute myeloid leukemia. Nat Med. 2002 Jul;8(7):743-50. doi: 10.1038/nm726. Epub 2002 Jun 24. PMID: 12091906.

Link KA, Lin S, Shrestha M, Bowman M, Wunderlich M, Bloomfield CD, Huang G, Mulloy JC. Supraphysiologic levels of the AML1-ETO isoform AE9a are essential for transformation. Proc Natl Acad Sci U S A. 2016 Aug 9;113(32):9075-80. doi: 10.1073/pnas.1524225113. Epub 2016 Jul 25. PMID: 27457952; PMCID: PMC4987773.

Linqing Z, Guohua J, Haoming L, Xuelei T, Jianbing Q, Meiling T. Runx1t1 regulates the neuronal differentiation of radial glial cells from the rat hippocampus. Stem Cells

Transl Med. 2015 Jan;4(1):110-6. doi: 10.5966/sctm.2014-0158. Epub 2014 Dec 3. PMID: 25473084; PMCID: PMC4275013.

Liu Y, Zhou K, Zhang N, Wei H, Tan YZ, Zhang Z, Carragher B, Potter CS, D'Arcy S, Luger K. FACT caught in the act of manipulating the nucleosome. Nature. 2020 Jan;577(7790):426-431. doi: 10.1038/s41586-019-1820-0. Epub 2019 Nov 27. PMID: 31775157; PMCID: PMC7441595.

Lovén J, Hoke HA, Lin CY, Lau A, Orlando DA, Vakoc CR, Bradner JE, Lee TI, Young RA. Selective inhibition of tumor oncogenes by disruption of super-enhancers. Cell. 2013 Apr 11;153(2):320-34. doi: 10.1016/j.cell.2013.03.036. PMID: 23582323; PMCID: PMC3760967.

Lu H, Zawel L, Fisher L, Egly JM, Reinberg D. Human general transcription factor IIH phosphorylates the C-terminal domain of RNA polymerase II. Nature. 1992 Aug 20;358(6388):641-5. doi: 10.1038/358641a0. PMID: 1495560.

Lu X, Zhu X, Li Y, Liu M, Yu B, Wang Y, Rao M, Yang H, Zhou K, Wang Y, Chen Y, Chen M, Zhuang S, Chen LF, Liu R, Chen R. Multiple P-TEFbs cooperatively regulate the release of promoter-proximally paused RNA polymerase II. Nucleic Acids Res. 2016 Aug 19;44(14):6853-67. doi: 10.1093/nar/gkw571. Epub 2016 Jun 28. PMID: 27353326; PMCID: PMC5001612.

Luan J, Xiang G, Gómez-García PA, Tome JM, Zhang Z, Vermunt MW, Zhang H, Huang A, Keller CA, Giardine BM, Zhang Y, Lan Y, Lis JT, Lakadamyali M, Hardison RC, Blobel GA. Distinct properties and functions of CTCF revealed by a rapidly inducible degron system. Cell Rep. 2021 Feb 23;34(8):108783. doi: 10.1016/j.celrep.2021.108783. PMID: 33626344; PMCID: PMC7999233.

Lutterbach B, Westendorf JJ, Linggi B, Patten A, Moniwa M, Davie JR, Huynh KD, Bardwell VJ, Lavinsky RM, Rosenfeld MG, Glass C, Seto E, Hiebert SW. ETO, a target of t(8;21) in acute leukemia, interacts with the N-CoR and mSin3 corepressors. Mol Cell Biol. 1998 Dec;18(12):7176-84. doi: 10.1128/MCB.18.12.7176. PMID: 9819404; PMCID: PMC109299.

Madan V, Han L, Hattori N, Teoh WW, Mayakonda A, Sun QY, Ding LW, Nordin HBM, Lim SL, Shyamsunder P, Dakle P, Sundaresan J, Doan NB, Sanada M, Sato-Otsubo A, Meggendorfer M, Yang H, Said JW, Ogawa S, Haferlach T, Liang DC, Shih LY, Nakamaki T, Wang QT, Koeffler HP. ASXL2 regulates hematopoiesis in mice and its deficiency promotes myeloid expansion. Haematologica. 2018 Dec;103(12):1980-1990. doi: 10.3324/haematol.2018.189928. Epub 2018 Aug 9. PMID: 30093396; PMCID: PMC6269306.

Maehara O, Suda G, Natsuizaka M, Shigesawa T, Kanbe G, Kimura M, Sugiyama M, Mizokami M, Nakai M, Sho T, Morikawa K, Ogawa K, Ohashi S, Kagawa S, Kinugasa H, Naganuma S, Okubo N, Ohnishi S, Takeda H, Sakamoto N. FGFR2 maintains cancer cell differentiation via AKT signaling in esophageal squamous cell carcinoma. Cancer Biol Ther. 2021 Jun 3;22(5-6):372-380. doi: 10.1080/15384047.2021.1939638. Epub 2021 Jul 5. PMID: 34224333; PMCID: PMC8386746.

Mahat DB, Kwak H, Booth GT, Jonkers IH, Danko CG, Patel RK, Waters CT, Munson K, Core LJ, Lis JT. Base-pair-resolution genome-wide mapping of active RNA polymerases using precision nuclear run-on (PRO-seq). Nat Protoc. 2016

Aug;11(8):1455-76. doi: 10.1038/nprot.2016.086. Epub 2016 Jul 21. PMID: 27442863; PMCID: PMC5502525.
Malik S, Roeder RG. Transcriptional regulation through Mediator-like coactivators in yeast and metazoan cells. Trends Biochem Sci. 2000 Jun;25(6):277-83. doi: 10.1016/s0968-0004(00)01596-6. PMID: 10838567.
Mandal R, Becker S, Strebhardt K. Targeting CDK9 for Anti-Cancer Therapeutics. Cancers (Basel). 2021 May 1;13(9):2181. doi: 10.3390/cancers13092181. PMID: 34062779; PMCID: PMC8124690.
Manolov G, Manolova Y. Marker band in one chromosome 14 from Burkitt lymphomas. Nature. 1972 May 5;237(5349):33-4. doi: 10.1038/237033a0. PMID: 4113130.
Mansour MR, Abraham BJ, Anders L, Berezovskaya A, Gutierrez A, Durbin AD, Etchin J, Lawton L, Sallan SE, Silverman LB, Loh ML, Hunger SP, Sanda T, Young RA, Look AT. Oncogene regulation. An oncogenic super-enhancer formed through somatic mutation of a noncoding intergenic element. Science. 2014 Dec 12;346(6215):1373-7. doi: 10.1126/science.1259037. Epub 2014 Nov 13. PMID: 25394790; PMCID: PMC4720521.
Mantovani F, Collavin L, Del Sal G. Mutant p53 as a guardian of the cancer cell. Cell Death Differ. 2019 Jan;26(2):199-212. doi: 10.1038/s41418-018-0246-9. Epub 2018 Dec 11. PMID: 30538286; PMCID: PMC6329812.
Marshall AD, Grosveld GC. Alveolar rhabdomyosarcoma - The molecular drivers of PAX3/7-FOXO1-induced tumorigenesis. Skelet Muscle. 2012 Dec 3;2(1):25. doi: 10.1186/2044-5040-2-25. PMID: 23206814; PMCID: PMC3564712.
Martell JD, Deerinck TJ, Sancak Y, Poulos TL, Mootha VK, Sosinsky GE, Ellisman MH, Ting AY. Engineered ascorbate peroxidase as a genetically encoded reporter for electron microscopy. Nat Biotechnol. 2012 Nov;30(11):1143-8. doi: 10.1038/nbt.2375. Epub 2012 Oct 21. PMID: 23086203; PMCID: PMC3699407.
Mateyak MK, Obaya AJ, Adachi S, Sedivy JM. Phenotypes of c-Myc-deficient rat fibroblasts isolated by targeted homologous recombination. Cell Growth Differ. 1997 Oct;8(10):1039-48. PMID: 9342182.
Mateyak MK, Obaya AJ, Sedivy JM. c-Myc regulates cyclin D-Cdk4 and -Cdk6 activity but affects cell cycle progression at multiple independent points. Mol Cell Biol. 1999 Jul;19(7):4672-83. doi: 10.1128/MCB.19.7.4672. PMID: 10373516; PMCID: PMC84265.
Mathur R, Alver BH, San Roman AK, Wilson BG, Wang X, Agoston AT, Park PJ, Shivdasani RA, Roberts CW. ARID1A loss impairs enhancer-mediated gene regulation and drives colon cancer in mice. Nat Genet. 2017 Feb;49(2):296-302. doi: 10.1038/ng.3744. Epub 2016 Dec 12. PMID: 27941798; PMCID: PMC5285448.
Matozaki S, Nakagawa T, Kawaguchi R, Aozaki R, Tsutsumi M, Murayama T, Koizumi T, Nishimura R, Isobe T, Chihara K. Establishment of a myeloid leukaemic cell line (SKNO-1) from a patient with t(8;21) who acquired monosomy 17 during disease progression. Br J Haematol. 1995 Apr;89(4):805-11. doi: 10.1111/j.1365-2141.1995.tb08418.x. PMID: 7772516.
Mattila MM, Ruohola JK, Valve EM, Tasanen MJ, Seppänen JA, Härkönen PL. FGF-8b increases angiogenic capacity and tumor growth of androgen-regulated S115

breast cancer cells. Oncogene. 2001 May 17;20(22):2791-804. doi: 10.1038/sj.onc.1204430. PMID: 11420691.

Mayer A, Heidemann M, Lidschreiber M, Schreieck A, Sun M, Hintermair C, Kremmer E, Eick D, Cramer P. CTD tyrosine phosphorylation impairs termination factor recruitment to RNA polymerase II. Science. 2012 Jun 29;336(6089):1723-5. doi: 10.1126/science.1219651. PMID: 22745433.

Meier N, Krpic S, Rodriguez P, Strouboulis J, Monti M, Krijgsveld J, Gering M, Patient R, Hostert A, Grosveld F. Novel binding partners of Ldb1 are required for haematopoietic development. Development. 2006 Dec;133(24):4913-23. doi: 10.1242/dev.02656. Epub 2006 Nov 15. PMID: 17108004.

Mertens F, Johansson B, Fioretos T, Mitelman F. The emerging complexity of gene fusions in cancer. Nat Rev Cancer. 2015 Jun;15(6):371-81. doi: 10.1038/nrc3947. PMID: 25998716.

Minezaki Y, Homma K, Kinjo AR, Nishikawa K. Human transcription factors contain a high fraction of intrinsically disordered regions essential for transcriptional regulation. J Mol Biol. 2006 Jun 16;359(4):1137-49. doi: 10.1016/j.jmb.2006.04.016. Epub 2006 Apr 25. Erratum in: J Mol Biol. 2006 Oct 13;363(1):309. PMID: 16697407.

Missiaglia E, Williamson D, Chisholm J, Wirapati P, Pierron G, Petel F, Concordet JP, Thway K, Oberlin O, Pritchard-Jones K, Delattre O, Delorenzi M, Shipley J. PAX3/FOXO1 fusion gene status is the key prognostic molecular marker in rhabdomyosarcoma and significantly improves current risk stratification. J Clin Oncol. 2012 May 10;30(14):1670-7. doi: 10.1200/JCO.2011.38.5591. Epub 2012 Mar 26. PMID: 22454413.

Mitelman F, Johansson B, Mertens F. The impact of translocations and gene fusions on cancer causation. Nat Rev Cancer. 2007 Apr;7(4):233-45. doi: 10.1038/nrc2091. Epub 2007 Mar 15. PMID: 17361217.

Mittal P, Shin YH, Yatsenko SA, Castro CA, Surti U, Rajkovic A. Med12 gain-of-function mutation causes leiomyomas and genomic instability. J Clin Invest. 2015 Aug 3;125(8):3280-4. doi: 10.1172/JCI81534. Epub 2015 Jul 20. PMID: 26193636; PMCID: PMC4563761.

Miyoshi H, Shimizu K, Kozu T, Maseki N, Kaneko Y, Ohki M. t(8;21) breakpoints on chromosome 21 in acute myeloid leukemia are clustered within a limited region of a single gene, AML1. Proc Natl Acad Sci U S A. 1991 Dec 1;88(23):10431-4. doi: 10.1073/pnas.88.23.10431. PMID: 1720541; PMCID: PMC52942.

Mochida K, Koda S, Inoue K, Nishii R. Statistical and Machine Learning Approaches to Predict Gene Regulatory Networks From Transcriptome Datasets. Front Plant Sci. 2018 Nov 29;9:1770. doi: 10.3389/fpls.2018.01770. PMID: 30555503; PMCID: PMC6281826.

Montalban-Bravo G, Garcia-Manero G. Novel drugs for older patients with acute myeloid leukemia. Leukemia. 2015 Apr;29(4):760-9. doi: 10.1038/leu.2014.244. Epub 2014 Aug 21. PMID: 25142817.

Muhar M, Ebert A, Neumann T, Umkehrer C, Jude J, Wieshofer C, Rescheneder P, Lipp JJ, Herzog VA, Reichholf B, Cisneros DA, Hoffmann T, Schlapansky MF, Bhat P, von Haeseler A, Köcher T, Obenauf AC, Popow J, Ameres SL, Zuber J. SLAM-seq defines direct gene-regulatory functions of the BRD4-MYC axis. Science. 2018

May 18;360(6390):800-805. doi: 10.1126/science.aao2793. Epub 2018 Apr 5. PMID: 29622725; PMCID: PMC6409205.
Muller PA, Vousden KH. p53 mutations in cancer. Nat Cell Biol. 2013 Jan;15(1):2-8. doi: 10.1038/ncb2641. PMID: 23263379.
Murakami K, Calero G, Brown CR, Liu X, Davis RE, Boeger H, Kornberg RD. Formation and fate of a complete 31-protein RNA polymerase II transcription preinitiation complex. J Biol Chem. 2013 Mar 1;288(9):6325-32. doi: 10.1074/jbc.M112.433623. Epub 2013 Jan 9. PMID: 23303183; PMCID: PMC3585067.
Nabet B, Roberts JM, Buckley DL, Paulk J, Dastjerdi S, Yang A, Leggett AL, Erb MA, Lawlor MA, Souza A, Scott TG, Vittori S, Perry JA, Qi J, Winter GE, Wong KK, Gray NS, Bradner JE. The dTAG system for immediate and target-specific protein degradation. Nat Chem Biol. 2018 May;14(5):431-441. doi: 10.1038/s41589-018-0021-8. Epub 2018 Mar 26. PMID: 29581585; PMCID: PMC6295913.
Nakae J, Kitamura T, Kitamura Y, Biggs WH 3rd, Arden KC, Accili D. The forkhead transcription factor Foxo1 regulates adipocyte differentiation. Dev Cell. 2003 Jan;4(1):119-29. doi: 10.1016/s1534-5807(02)00401-x. PMID: 12530968.
Nakamura N, Ramaswamy S, Vazquez F, Signoretti S, Loda M, Sellers WR. Forkhead transcription factors are critical effectors of cell death and cell cycle arrest downstream of PTEN. Mol Cell Biol. 2000 Dec;20(23):8969-82. doi: 10.1128/MCB.20.23.8969-8982.2000. PMID: 11073996; PMCID: PMC86551.
Nebert DW. Transcription factors and cancer: an overview. Toxicology. 2002 Dec 27;181-182:131-41. doi: 10.1016/s0300-483x(02)00269-x. PMID: 12505298.
Noguera NI, Piredda ML, Taulli R, Catalano G, Angelini G, Gaur G, Nervi C, Voso MT, Lunardi A, Pandolfi PP, Lo-Coco F. PML/RARa inhibits PTEN expression in hematopoietic cells by competing with PU.1 transcriptional activity. Oncotarget. 2016 Oct 11;7(41):66386-66397. doi: 10.18632/oncotarget.11964. PMID: 27626703; PMCID: PMC5341808.
Nojima T, Rebelo K, Gomes T, Grosso AR, Proudfoot NJ, Carmo-Fonseca M. RNA Polymerase II Phosphorylated on CTD Serine 5 Interacts with the Spliceosome during Co-transcriptional Splicing. Mol Cell. 2018 Oct 18;72(2):369-379.e4. doi: 10.1016/j.molcel.2018.09.004. PMID: 30340024; PMCID: PMC6201815.
Nora EP, Goloborodko A, Valton AL, Gibcus JH, Uebersohn A, Abdennur N, Dekker J, Mirny LA, Bruneau BG. Targeted Degradation of CTCF Decouples Local Insulation of Chromosome Domains from Genomic Compartmentalization. Cell. 2017 May 18;169(5):930-944.e22. doi: 10.1016/j.cell.2017.05.004. PMID: 28525758; PMCID: PMC5538188.
Nucifora G, Rowley JD. The AML1 and ETO genes in acute myeloid leukemia with a t(8;21). Leuk Lymphoma. 1994 Aug;14(5-6):353-62. doi: 10.3109/10428199409049690. PMID: 7812194.
O'Meara E, Stack D, Phelan S, McDonagh N, Kelly L, Sciot R, Debiec-Rychter M, Morris T, Cochrane D, Sorensen P, O'Sullivan MJ. Identification of an MLL4-GPS2 fusion as an oncogenic driver of undifferentiated spindle cell sarcoma in a child. Genes Chromosomes Cancer. 2014 Dec;53(12):991-8. doi: 10.1002/gcc.22208. Epub 2014 Aug 19. PMID: 25139254.
Odore E, Lokiec F, Cvitkovic E, Bekradda M, Herait P, Bourdel F, Kahatt C, Raffoux E, Stathis A, Thieblemont C, Quesnel B, Cunningham D, Riveiro ME, Rezaï K. Phase

l Population Pharmacokinetic Assessment of the Oral Bromodomain Inhibitor OTX015 in Patients with Haematologic Malignancies. Clin Pharmacokinet. 2016 Mar;55(3):397-405. doi: 10.1007/s40262-015-0327-6. PMID: 26341814.

Ognjanovic S, Carozza SE, Chow EJ, Fox EE, Horel S, McLaughlin CC, Mueller BA, Puumala S, Reynolds P, Von Behren J, Spector L. Birth characteristics and the risk of childhood rhabdomyosarcoma based on histological subtype. Br J Cancer. 2010 Jan 5;102(1):227-31. doi: 10.1038/sj.bjc.6605484. Epub 2009 Dec 8. PMID: 19997102; PMCID: PMC2813761.

Omoteyama K, Takagi M. FGF8 regulates myogenesis and induces Runx2 expression and osteoblast differentiation in cultured cells. J Cell Biochem. 2009 Mar 1;106(4):546-52. doi: 10.1002/jcb.22012. PMID: 19170063.

Orphanides G, Wu WH, Lane WS, Hampsey M, Reinberg D. The chromatin-specific transcription elongation factor FACT comprises human SPT16 and SSRP1 proteins. Nature. 1999 Jul 15;400(6741):284-8. doi: 10.1038/22350. PMID: 10421373.

Ortega E, Rengachari S, Ibrahim Z, Hoghoughi N, Gaucher J, Holehouse AS, Khochbin S, Panne D. Transcription factor dimerization activates the p300 acetyltransferase. Nature. 2018 Oct;562(7728):538-544. doi: 10.1038/s41586-018-0621-1. Epub 2018 Oct 15. PMID: 30323286; PMCID: PMC6914384.

Osthus RC, Shim H, Kim S, Li Q, Reddy R, Mukherjee M, Xu Y, Wonsey D, Lee LA, Dang CV. Deregulation of glucose transporter 1 and glycolytic gene expression by c-Myc. J Biol Chem. 2000 Jul 21;275(29):21797-800. doi: 10.1074/jbc.C000023200. PMID: 10823814.

Ott CJ, Kopp N, Bird L, Paranal RM, Qi J, Bowman T, Rodig SJ, Kung AL, Bradner JE, Weinstock DM. BET bromodomain inhibition targets both c-Myc and IL7R in high-risk acute lymphoblastic leukemia. Blood. 2012 Oct 4;120(14):2843-52. doi: 10.1182/blood-2012-02-413021. Epub 2012 Aug 17. PMID: 22904298; PMCID: PMC3466965.

Pappo AS, Anderson JR, Crist WM, Wharam MD, Breitfeld PP, Hawkins D, Raney RB, Womer RB, Parham DM, Qualman SJ, Grier HE. Survival after relapse in children and adolescents with rhabdomyosarcoma: A report from the Intergroup Rhabdomyosarcoma Study Group. J Clin Oncol. 1999 Nov;17(11):3487-93. doi: 10.1200/JCO.1999.17.11.3487. PMID: 10550146.

Pelletier A, Mayran A, Gouhier A, Omichinski JG, Balsalobre A, Drouin J. Pax7 pioneer factor action requires both paired and homeo DNA binding domains. Nucleic Acids Res. 2021 Jul 21;49(13):7424-7436. doi: 10.1093/nar/gkab561. PMID: 34197620; PMCID: PMC8287922.

Pingault V, Ente D, Dastot-Le Moal F, Goossens M, Marlin S, Bondurand N. Review and update of mutations causing Waardenburg syndrome. Hum Mutat. 2010 Apr;31(4):391-406. doi: 10.1002/humu.21211. PMID: 20127975.

Pott S, Lieb JD. What are super-enhancers? Nat Genet. 2015 Jan;47(1):8-12. doi: 10.1038/ng.3167. PMID: 25547603.

Prozzillo Y, Fattorini G, Santopietro MV, Suglia L, Ruggiero A, Ferreri D, Messina G. Targeted Protein Degradation Tools: Overview and Future Perspectives. Biology (Basel). 2020 Nov 26;9(12):421. doi: 10.3390/biology9120421. PMID: 33256092; PMCID: PMC7761331.

Ptasinska A, Assi SA, Martinez-Soria N, Imperato MR, Piper J, Cauchy P, Pickin A, James SR, Hoogenkamp M, Williamson D, Wu M, Tenen DG, Ott S, Westhead DR, Cockerill PN, Heidenreich O, Bonifer C. Identification of a dynamic core transcriptional network in t(8;21) AML that regulates differentiation block and self-renewal. Cell Rep. 2014 Sep 25;8(6):1974-1988. doi: 10.1016/j.celrep.2014.08.024. Epub 2014 Sep 18. PMID: 25242324; PMCID: PMC4487811.

Rabbitts TH, Forster A, Baer R, Hamlyn PH. Transcription enhancer identified near the human C mu immunoglobulin heavy chain gene is unavailable to the translocated c-myc gene in a Burkitt lymphoma. Nature. 1983 Dec 22-1984 Jan 4;306(5945):806-9. doi: 10.1038/306806a0. PMID: 6419124.

Rabbitts TH, Hamlyn PH, Baer R. Altered nucleotide sequences of a translocated c-myc gene in Burkitt lymphoma. Nature. 1983 Dec 22-1984 Jan 4;306(5945):760-5. doi: 10.1038/306760a0. PMID: 6419122.

Rabbitts TH, van Straaten P, Rabbitts PH, Watson J. Discussion on the metabolism of c-myc mRNA and protein. Proc R Soc Lond B Biol Sci. 1985 Oct 22;226(1242):79-82. doi: 10.1098/rspb.1985.0081. PMID: 2866526.

Rabbitts TH. Chromosomal translocations in human cancer. Nature. 1994 Nov 10;372(6502):143-9. doi: 10.1038/372143a0. PMID: 7969446.

Rada-Iglesias A, Bajpai R, Swigut T, Brugmann SA, Flynn RA, Wysocka J. A unique chromatin signature uncovers early developmental enhancers in humans. Nature. 2011 Feb 10;470(7333):279-83. doi: 10.1038/nature09692. Epub 2010

Rahl PB, Lin CY, Seila AC, Flynn RA, McCuine S, Burge CB, Sharp PA, Young RA. c-Myc regulates transcriptional pause release. Cell. 2010 Apr 30;141(3):432-45. doi: 10.1016/j.cell.2010.03.030. PMID: 20434984; PMCID: PMC2864022.

Rakhra K, Bachireddy P, Zabuawala T, Zeiser R, Xu L, Kopelman A, Fan AC, Yang Q, Braunstein L, Crosby E, Ryeom S, Felsher DW. CD4(+) T cells contribute to the remodeling of the microenvironment required for sustained tumor regression upon oncogene inactivation. Cancer Cell. 2010 Nov 16;18(5):485-98. doi: 10.1016/j.ccr.2010.10.002. Epub 2010 Oct 28. Erratum in: Cancer Cell. 2010 Dec 14;18(6):696. PMID: 21035406; PMCID: PMC2991103.

Ramsey HE, Fischer MA, Lee T, Gorska AE, Arrate MP, Fuller L, Boyd KL, Strickland SA, Sensintaffar J, Hogdal LJ, Ayers GD, Olejniczak ET, Fesik SW, Savona MR. A Novel MCL1 Inhibitor Combined with Venetoclax Rescues Venetoclax-Resistant Acute Myelogenous Leukemia. Cancer Discov. 2018 Dec;8(12):1566-1581. doi: 10.1158/2159-8290.CD-18-0140. Epub 2018 Sep 5. PMID: 30185627; PMCID: PMC6279595.

Razaghi-Moghadam Z, Nikoloski Z. Supervised learning of gene-regulatory networks based on graph distance profiles of transcriptomics data. NPJ Syst Biol Appl. 2020 Jun 30;6(1):21. doi: 10.1038/s41540-020-0140-1. PMID: 32606380; PMCID: PMC7327016.

Rena G, Guo S, Cichy SC, Unterman TG, Cohen P. Phosphorylation of the transcription factor forkhead family member FKHR by protein kinase B. J Biol Chem. 1999 Jun 11;274(24):17179-83. doi: 10.1074/jbc.274.24.17179. PMID: 10358075.

Rhoades KL, Hetherington CJ, Harakawa N, Yergeau DA, Zhou L, Liu LQ, Little MT, Tenen DG, Zhang DE. Analysis of the role of AML1-ETO in leukemogenesis, using

an inducible transgenic mouse model. Blood. 2000 Sep 15;96(6):2108-15. PMID: 10979955.

Roberts KG, Janke LJ, Zhao Y, Seth A, Ma J, Finkelstein D, Smith S, Ebata K, Tuch BB, Hunger SP, Mullighan CG. ETV6-NTRK3 induces aggressive acute lymphoblastic leukemia highly sensitive to selective TRK inhibition. Blood. 2018 Aug 23;132(8):861-865. doi: 10.1182/blood-2018-05-849554. Epub 2018 Jun 7. PMID: 29880614; PMCID: PMC6107883.

Robson MI, Ringel AR, Mundlos S. Regulatory Landscaping: How Enhancer-Promoter Communication Is Sculpted in 3D. Mol Cell. 2019 Jun 20;74(6):1110-1122. doi: 10.1016/j.molcel.2019.05.032. PMID: 31226276.

Rodriguez CR, Cho EJ, Keogh MC, Moore CL, Greenleaf AL, Buratowski S. Kin28, the TFIIH-associated carboxy-terminal domain kinase, facilitates the recruitment of mRNA processing machinery to RNA polymerase II. Mol Cell Biol. 2000 Jan;20(1):104-12. doi: 10.1128/MCB.20.1.104-112.2000. PMID: 10594013; PMCID: PMC85066.

Roeb W, Boyer A, Cavenee WK, Arden KC. PAX3-FOXO1 controls expression of the p57Kip2 cell-cycle regulator through degradation of EGR1. Proc Natl Acad Sci U S A. 2007 Nov 13;104(46):18085-90. doi: 10.1073/pnas.0708910104. Epub 2007 Nov 6. PMID: 17986608; PMCID: PMC2084300.

Roeder RG. The role of general initiation factors in transcription by RNA polymerase II. Trends Biochem Sci. 1996 Sep;21(9):327-35. PMID: 8870495.

Rowley JD. A new consistent chromosomal abnormality in chronic myelogenous leukaemia identified by quinacrine fluorescence and giemsa staining. Nautre. 1973 Jan;243:190-293. PMID: 4126434.

Rowley JD. Identificaton of a translocation with quinacrine fluorescence in a patient with acute leukemia. Ann Genet. 1973 Jun;16(2):109-12. PMID: 4125056.

Rubin BP, Nishijo K, Chen HI, Yi X, Schuetze DP, Pal R, Prajapati SI, Abraham J, Arenkiel BR, Chen QR, Davis S, McCleish AT, Capecchi MR, Michalek JE, Zarzabal LA, Khan J, Yu Z, Parham DM, Barr FG, Meltzer PS, Chen Y, Keller C. Evidence for an unanticipated relationship between undifferentiated pleomorphic sarcoma and embryonal rhabdomyosarcoma. Cancer Cell. 2011 Feb 15;19(2):177-91. doi: 10.1016/j.ccr.2010.12.023. PMID: 21316601; PMCID: PMC3040414.

Sabari BR, Dall'Agnese A, Boija A, Klein IA, Coffey EL, Shrinivas K, Abraham BJ, Hannett NM, Zamudio AV, Manteiga JC, Li CH, Guo YE, Day DS, Schuijers J, Vasile E, Malik S, Hnisz D, Lee TI, Cisse II, Roeder RG, Sharp PA, Chakraborty AK, Young RA. Coactivator condensation at super-enhancers links phase separation and gene control. Science. 2018 Jul 27;361(6400):eaar3958. doi: 10.1126/science.aar3958. Epub 2018 Jun 21. PMID: 29930091; PMCID: PMC6092193.

Sabò A, Kress TR, Pelizzola M, de Pretis S, Gorski MM, Tesi A, Morelli MJ, Bora P, Doni M, Verrecchia A, Tonelli C, Fagà G, Bianchi V, Ronchi A, Low D, Müller H, Guccione E, Campaner S, Amati B. Selective transcriptional regulation by Myc in cellular growth control and lymphomagenesis. Nature. 2014 Jul 24;511(7510):488-492. doi: 10.1038/nature13537. Epub 2014 Jul 9. PMID: 25043028; PMCID: PMC4110711.

Saha A, Wittmeyer J, Cairns BR. Chromatin remodelling: the industrial revolution of DNA around histones. Nat Rev Mol Cell Biol. 2006 Jun;7(6):437-47. doi: 10.1038/nrm1945. PMID: 16723979.

Sakamoto KM, Kim KB, Kumagai A, Mercurio F, Crews CM, Deshaies RJ. Protacs: chimeric molecules that target proteins to the Skp1-Cullin-F box complex for ubiquitination and degradation. Proc Natl Acad Sci U S A. 2001 Jul 17;98(15):8554-9. doi: 10.1073/pnas.141230798. Epub 2001 Jul 3. PMID: 11438690; PMCID: PMC37474.

Sampathi S, Acharya P, Zhao Y, Wang J, Stengel KR, Liu Q, Savona MR, Hiebert SW. The CDK7 inhibitor THZ1 alters RNA polymerase dynamics at the 5' and 3' ends of genes. Nucleic Acids Res. 2019 May 7;47(8):3921-3936. doi: 10.1093/nar/gkz127. PMID: 30805632; PMCID: PMC6486546.

Schäfer BW, Czerny T, Bernasconi M, Genini M, Busslinger M. Molecular cloning and characterization of a human PAX-7 cDNA expressed in normal and neoplastic myocytes. Nucleic Acids Res. 1994 Nov 11;22(22):4574-82. doi: 10.1093/nar/22.22.4574. PMID: 7527137; PMCID: PMC308503.

Schoenfelder S, Fraser P. Long-range enhancer-promoter contacts in gene expression control. Nat Rev Genet. 2019 Aug;20(8):437-455. doi: 10.1038/s41576-019-0128-0. PMID: 31086298.

Schulte TW, Toretsky JA, Ress E, Helman L, Neckers LM. Expression of PAX3 in Ewing's sarcoma family of tumors. Biochem Mol Med. 1997 Apr;60(2):121-6. doi: 10.1006/bmme.1997.2567. PMID: 9169092.

Segalla S, Rinaldi L, Kilstrup-Nielsen C, Badaracco G, Minucci S, Pelicci PG, Landsberger N. Retinoic acid receptor alpha fusion to PML affects its transcriptional and chromatin-remodeling properties. Mol Cell Biol. 2003 Dec;23(23):8795-808. doi: 10.1128/MCB.23.23.8795-8808.2003. PMID: 14612419; PMCID: PMC262687.

Shao W, Zeitlinger J. Paused RNA polymerase II inhibits new transcriptional initiation. Nat Genet. 2017 Jul;49(7):1045-1051. doi: 10.1038/ng.3867. Epub 2017 May 15. PMID: 28504701.

Shapiro DN, Sublett JE, Li B, Downing JR, Naeve CW. Fusion of PAX3 to a member of the forkhead family of transcription factors in human alveolar rhabdomyosarcoma. Cancer Res. 1993 Nov 1;53(21):5108-12. PMID: 8221646.

Shen ZX, Shi ZZ, Fang J, Gu BW, Li JM, Zhu YM, Shi JY, Zheng PZ, Yan H, Liu YF, Chen Y, Shen Y, Wu W, Tang W, Waxman S, De Thé H, Wang ZY, Chen SJ, Chen Z. All-trans retinoic acid/As2O3 combination yields a high quality remission and survival in newly diagnosed acute promyelocytic leukemia. Proc Natl Acad Sci U S A. 2004 Apr 13;101(15):5328-35. doi: 10.1073/pnas.0400053101. Epub 2004 Mar 24. PMID: 15044693; PMCID: PMC397380.

Shern JF, Chen L, Chmielecki J, Wei JS, Patidar R, Rosenberg M, Ambrogio L, Auclair D, Wang J, Song YK, Tolman C, Hurd L, Liao H, Zhang S, Bogen D, Brohl AS, Sindiri S, Catchpoole D, Badgett T, Getz G, Mora J, Anderson JR, Skapek SX, Barr FG, Meyerson M, Hawkins DS, Khan J. Comprehensive genomic analysis of rhabdomyosarcoma reveals a landscape of alterations affecting a common genetic axis in fusion-positive and fusion-negative tumors. Cancer Discov. 2014

Feb;4(2):216-31. doi: 10.1158/2159-8290.CD-13-0639. Epub 2014 Jan 23. PMID: 24436047; PMCID: PMC4462130.

Shlyueva D, Stampfel G, Stark A. Transcriptional enhancers: from properties to genome-wide predictions. Nat Rev Genet. 2014 Apr;15(4):272-86. doi: 10.1038/nrg3682. Epub 2014 Mar 11. PMID: 24614317.

Skene PJ, Henikoff S. An efficient targeted nuclease strategy for high-resolution mapping of DNA binding sites. Elife. 2017 Jan 16;6:e21856. doi: 10.7554/eLife.21856. PMID: 28079019; PMCID: PMC5310842.

Skrzypek K, Kusienicka A, Trzyna E, Szewczyk B, Ulman A, Konieczny P, Adamus T, Badyra B, Kortylewski M, Majka M. SNAIL is a key regulator of alveolar rhabdomyosarcoma tumor growth and differentiation through repression of MYF5 and MYOD function. Cell Death Dis. 2018 May 29;9(6):643. doi: 10.1038/s41419-018-0693-8. PMID: 29844345; PMCID: PMC5974324.

Slany RK. When epigenetics kills: MLL fusion proteins in leukemia. Hematol Oncol. 2005 Mar;23(1):1-9. doi: 10.1002/hon.739. PMID: 16118769.

Song HM, Song JL, Li DF, Hua KY, Zhao BK, Fang L. Inhibition of FOXO1 by small interfering RNA enhances proliferation and inhibits apoptosis of papillary thyroid carcinoma cells via Akt/FOXO1/Bim pathway. Onco Targets Ther. 2015 Dec 1;8:3565-73. doi: 10.2147/OTT.S95395. PMID: 26664140; PMCID: PMC4671809.

Song L, Crawford GE. DNase-seq: a high-resolution technique for mapping active gene regulatory elements across the genome from mammalian cells. Cold Spring Harb Protoc. 2010 Feb;2010(2):pdb.prot5384. doi: 10.1101/pdb.prot5384. PMID: 20150147; PMCID: PMC3627383.

Sorensen PH, Lynch JC, Qualman SJ, Tirabosco R, Lim JF, Maurer HM, Bridge JA, Crist WM, Triche TJ, Barr FG. PAX3-FKHR and PAX7-FKHR gene fusions are prognostic indicators in alveolar rhabdomyosarcoma: a report from the children's oncology group. J Clin Oncol. 2002 Jun 1;20(11):2672-9. doi: 10.1200/JCO.2002.03.137. PMID: 12039929.

Stadler MB, Murr R, Burger L, Ivanek R, Lienert F, Schöler A, van Nimwegen E, Wirbelauer C, Oakeley EJ, Gaidatzis D, Tiwari VK, Schübeler D. DNA-binding factors shape the mouse methylome at distal regulatory regions. Nature. 2011 Dec 14;480(7378):490-5. doi: 10.1038/nature10716. Erratum in: Nature. 2012 Apr 26;484(7395):550. van Nimwegen, Erik [added]. PMID: 22170606.

Stengel KR, Ellis JD, Spielman CL, Bomber ML, Hiebert SW. Definition of a small core transcriptional circuit regulated by AML1-ETO. Mol Cell. 2021 Feb 4;81(3):530-545.e5. doi: 10.1016/j.molcel.2020.12.005. Epub 2020 Dec 30. PMID: 33382982; PMCID: PMC7867650.

Storlazzi CT, Anelli L, Albano F, Zagaria A, Ventura M, Rocchi M, Panagopoulos I, Pannunzio A, Ottaviani E, Liso V, Specchia G. A novel chromosomal translocation t(3;7)(q26;q21) in myeloid leukemia resulting in overexpression of EVI1. Ann Hematol. 2004 Feb;83(2):78-83. doi: 10.1007/s00277-003-0778-y. Epub 2003 Oct 10. PMID: 14551738.

Stratton MR, Fisher C, Gusterson BA, Cooper CS. Detection of point mutations in N-ras and K-ras genes of human embryonal rhabdomyosarcomas using oligonucleotide probes and the polymerase chain reaction. Cancer Res. 1989 Nov 15;49(22):6324-7. PMID: 2680062.

Stratton MR, Fisher C, Gusterson BA, Cooper CS. Detection of point mutations in N-ras and K-ras genes of human embryonal rhabdomyosarcomas using oligonucleotide probes and the polymerase chain reaction. Cancer Res. 1989 Nov 15;49(22):6324-7. PMID: 2680062.

Su W, Jackson S, Tjian R, Echols H. DNA looping between sites for transcriptional activation: self-association of DNA-bound Sp1. Genes Dev. 1991 May;5(5):820-6. doi: 10.1101/gad.5.5.820. PMID: 1851121.

Suh DS, Yoon MS, Choi KU, Kim JY. Significance of E2F-1 overexpression in epithelial ovarian cancer. Int J Gynecol Cancer. 2008 May-Jun;18(3):492-8. doi: 10.1111/j.1525-1438.2007.01044.x. Epub 2007 Aug 10. PMID: 17692085.

Sultan I, Qaddoumi I, Yaser S, Rodriguez-Galindo C, Ferrari A. Comparing adult and pediatric rhabdomyosarcoma in the surveillance, epidemiology and end results program, 1973 to 2005: an analysis of 2,600 patients. J Clin Oncol. 2009 Jul 10;27(20):3391-7. doi: 10.1200/JCO.2008.19.7483. Epub 2009 Apr 27. PMID: 19398574.

Sunkel BD, Wang M, LaHaye S, Kelly BJ, Fitch JR, Barr FG, White P, Stanton BZ. Evidence of pioneer factor activity of an oncogenic fusion transcription factor. iScience. 2021 Jul 16;24(8):102867. doi: 10.1016/j.isci.2021.102867. PMID: 34386729; PMCID: PMC8346656.

Swanson CI, Evans NC, Barolo S. Structural rules and complex regulatory circuitry constrain expression of a Notch- and EGFR-regulated eye enhancer. Dev Cell. 2010 Mar 16;18(3):359-70. doi: 10.1016/j.devcel.2009.12.026. PMID: 20230745; PMCID: PMC2847355.

Swift J, Coruzzi GM. A matter of time - How transient transcription factor interactions create dynamic gene regulatory networks. Biochim Biophys Acta Gene Regul Mech. 2017 Jan;1860(1):75-83. doi: 10.1016/j.bbagrm.2016.08.007. Epub 2016 Aug 18. PMID: 27546191; PMCID: PMC5203810.

Taatjes DJ. The human Mediator complex: a versatile, genome-wide regulator of transcription. Trends Biochem Sci. 2010 Jun;35(6):315-22. doi: 10.1016/j.tibs.2010.02.004. Epub 2010 Mar 17. PMID: 20299225; PMCID: PMC2891401.

Takahashi H, Parmely TJ, Sato S, Tomomori-Sato C, Banks CA, Kong SE, Szutorisz H, Swanson SK, Martin-Brown S, Washburn MP, Florens L, Seidel CW, Lin C, Smith ER, Shilatifard A, Conaway RC, Conaway JW. Human mediator subunit MED26 functions as a docking site for transcription elongation factors. Cell. 2011 Jul 8;146(1):92-104. doi: 10.1016/j.cell.2011.06.005. PMID: 21729782; PMCID: PMC3145325.

Tanaka M, Herr W. Differential transcriptional activation by Oct-1 and Oct-2: interdependent activation domains induce Oct-2 phosphorylation. Cell. 1990 Feb 9;60(3):375-86. doi: 10.1016/0092-8674(90)90589-7. PMID: 2302733.

Tanese N, Pugh BF, Tjian R. Coactivators for a proline-rich activator purified from the multisubunit human TFIID complex. Genes Dev. 1991 Dec;5(12A):2212-24. doi: 10.1101/gad.5.12a.2212. PMID: 1748279.

Taub R, Kirsch I, Morton C, Lenoir G, Swan D, Tronick S, Aaronson S, Leder P. Translocation of the c-myc gene into the immunoglobulin heavy chain locus in human Burkitt lymphoma and murine plasmacytoma cells. Proc Natl Acad Sci U S

A. 1982 Dec;79(24):7837-41. doi: 10.1073/pnas.79.24.7837. PMID: 6818551; PMCID: PMC347444.

Taylor AC, Shu L, Danks MK, Poquette CA, Shetty S, Thayer MJ, Houghton PJ, Harris LC. P53 mutation and MDM2 amplification frequency in pediatric rhabdomyosarcoma tumors and cell lines. Med Pediatr Oncol. 2000 Aug;35(2):96-103. doi: 10.1002/1096-911x(200008)35:2<96::aid-mpo2>3.0.co;2-z. PMID: 10918230.

Tiwari A, Swamynathan S, Alexander N, Gnalian J, Tian S, Kinchington PR, Swamynathan SK. KLF4 Regulates Corneal Epithelial Cell Cycle Progression by Suppressing Canonical TGF-β Signaling and Upregulating CDK Inhibitors P16 and P27. Invest Ophthalmol Vis Sci. 2019 Feb 1;60(2):731-740. doi: 10.1167/iovs.18-26423. PMID: 30786277; PMCID: PMC6383833.

Trapnell C, Hendrickson DG, Sauvageau M, Goff L, Rinn JL, Pachter L. Differential analysis of gene regulation at transcript resolution with RNA-seq. Nat Biotechnol. 2013 Jan;31(1):46-53. doi: 10.1038/nbt.2450. Epub 2012 Dec 9. PMID: 23222703; PMCID: PMC3869392.

Trapnell C, Roberts A, Goff L, Pertea G, Kim D, Kelley DR, Pimentel H, Salzberg SL, Rinn JL, Pachter L. Differential gene and transcript expression analysis of RNA-seq experiments with TopHat and Cufflinks. Nat Protoc. 2012 Mar 1;7(3):562-78. doi: 10.1038/nprot.2012.016. Erratum in: Nat Protoc. 2014 Oct;9(10):2513. PMID: 22383036; PMCID: PMC3334321.

Tremblay P, Gruss P. Pax: genes for mice and men. Pharmacol Ther. 1994;61(1-2):205-26. doi: 10.1016/0163-7258(94)90063-9. PMID: 7938171.

Tsai KL, Sato S, Tomomori-Sato C, Conaway RC, Conaway JW, Asturias FJ. A conserved Mediator-CDK8 kinase module association regulates Mediator-RNA polymerase II interaction. Nat Struct Mol Biol. 2013 May;20(5):611-9. doi: 10.1038/nsmb.2549. Epub 2013 Apr 7. PMID: 23563140; PMCID: PMC3648612.

Tsai KL, Tomomori-Sato C, Sato S, Conaway RC, Conaway JW, Asturias FJ. Subunit architecture and functional modular rearrangements of the transcriptional mediator complex. Cell. 2014 Jun 5;157(6):1430-1444. doi: 10.1016/j.cell.2014.05.015. Epub 2014 May 29. Erratum in: Cell. 2014 Jul 17;158(2):463. PMID: 24882805; PMCID: PMC4104964.

Tsompana M, Buck MJ. Chromatin accessibility: a window into the genome. Epigenetics Chromatin. 2014 Nov 20;7(1):33. doi: 10.1186/1756-8935-7-33. PMID: 25473421; PMCID: PMC4253006.

Turc-Carel C, Dal Cin P, Rao U, Karakousis C, Sandberg AA. Cytogenetic studies of adipose tissue tumors. I. A benign lipoma with reciprocal translocation t(3;12)(q28;q14). Cancer Genet Cytogenet. 1986 Dec;23(4):283-9. doi: 10.1016/0165-4608(86)90010-5. PMID: 3779624.

Turc-Carel C, Lizard-Nacol S, Justrabo E, Favrot M, Philip T, Tabone E. Consistent chromosomal translocation in alveolar rhabdomyosarcoma. Cancer Genet Cytogenet. 1986 Jan 15;19(3-4):361-2. doi: 10.1016/0165-4608(86)90069-5. PMID: 3943053.

Valen E, Sandelin A. Genomic and chromatin signals underlying transcription start-site selection. Trends Genet. 2011 Nov;27(11):475-85. doi: 10.1016/j.tig.2011.08.001. Epub 2011 Sep 15. PMID: 21924514.

van Berkum NL, Dekker J. Determining spatial chromatin organization of large genomic regions using 5C technology. Methods Mol Biol. 2009;567:189-213. doi: 10.1007/978-1-60327-414-2_13. PMID: 19588094; PMCID: PMC3880132.

van der Horst A, Tertoolen LG, de Vries-Smits LM, Frye RA, Medema RH, Burgering BM. FOXO4 is acetylated upon peroxide stress and deacetylated by the longevity protein hSir2(SIRT1). J Biol Chem. 2004 Jul 9;279(28):28873-9. doi: 10.1074/jbc.M401138200. Epub 2004 May 4. PMID: 15126506.

van Riggelen J, Yetil A, Felsher DW. MYC as a regulator of ribosome biogenesis and protein synthesis. Nat Rev Cancer. 2010 Apr;10(4):301-9. doi: 10.1038/nrc2819. PMID: 20332779.

Verrijzer CP, Chen JL, Yokomori K, Tjian R. Binding of TAFs to core elements directs promoter selectivity by RNA polymerase II. Cell. 1995 Jun 30;81(7):1115-25. doi: 10.1016/s0092-8674(05)80016-9. PMID: 7600579.

Vos SM, Farnung L, Urlaub H, Cramer P. Structure of paused transcription complex Pol II-DSIF-NELF. Nature. 2018 Aug;560(7720):601-606. doi: 10.1038/s41586-018-0442-2. Epub 2018 Aug 22. PMID: 30135580; PMCID: PMC6245578.

Wada T, Takagi T, Yamaguchi Y, Ferdous A, Imai T, Hirose S, Sugimoto S, Yano K, Hartzog GA, Winston F, Buratowski S, Handa H. DSIF, a novel transcription elongation factor that regulates RNA polymerase II processivity, is composed of human Spt4 and Spt5 homologs. Genes Dev. 1998 Feb 1;12(3):343-56. doi: 10.1101/gad.12.3.343. PMID: 9450929; PMCID: PMC316480.

Walker BA, Wardell CP, Brioli A, Boyle E, Kaiser MF, Begum DB, Dahir NB, Johnson DC, Ross FM, Davies FE, Morgan GJ. Translocations at 8q24 juxtapose MYC with genes that harbor superenhancers resulting in overexpression and poor prognosis in myeloma patients. Blood Cancer J. 2014 Mar 14;4(3):e191. doi: 10.1038/bcj.2014.13. PMID: 24632883; PMCID: PMC3972699.

Walters ZS, Villarejo-Balcells B, Olmos D, Buist TW, Missiaglia E, Allen R, Al-Lazikani B, Garrett MD, Blagg J, Shipley J. JARID2 is a direct target of the PAX3-FOXO1 fusion protein and inhibits myogenic differentiation of rhabdomyosarcoma cells. Oncogene. 2014 Feb 27;33(9):1148-57. doi: 10.1038/onc.2013.46. Epub 2013 Feb 25. PMID: 23435416; PMCID: PMC3982124.

Walz S, Lorenzin F, Morton J, Wiese KE, von Eyss B, Herold S, Rycak L, Dumay-Odelot H, Karim S, Bartkuhn M, Roels F, Wüstefeld T, Fischer M, Teichmann M, Zender L, Wei CL, Sansom O, Wolf E, Eilers M. Activation and repression by oncogenic MYC shape tumour-specific gene expression profiles. Nature. 2014 Jul 24;511(7510):483-7. doi: 10.1038/nature13473. Epub 2014 Jul 9. Erratum in: Nature. 2014 Dec 18;516(7531):440. PMID: 25043018; PMCID: PMC6879323.

Wang J, Zhao Y, Zhou X, Hiebert SW, Liu Q, Shyr Y. Nascent RNA sequencing analysis provides insights into enhancer-mediated gene regulation. BMC Genomics. 2018 Aug 23;19(1):633. doi: 10.1186/s12864-018-5016-z. PMID: 30139328; PMCID: PMC6107967.

Wang L, Gural A, Sun XJ, Zhao X, Perna F, Huang G, Hatlen MA, Vu L, Liu F, Xu H, Asai T, Xu H, Deblasio T, Menendez S, Voza F, Jiang Y, Cole PA, Zhang J, Melnick A, Roeder RG, Nimer SD. The leukemogenicity of AML1-ETO is dependent on site-specific lysine acetylation. Science. 2011 Aug 5;333(6043):765-9. doi:

10.1126/science.1201662. Epub 2011 Jul 14. PMID: 21764752; PMCID: PMC3251012.

Wang R, Liu W, Helfer CM, Bradner JE, Hornick JL, Janicki SM, French CA, You J. Activation of SOX2 expression by BRD4-NUT oncogenic fusion drives neoplastic transformation in NUT midline carcinoma. Cancer Res. 2014 Jun 15;74(12):3332-43. doi: 10.1158/0008-5472.CAN-13-2658. Epub 2014 Apr 15. PMID: 24736545; PMCID: PMC4097982.

Wang W, Kumar P, Wang W, Epstein J, Helman L, Moore JV, Kumar S. Insulin-like growth factor II and PAX3-FKHR cooperate in the oncogenesis of rhabdomyosarcoma. Cancer Res. 1998 Oct 1;58(19):4426-33. PMID: 9766674.

Ward E, DeSantis C, Robbins A, Kohler B, Jemal A. Childhood and adolescent cancer statistics, 2014. CA Cancer J Clin. 2014 Mar-Apr;64(2):83-103. doi: 10.3322/caac.21219. Epub 2014 Jan 31. PMID: 24488779.

Weintraub AS, Li CH, Zamudio AV, Sigova AA, Hannett NM, Day DS, Abraham BJ, Cohen MA, Nabet B, Buckley DL, Guo YE, Hnisz D, Jaenisch R, Bradner JE, Gray NS, Young RA. YY1 Is a Structural Regulator of Enhancer-Promoter Loops. Cell. 2017 Dec 14;171(7):1573-1588.e28. doi: 10.1016/j.cell.2017.11.008. Epub 2017 Dec 7. PMID: 29224777; PMCID: PMC5785279.

Whitehouse I, Flaus A, Cairns BR, White MF, Workman JL, Owen-Hughes T. Nucleosome mobilization catalysed by the yeast SWI/SNF complex. Nature. 1999 Aug 19;400(6746):784-7. doi: 10.1038/23506. PMID: 10466730.

Whyte WA, Orlando DA, Hnisz D, Abraham BJ, Lin CY, Kagey MH, Rahl PB, Lee TI, Young RA. Master transcription factors and mediator establish super-enhancers at key cell identity genes. Cell. 2013 Apr 11;153(2):307-19. doi: 10.1016/j.cell.2013.03.035. PMID: 23582322; PMCID: PMC3653129.

Wilson NK, Foster SD, Wang X, Knezevic K, Schütte J, Kaimakis P, Chilarska PM, Kinston S, Ouwehand WH, Dzierzak E, Pimanda JE, de Bruijn MF, Göttgens B. Combinatorial transcriptional control in blood stem/progenitor cells: genome-wide analysis of ten major transcriptional regulators. Cell Stem Cell. 2010 Oct 8;7(4):532-44. doi: 10.1016/j.stem.2010.07.016. PMID: 20887958.

Winter GE, Buckley DL, Paulk J, Roberts JM, Souza A, Dhe-Paganon S, Bradner JE. DRUG DEVELOPMENT. Phthalimide conjugation as a strategy for in vivo target protein degradation. Science. 2015 Jun 19;348(6241):1376-81. doi: 10.1126/science.aab1433. Epub 2015 May 21. PMID: 25999370; PMCID: PMC4937790.

Wu C, Wong YC, Elgin SC. The chromatin structure of specific genes: II. Disruption of chromatin structure during gene activity. Cell. 1979 Apr;16(4):807-14. doi: 10.1016/0092-8674(79)90096-5. PMID: 455450.

Wu CH, Yamaguchi Y, Benjamin LR, Horvat-Gordon M, Washinsky J, Enerly E, Larsson J, Lambertsson A, Handa H, Gilmour D. NELF and DSIF cause promoter proximal pausing on the hsp70 promoter in Drosophila. Genes Dev. 2003 Jun 1;17(11):1402-14. doi: 10.1101/gad.1091403. PMID: 12782658; PMCID: PMC196072.

Wu TF, Yao YL, Lai IL, Lai CC, Lin PL, Yang WM. Loading of PAX3 to Mitotic Chromosomes Is Mediated by Arginine Methylation and Associated with Waardenburg Syndrome. J Biol Chem. 2015 Aug 14;290(33):20556-64. doi:

10.1074/jbc.M114.607713. Epub 2015 Jul 6. PMID: 26149688; PMCID: PMC4536459.

Xiao Q, Li L, Xie Y, Tan N, Wang C, Xu J, Xia K, Gardner K, Li QQ. Transcription factor E2F-1 is upregulated in human gastric cancer tissues and its overexpression suppresses gastric tumor cell proliferation. Cell Oncol. 2007;29(4):335-49. doi: 10.1155/2007/147615. PMID: 17641417; PMCID: PMC4617805.

Yamaguchi Y, Takagi T, Wada T, Yano K, Furuya A, Sugimoto S, Hasegawa J, Handa H. NELF, a multisubunit complex containing RD, cooperates with DSIF to repress RNA polymerase II elongation. Cell. 1999 Apr 2;97(1):41-51. doi: 10.1016/s0092-8674(00)80713-8. PMID: 10199401.

Yan M, Burel SA, Peterson LF, Kanbe E, Iwasaki H, Boyapati A, Hines R, Akashi K, Zhang DE. Deletion of an AML1-ETO C-terminal NcoR/SMRT-interacting region strongly induces leukemia development. Proc Natl Acad Sci U S A. 2004 Dec 7;101(49):17186-91. doi: 10.1073/pnas.0406702101. Epub 2004 Nov 29. PMID: 15569932; PMCID: PMC535382.

Yan M, Kanbe E, Peterson LF, Boyapati A, Miao Y, Wang Y, Chen IM, Chen Z, Rowley JD, Willman CL, Zhang DE. A previously unidentified alternatively spliced isoform of t(8;21) transcript promotes leukemogenesis. Nat Med. 2006 Aug;12(8):945-9. doi: 10.1038/nm1443. Epub 2006 Jul 30. PMID: 16892037.

Yang C, Bolotin E, Jiang T, Sladek FM, Martinez E. Prevalence of the initiator over the TATA box in human and yeast genes and identification of DNA motifs enriched in human TATA-less core promoters. Gene. 2007 Mar 1;389(1):52-65. doi: 10.1016/j.gene.2006.09.029. Epub 2006 Oct 10. PMID: 17123746; PMCID: PMC1955227.

Yang J, Zhang X, Feng J, Leng H, Li S, Xiao J, Liu S, Xu Z, Xu J, Li D, Wang Z, Wang J, Li Q. The Histone Chaperone FACT Contributes to DNA Replication-Coupled Nucleosome Assembly. Cell Rep. 2016 Feb 9;14(5):1128-1141. doi: 10.1016/j.celrep.2015.12.096. Epub 2016 Jan 21. Erratum in: Cell Rep. 2016 Sep 20;16(12):3414. PMID: 26804921.

Yang Z, Yik JH, Chen R, He N, Jang MK, Ozato K, Zhou Q. Recruitment of P-TEFb for stimulation of transcriptional elongation by the bromodomain protein Brd4. Mol Cell. 2005 Aug 19;19(4):535-45. doi: 10.1016/j.molcel.2005.06.029. PMID: 16109377.

Yankulov K, Blau J, Purton T, Roberts S, Bentley DL. Transcriptional elongation by RNA polymerase II is stimulated by transactivators. Cell. 1994 Jun 3;77(5):749-59. doi: 10.1016/0092-8674(94)90058-2. PMID: 8205623.

Yankulov K, Yamashita K, Roy R, Egly JM, Bentley DL. The transcriptional elongation inhibitor 5,6-dichloro-1-beta-D-ribofuranosylbenzimidazole inhibits transcription factor IIH-associated protein kinase. J Biol Chem. 1995 Oct 13;270(41):23922-5. doi: 10.1074/jbc.270.41.23922. PMID: 7592583.

Yoo KH, Hennighausen L. EZH2 methyltransferase and H3K27 methylation in breast cancer. Int J Biol Sci. 2012;8(1):59-65. doi: 10.7150/ijbs.8.59. Epub 2011 Nov 18. PMID: 22211105; PMCID: PMC3226033.

Yoshida H, Kitamura K, Tanaka K, Omura S, Miyazaki T, Hachiya T, Ohno R, Naoe T. Accelerated degradation of PML-retinoic acid receptor alpha (PML-RARA) oncoprotein by all-trans-retinoic acid in acute promyelocytic leukemia: possible

role of the proteasome pathway. Cancer Res. 1996 Jul 1;56(13):2945-8. PMID: 8674046.

Yuan Y, Zhou L, Miyamoto T, Iwasaki H, Harakawa N, Hetherington CJ, Burel SA, Lagasse E, Weissman IL, Akashi K, Zhang DE. AML1-ETO expression is directly involved in the development of acute myeloid leukemia in the presence of additional mutations. Proc Natl Acad Sci U S A. 2001 Aug 28;98(18):10398-403. doi: 10.1073/pnas.171321298. PMID: 11526243; PMCID: PMC56972.

Zech L, Haglund U, Nilsson K, Klein G. Characteristic chromosomal abnormalities in biopsies and lymphoid-cell lines from patients with Burkitt and non-Burkitt lymphomas. Int J Cancer. 1976 Jan 15;17(1):47-56. doi: 10.1002/ijc.2910170108. PMID: 946170.

Zentner GE, Tesar PJ, Scacheri PC. Epigenetic signatures distinguish multiple classes of enhancers with distinct cellular functions. Genome Res. 2011 Aug;21(8):1273-83. doi: 10.1101/gr.122382.111. Epub 2011 Jun 1. PMID: 21632746; PMCID: PMC3149494.

Zhai Y, Wei R, Sha S, Lin C, Wang H, Jiang X, Liu G. Effect of NELL1 on lung cancer stem-like cell differentiation. Oncol Rep. 2019 Mar;41(3):1817-1826. doi: 10.3892/or.2019.6954. Epub 2019 Jan 3. PMID: 30628703.

Zhang G, Liu R, Zhong Y, Plotnikov AN, Zhang W, Zeng L, Rusinova E, Gerona-Nevarro G, Moshkina N, Joshua J, Chuang PY, Ohlmeyer M, He JC, Zhou MM. Down-regulation of NF-κB transcriptional activity in HIV-associated kidney disease by BRD4 inhibition. J Biol Chem. 2012 Aug 17;287(34):28840-51. doi: 10.1074/jbc.M112.359505. Epub 2012 May 29. Erratum in: J Biol Chem. 2012 Nov 9;287(46):38956. PMID: 22645123; PMCID: PMC3436579.

Zhang J, Kalkum M, Yamamura S, Chait BT, Roeder RG. E protein silencing by the leukemogenic AML1-ETO fusion protein. Science. 2004 Aug 27;305(5688):1286-9. doi: 10.1126/science.1097937. PMID: 15333839.

Zhang S, Zhao Y, Heaster TM, Fischer MA, Stengel KR, Zhou X, Ramsey H, Zhou MM, Savona MR, Skala MC, Hiebert SW. BET inhibitors reduce cell size and induce reversible cell cycle arrest in AML. J Cell Biochem. 2018 Nov 11:10.1002/jcb.28005. doi: 10.1002/jcb.28005. Epub ahead of print. PMID: 30417424; PMCID: PMC6513713.

Zhao Y, Liu Q, Acharya P, Stengel KR, Sheng Q, Zhou X, Kwak H, Fischer MA, Bradner JE, Strickland SA, Mohan SR, Savona MR, Venters BJ, Zhou MM, Lis JT, Hiebert SW. High-Resolution Mapping of RNA Polymerases Identifies Mechanisms of Sensitivity and Resistance to BET Inhibitors in t(8;21) AML. Cell Rep. 2016 Aug 16;16(7):2003-16. doi: 10.1016/j.celrep.2016.07.032. Epub 2016 Aug 4. PMID: 27498870; PMCID: PMC4996374.

Zhou H, Bai L, Xu R, Zhao Y, Chen J, McEachern D, Chinnaswamy K, Wen B, Dai L, Kumar P, Yang CY, Liu Z, Wang M, Liu L, Meagher JL, Yi H, Sun D, Stuckey JA, Wang S. Structure-Based Discovery of SD-36 as a Potent, Selective, and Efficacious PROTAC Degrader of STAT3 Protein. J Med Chem. 2019 Dec 26;62(24):11280-11300. doi: 10.1021/acs.jmedchem.9b01530. Epub 2019 Dec 10. PMID: 31747516; PMCID: PMC8848307.

Zhou Q, Li T, Price DH. RNA polymerase II elongation control. Annu Rev Biochem. 2012;81:119-43. doi: 10.1146/annurev-biochem-052610-095910. Epub 2012 Mar 9. PMID: 22404626; PMCID: PMC4273853.

Zhu J, Gianni M, Kopf E, Honoré N, Chelbi-Alix M, Koken M, Quignon F, Rochette-Egly C, de Thé H. Retinoic acid induces proteasome-dependent degradation of retinoic acid receptor alpha (RARalpha) and oncogenic RARalpha fusion proteins. Proc Natl Acad Sci U S A. 1999 Dec 21;96(26):14807-12. doi: 10.1073/pnas.96.26.14807. PMID: 10611294; PMCID: PMC24729.

Zou L, Li H, Han X, Qin J, Song G. Runx1t1 promotes the neuronal differentiation in rat hippocampus. Stem Cell Res Ther. 2020 Apr 22;11(1):160. doi: 10.1186/s13287-020-01667-x. PMID: 32321587; PMCID: PMC7178948.

Zuber J, Shi J, Wang E, Rappaport AR, Herrmann H, Sison EA, Magoon D, Qi J, Blatt K, Wunderlich M, Taylor MJ, Johns C, Chicas A, Mulloy JC, Kogan SC, Brown P, Valent P, Bradner JE, Lowe SW, Vakoc CR. RNAi screen identifies Brd4 as a therapeutic target in acute myeloid leukaemia. Nature. 2011 Aug 3;478(7370):524-8. doi: 10.1038/nature10334. PMID: 21814200; PMCID: PMC3328300.